Table of contents:

1. General information

NMR Spectroscopy. ^{1}H NMR spectra were recorded on a high-field spectrometer (^{1}H 600.15 MHz and 500 MHz, ^{13}C 151 MHz and 125.75 MHz), equipped with a broadband inverse gradient probe head. Spectra were referenced to the residual solvent signal (chloroform-d, 7.26 ppm and methanol-d_4, 3.31 ppm in ^{1}H spectra and chloroform-d, 76.16 ppm and methanol-d_4, 49.00 ppm in ^{13}C spectra). The experiments were performed at 300K if not specified.

Mass Spectrometry. High resolution and Accurate Mass spectra were recorded on a Bruker apex ultra FTMS and a Bruker microTOF-Q spectrometers using the electrospray technique.

UV-Vis Spectroscopy. Electronic spectra were recorded on an Agilent Technologies Carry-60 spectrophotometer.

Fluorescence. For recording photoluminescence excitation (PLE) and emission (PL) spectra the FSL980 Fluorescence Spectrometer from Edinburgh Instruments Ltd was used with a 450 W Xenon arc lamp (PL and PLE) as an excitation source. Emission spectra were corrected for the recording system efficiency and excitation spectra were corrected for the incident light intensity. PLE and PL spectra and QY were measured using a cooled extended-red Hamamatsu photomultiplier operating in a 200 – 1050 nm range. Quantum yield measurements were performed by using an Edinburgh Instruments integrating sphere equipped with a small elliptical mirror and a baffle plate for beam steering and shielding against directly detected light. For the measurement, the integrating sphere replaced the standard sample holder inside the sample chamber. Calculations of quantum yields were made using the software provided by Edinburgh Instruments. The decay curves of the luminescence excited by pulsed diode with excitation line 280 nm were recorded with the low-noise F-G05 detector featuring a Hamamatsu H5773-04 photomultiplier. The maximum of emission was chosen as an observation wavelength.

X-Ray Analysis. X-Ray quality crystals were prepared by slow evaporation or vapor diffusion in different solvents sets, based on the structure. SCXRD measurements for **1c**, **1e** and **5**, were performed using the following instrument: Bruker D8 Quest Eco diffractometer at 100K equipped with Photon II CPAD detector, MoKα (λ = 0.71073 Å) sealed tube radiation source and Triumph® optics. For structures **1b**, **2a** and **3**-*O*-**3** a Rigaku Oxford Diffraction XtaLAB Synergy-R DW diffractometer equipped with a HyPix ARC 150° Hybrid Photon Counting (HPC) detector using CuKα (λ = 1.54184 Å) was used. For structure **1d** a Xcalibur R diffractometer equipped with Ruby CCD detector using CuKα (λ = 1.54184 Å) was employed. For structure **1a**, a Xcalibur Gemini Ultra diffractometer equipped with Ruby CCD detector using CuKα (λ = 1.54184 Å) was used.

Data were processed using the CrystAlisPro software. The structures were solved by intrinsic phasing with SHELXT (2015 release) and refined by full-matrix least-squares methods based F 2 using SHELXL. For all structures, H atoms bound to C atoms were placed in the geometrically idealized positions and treated in riding mode, with C-H = 0.95 Å and Uiso(H) = 1.2Ueq(C) for C-H groups, and C-H = 0.98 Å and Uiso(H) = 1.5Ueq(C) for CH_3 groups, while the O- and N-bound H atoms were refined freely.

Theoretical calculations. Geometry optimizations for all the derivatives were carried out with the Gaussian 09[1] software package within unconstrained C1 symmetry, with starting coordinates derived from semi-empirical calculations. Becke's three-parameter exchange functional with the gradient-corrected correlation formula of Lee, Yang and Parr (DFT-B3LYP)[2] were used with the 6-31G(d,p) basis set. The polarizable continuum model of solvation was used (PCM, standard dichloromethane) for all optimizations.
The electronic spectra were simulated by means of time-dependent density functional theory (TD-DFT) using the Tamm-Dancoff approximation for 50 states and 6-31G(d,p) basis set for all the derivatives. The electronic transitions and UV/Vis were analyzed by means of the GaussSum program. The transitions were convoluted by Gaussian curves with 2000 cm^{-1} half line width for all the derivatives.
The SCF GIAO NMR predictions were determined starting from the optimized geometries and using a shielding value of 31.75 ppm when calculated in $CDCl_3$ and a shielding value of 31.74 when calculated in CD_3OD. Shielding values were calculated on the TMS (tetramethyl silane) optimized structure.
LC-MS analysis. The LC-MS analysis was performed on Shimadzu LC IT-TOF. Separation was carried out on an RP-Zorbax (50×2.1 mm, 3.5 µm) column with a gradient elution of 0-80% B in A (A = 0.1% HCOOH in water; B = 0.1% HCOOH in MeCN) at room temperature over a period of 20 min (flow rate: 0.1 mL/min).
SEC chromatography. SEC column were performed using Bio-Beads S-X1 Support, styrene divinylbenzene with 1% crosslinkage, 40-80 µm bead size, 600-14,000 MW exclusion range as stationary phase and THF as eluent.

[1] Gaussian 09, Revision E.01; M. J. Frisch et al., Gaussian, Inc.: Wallingford CT, 2009.
[2] a) C. T. Lee, W. T. Yang, R. G. Parr, *Phys. Rev. B*, 1988, **37**, 785-789. b) A. D. Becke, *Phys. Rev. A*, 1988, **38**, 3098-3100.

2. Experimental section.

All solvents (methanol, ethyl acetate, chloroform, *n*-hexane, toluene, acetone, water and tetrahydrofuran) if not indicated differently were used without purification. CH_2Cl_2 was distilled over CaH_2. Chloroform-*d* was prepared directly before using by passing through a basic alumina column. All reactions were performed under inert atmosphere.

2.1 Experimental procedures.

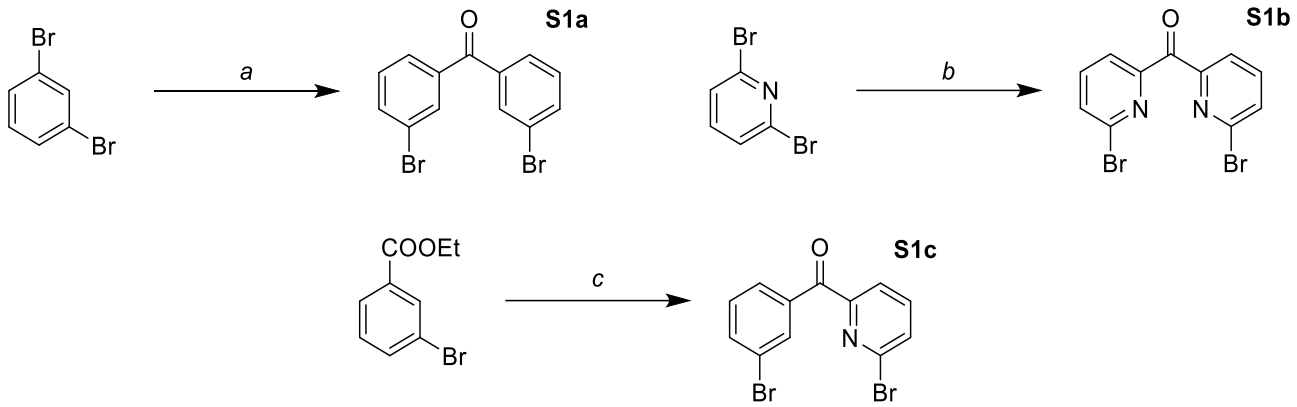

Scheme S1. Synthetic approach for **S1a, S1b** and **S1c** synthons used in this work. Conditions: *a*, 1,3-dibromobenzene (1.0 eq.), *n*BuLi (1.001 eq.), diethyl carbonate (2.01 eq.), THF, -78 °C to RT, Ar, 16h; *b*, 2,6-dibromopyridine (2.2 eq.), *n*Buli (2.4 eq.), diethyl carbonate (1.0 eq.), THF, -78 °C to 0 °C, Ar, 2h; *c*, ethyl 3-bromobenzoate (1.0 eq.), 2,6-dibromopyridine (1.0 eq.), *n*BuLi (1.01 eq.), THF, -78 °C to RT, Ar, 2h.

S1a was prepared according to Gibb et al. procedure.[3]
S1b was prepared according to Mayor et al. procedure.[4]
S1c was prepared according to a modified procedure of Mayor et al.[4]

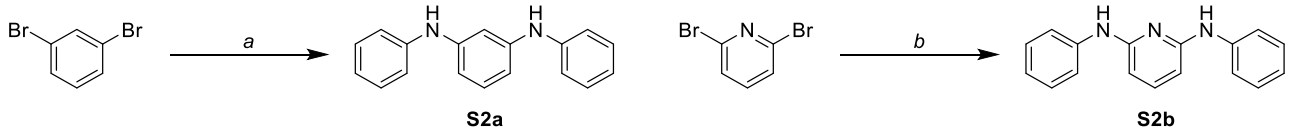

Scheme S2. Synthetic approach for motifs **S2a** and **S2b** used in this work. Conditions: *a*, 1,3-dibromobenzene (1.0 eq.), aniline (3.0 eq.), $Pd_2(dba)_3$ (2.0% eq.), racBINAP (4.0% eq.), NaO^tBu (3.6 eq.); *b,* 2,6-dibromopyridine (1.0 eq.), aniline (2.4 eq.), $Pd_2(dba)_3$ (2.0% eq.), racBINAP (4.0% eq.), NaO^tBu (2.8 eq.).

[3] X. Li, C. L. D. Gibb, M. E. Kuebel, and B. C. Gibb, *Tetrahedron*, **2001**, 57, 1175-1182.
[4] M. Lindner, M. Valàsek, J. Homberg, K. Edelmann, L. Gerhard, W. Wulfhekel, O. Fuhr, T. Wächter, M. Zharnikov, V. Kolivoska, L. Pospìsil, G. Mészàros, M. Hromadovà, and M. Mayor, *Chem. Eur J.*, **2016**, 22, 13218-13235.

S2a was prepared according to Hatakeyama et al. procedure.[5]
S2b was prepared according to the procedure of Buchwald and co-worker. [6]

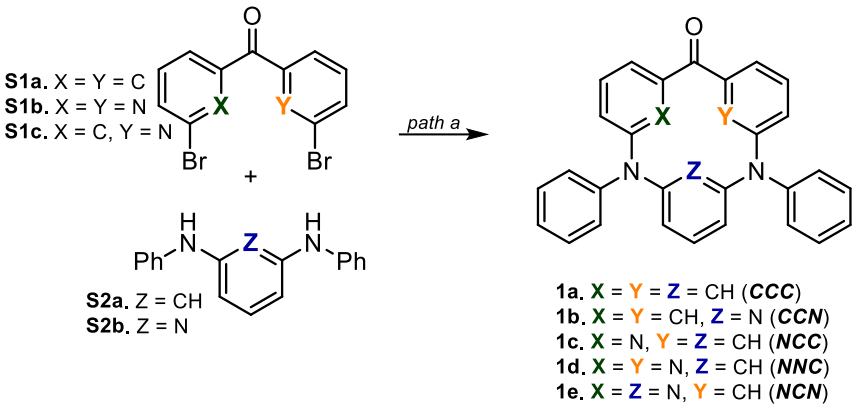

Scheme S3. Synthetic approach for the formation of macrocycles **1a-e**.

General procedure for the preparation of Macrocycles 1a-1e.[5]
A Schlenk tube was charged with **S1a** or **S1b** or **S1c** (0.15 mmol), $Pd_2(dba)_3$ (7.5% mol. halo), RuPhos (30% mol. halo), **S2a** or **S2b** (0.15 mmol) and K_3PO_4 (10 eq.) and was allowed to dry under high vacuum overnight. In the morning, 15 mL of degassed toluene (**1b**, **1d**) or *o*-xylene (**1a**, **1c**, **1e**) was added to the tube and the reaction mixture was refluxed for 24 hours. After reaction completion, the crude product was allowed to chill to room temperature and it was passed through a silica plug (eluent: ethyl acetate). The obtained solution was dried under reduced pressure and subjected to column chromatography purification.

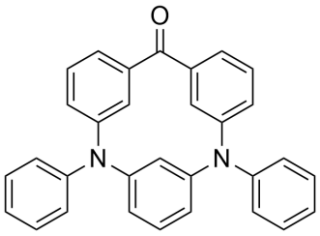

Macrocycle, 1a. The product was obtained in 71% yield as a pale yellow solid (column chromatography conditions: *n*Hexane/ CH_2Cl_2 1:1 to 100% CH_2Cl_2). **^{1}H NMR (600 MHz, 300K, $CDCl_3$)** δ 7.58 (m, 3H), 7.47 (ddd, ^3J = 8.0 Hz, ^4J = 2.4 Hz, ^4J = 0.9 Hz, 2H), 7.37 (t, ^3J = 7.8 Hz, 2H), 7.29 (m, 4H), 7.17-7.14 (m, 5H), 7.01 (t, ^4J = 1.9 Hz, 2H) 7.00-6.96 (m, 4H). **^{13}C NMR (151 MHz, 300K, $CDCl_3$)** δ 196.1, 149.2, 147.3, 146.3, 139.9, 132.5, 130.5, 129.7, 129.6, 128.6, 127.6, 123.8, 122.9, 121.6, 119.4, **HRMS (m/z)**: 439.1811 $[M+H]^+$ (theor. calc. 439.1805 for $C_{31}H_{22}N_2O$), **UV-Vis**: 284, 404 nm, **Extinction**: $2.3 \cdot 10^4$ $M^{-1}cm^{-1}$, **Emission**: 495 nm.

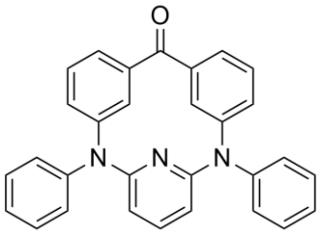

Macrocycle, 1b. In this case, Pd_2dba_3 (5% halo.) and XantPhos (10% halo.) were used. The product was obtained in 35% yield as a pale yellow solid (column chromatography conditions: 100% CH_2Cl_2). **^{1}H NMR (600 MHz, 300K, $CDCl_3$)** δ = 8.66 (t, ^4J = 1.9 Hz, 2H), 7.68 (ddd, ^3J = 7.6, ^4J = 1.5, 1.0 Hz, 2H), 7.51-7.44 (m, 4H), 7.39-7.29 (m, 8H), 7.24 (t, ^3J = 8.1 Hz, 1H), 7.00 (ddd, ^3J = 8.1, ^4J = 2.3, 0.9 Hz, 2H), 6.23 (d, ^3J = 8.1 Hz, 2H). **^{13}C NMR (151 MHz, 300K, $CDCl_3$)** δ = 196.6, 155.9, 143.8, 142.9, 138.7, 137.8, 134.9, 130.2, 128.0, 127.8, 127.3, 126.5, 123.1, 104.9,

[5] S. Nakatsuka, H. Gotoh, K. Kinoshita, N. Yasuda, T. Hatakeyama, *Angew. Chem. Int. Ed.*, **2017**, 56, 5087-5090.
[6] S. Wagaw and S. L. Buchwald. *J. Org. Chem.*, **1996**, 61, 21, 7240-7241.

HRMS (m/z): 440.1743 $[M+H]^+$ (theor. calc. 440.1757 for $C_{30}H_{21}N_3O$), **UV-Vis**: 268, 336 nm, **Extinction**: $2.5 \cdot 10^4$ $M^{-1}cm^{-1}$, **Emission**: 487 nm.

Macrocycle, 1c. The product was obtained in 54% yield as a yellow solid (column chromatography conditions: *n*Hexane/ CH_2Cl_2 1:1 to 80% CH_2Cl_2). 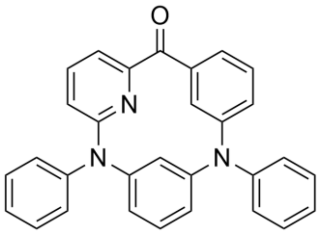 **^{1}H NMR (600 MHz, 300K, $CDCl_3$)** δ 8.77 (s, 1H), 8.00 (t, ^3J = 2.1 Hz, 1H), 7.59 (d, ^3J = 7.4 Hz, 1H), 7.54 – 7.47 (m, 3H), 7.47 – 7.35 (m, 7H), 7.21 – 7.12 (m, 4H), 7.01 (t, ^3J = 8.1 Hz, 1H), 6.72 (dd, ^3J = 8.1, ^4J = 2.2 Hz, 1H), 6.64 (d, ^3J = 8.5 Hz, 1H), 6.33 (ddd, ^3J = 8.0, ^4J = 2.0, 0.6 Hz, 1H). **^{13}C NMR (151 MHz, 300K, $CDCl_3$)** δ 192.2, 155.4, 151.8, 146.0, 145.5, 144.2, 143.1, 142.4, 137.2, 136.8, 129.4, 128.7, 127.9, 127.6, 127.4, 126.4, 126.3, 124.6, 124.1, 123.4, 122.1, 119.7, 117.3, 116.7, 114.4, 111.7, **HRMS (m/z)**: 440.1771 $[M+H]^+$ (theor. calc. 441.1757 for $C_{30}H_{21}N_3O$), **UV-Vis**: 292, 386 nm, **Extinction**: $3.45 \cdot 10^4$ $M^{-1}cm^{-1}$, **Emission**: 576 nm.

Macrocycle, 1d. The product was obtained in 77% yield as an orange solid (column chromatography conditions: ethyl acetate/ CH_2Cl_2 1:10). 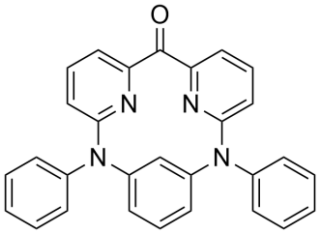 **^{1}H NMR (600 MHz, 300K, $CDCl_3$)** δ 8.51 (t, ^4J = 2.2 Hz, 1H), 7.55-7.44 (m, 12H), 7.34 (tt, ^3J = 7.2 Hz, ^4J = 1.4 Hz, 2H), 6.98 (t, ^3J = 8.1 Hz, 1H), 6.77 (dd, ^3J = 7.8 Hz, ^4J = 1.3 Hz, 2H), 6.42 (dd, ^3J = 8.1 Hz, ^4J = 2.2 Hz, 2H). **^{13}C NMR (151 MHz, 300K, $CDCl_3$)** δ 189.6, 157.0, 153.0, 143.8, 143.1, 138.2, 130.3, 128.3, 127.4, 126.8, 126.7, 118.2, 116.5, 113.9, **HRMS (m/z)**: 441.1715 $[M+H]^+$ (theor. calc. 441.1710 for $C_{29}H_{20}N_4O$), **UV-Vis**: 277, 405 nm, **Extinction**: $5.8 \cdot 10^4$ $M^{-1}cm^{-1}$, **Emission**: 576 nm.

Macrocycle, 1e. The product was obtained in 59% yield as a yellow solid (column chromatography conditions: 100% CH_2Cl_2 to ethyl acetate/ CH_2Cl_2 1:10 and the purification was concluded with an additional SEC column with THF as solvent). 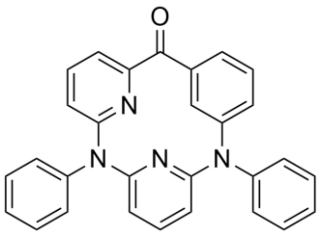 **^{1}H NMR (600 MHz, 300K, $CDCl_3$)** δ = 9.67 (t, ^4J = 1.9 Hz, 1H), 7.60 (d, ^3J = 7.4 Hz, 2H), 7.55 (m, 2H), 7.52-7.41 (m, 8H), 7.30 (tt, ^3J = 7.1, ^4J = 1.3, 1H), 7.28-7.24 (m, 1H), 7.15 (t, ^3J = 7.8 Hz, 1H), 6.88 (ddd, ^3J = 8.1, ^4J = 2.4, 0.75, 1H), 6.44 (d, ^3J = 8.5 Hz, 1H), 6.28 (d, ^4J = 8.0 Hz, 1H), 5.94 (d, ^4J = 8.0, 1H). **^{13}C NMR (151 MHz, 300K, $CDCl_3$)** δ = 192.9, 156.6, 155.6, 155.5, 153.6, 144.2, 143.0, 139.0, 138.1, 136.6, 130.9, 130.3, 129.9, 128.2, 127.7, 127,5, 126.3, 124.4, 121.9, 116.2, 114.7, 108.7, 107.9,
HRMS (m/z): 441.1736 $[M+H]^+$ (theor. calc. 441.1710 for $C_{29}H_{20}N_4O$), **UV-Vis**: 288, 343 nm, **Extinction**: $3.8 \cdot 10^4$ $M^{-1}cm^{-1}$, **Emission**: 539 nm.

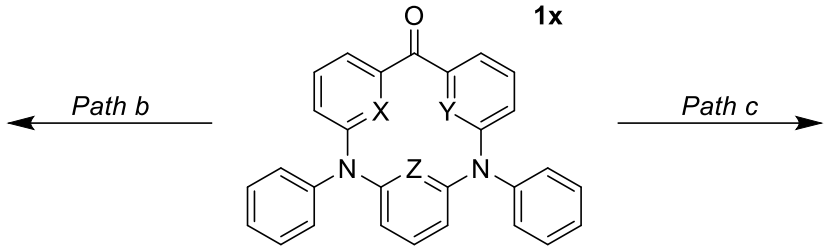

Scheme S4. Schematic representation of the Boron(III) insertion reactions.

General procedure for Boron(III) insertion.[7]

Path *b*: A Schlenk tube was charged with a macrocycle **1a-e** (0.1 mmol), degassed toluene (10 mL) was added and the mixture was brought to reflux. BBr_3 (10 equiv.) was added was allowed to reflux for additional 20 minutes. After this time, TEA (10 equiv.) was added and the reaction was refluxed for 2 hours. After that time, the reaction mixture was allowed to cool to room temperature and water (50 mL) was added. The mixture was extracted with CH_2Cl_2 (3X30 mL) , the collected organic phase was dried over Na_2SO_4, filtered and dried to solid. The solids were then purified with different methods.

Path *c*: A Schlenk tube was charged with a macrocycle **1a-e** (0.1 mmol) and degassed 1,2-dichlorobenzene (5 mL). BBr_3 (10 equiv.) was added dropwise and the reaction was allowed to reflux for 5 hours. After that time, the reaction mixture was allowed to cool to room temperature and water (50 mL) was added. The mixture was extracted with CH_2Cl_2 (3X30 mL), the collected organic phase was dried over Na_2SO_4, filtered and dried to solid. The solids were then purified with different methods.

Macrocycle *meso*-bromine, 2a. The product was obtained as an off white solid (column chromatography conditions: 100% *n*Hexane to 100% CH_2Cl_2 with gradient), from starting material **1a**, following conditions from **Path *b***. **^{1}H NMR (600 MHz, 300K, $CDCl_3$)** δ 7.80 (s, 2H), 7.13 – 7.05 (m, 2H), 7.03 (t, ^3J = 8.1 Hz, 1H), 6.92 (t, ^3J = 7.8 Hz, 2H), 6.79 (ddd, ^3J = 8.2, ^4J = 2.3, ^4J = 0.8 Hz, 2H), 6.65 (t, ^3J = 7.0 Hz, 3H), 6.63 (dd, ^3J = 8.1, ^4J = 2.2 Hz, 2H), 5.64 (s, 1H), 1.25 (s, 2H). **^{13}C NMR (150 MHz, 300K, $CDCl_3$)** δ 149.0, 148.4, 144.3, 144.1, 129.0, 128.5, 127.8, 124.5, 123.7, 122.9, 120.7, 120.2, 117.9, 116.0, 28.9. **HRMS (m/z)**: 927.27735 $[M+H]^+$, **UV-Vis**: 298 nm, **Extinction**: $5.9\cdot10^4$ $M^{-1}cm^{-1}$, **Emission**: 402 nm.

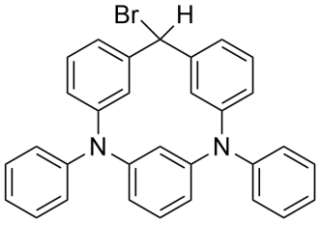

Fused Dimer, 3. The product was obtained in 49% yield as a dark green-brown solid, from starting material **1d**, following conditions from **Path *b***. The product was purified using a SEC chromatography (eluent: THF) and precipitation (CH_2Cl_2/*n*Hexane). **^{1}H NMR (600 MHz, CD_3OD)** δ = 9.01 (d, ^3J = 10.1 Hz, 2H), 8.14 (dd, ^3J = 8.8 Hz, 7.9 Hz, 2H), 7.95-7.77 (m, 14H), 7.72 (d, ^3J = 7.2 Hz, 2H), 7.64-7.56 (m, 6H), 7.34 (t, ^3J = 8.2 Hz, 2H), 7.24 (d, ^3J = 10.1 Hz, 2H), 7.03 (d, ^3J = 9.1 Hz, 2H), 6.52 (d, ^3J = 8.2 Hz, 2H), 6.45 (d, ^3J = 8.2 Hz, 2H). **^{13}C NMR (151 MHz, CD_3OD)** δ = 153.0, 151.6, 143.7, 143.4, 142.7, 141.9, 140.6, 139.0, 138.7, 135.9, 133.6, 133.1, 132.8, 132.4, 131.9, 131.3, 130.9, 129.7, 125.8, 123.6, 118.9, 117.1, 113.7, 113.5. **HRMS (m/z)**: 450.16112

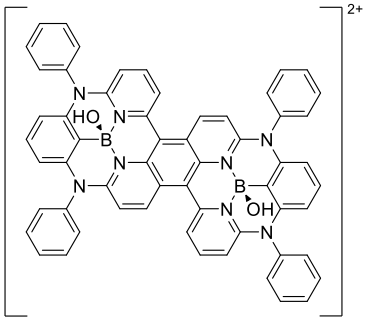

[7] M. Kijewska, M. Siczek, and M. Pawlicki, *Org. Lett.*, **2021**, 23, 9, 3652-3656.

$[M]^{+2}$ (theor. calc. 450.16466 for $C_{58}H_{38}B_2N_8O_2$), **UV-Vis**: 309, 389, 460, 486, 580 nm, **Extinction**: $2.5 \cdot 10^4$ $M^{-1}cm^{-1}$, **Emission**: 637 nm.

Fused dimer, 4. The product was obtained in 44% yield as a dark red-brown solid, from starting

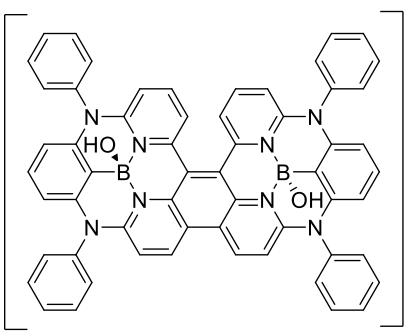

material **1d**, following conditions from **Path *c***. The product was purified using SEC chromatography (eluent: THF) and precipitation (CH_2Cl_2/*n*Hexane). **^{1}H NMR (600 MHz, CD_3OD)** δ = 9.13 (d, ^3J = 9.9 Hz, 1H), 7.83 (m, 10H), 7.68 (d, ^3J = 7.4 Hz, 1H), 7.65 (d, ^3J = 7.2 Hz, 1H), 7.30 (m, 2H), 6.95 (d, ^3J = 9.0 Hz, 1H), 6.46 (d, ^3J = 8.2 Hz, 1H), 6.42 (d, ^3J = 8.2 Hz, 1H). **^{13}C NMR (151 MHz, CD_3OD)** δ = 152.2, 151.5, 149.1, 148.0, 146.7, 144.8, 143.4, 142.4, 139.2, 139.1, 137.6, 133.0, 132.2, 131.9, 131.1, 131.0, 129.0, 125.1, 121.9, 119.2, 117.5, 113.4, 113.4. **HRMS (m/z)**: 450.1695 $[M]^{+2}$ (theor. calc. 450.1655 for $C_{58}H_{38}B_2N_8O_2$), UV-Vis: 311, 368, 382, 448, 472, 554 nm, **Extinction**: $3.2 \cdot 10^4$ $M^{-1}cm^{-1}$, **Emission**: 614 nm.

Fused Tetramer, 3-*O*-3. The product was obtained as result of slow conversion from mono

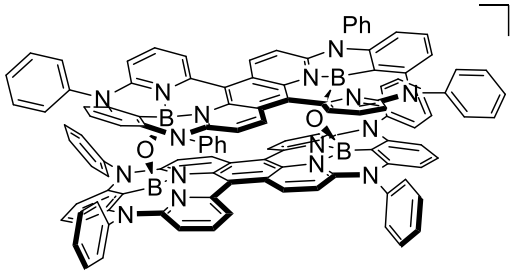

layered system **3** with the elimination of 2 molecules of H_2O. **HRMS (m/z)**: 441.15866 $[M]^{+4}$ (theor. calc. 441.16111 for $C_{116}H_{72}B_4N_{16}O_2$), **UV-Vis**: 303, 388, 455, 481, 580 nm, **Extinction**: $2.4 \cdot 10^4$ $M^{-1}cm^{-1}$.

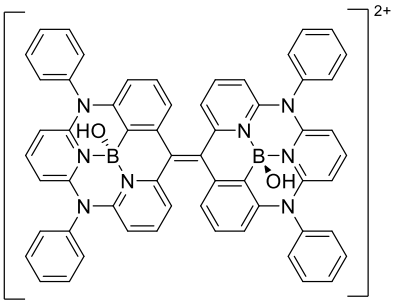

Dimer, 5. The product was obtained in 51% yield as a dark green solid, from starting material **1e**, following conditions from **Path *c*** (using longer reaction time, 18 hours). The product was purified using a preparative HPLC (eluent: acetonitrile and H_2O with TFA). **^{1}H NMR (500 MHz, CD_3OD)** δ = 7.88-7.69 (m, 20H), 7.56 (d, ^3J = 7.2 Hz, 4H), 7.41 (dd, ^3J = 7.8, ^4J = 0.8 Hz, 2H), 7.09 (dd, ^3J = 8.3, 7.7 Hz, 2H), 6.93 (d, ^3J = 7.6 Hz, 2H), 6.79 (dd, ^3J = 8.8, ^4J = 0.8 Hz, 2H), 6.44 (d, ^3J = 8.4 Hz, 2H), 6.35 (dd, ^3J = 8.8, ^4J = 0.6 Hz, 2H), 6.14 (dd, ^3J = 8.2, ^4J = 0.6 Hz, 2H). **^{13}C NMR (126 MHz, CD_3OD)** δ = 151.7, 150.8, 150.7, 149.4, 144.8, 144.0, 143.3, 139.6, 138.0, 136.40, 136.38, 133.2, 132.8, 132.7, 131.6, 131.0, 130.8, 130.2, 124.5, 124.0, 117.8, 116.5, 108.6, 104.3. **HRMS (m/z)**: 451.1761 $[M]^{+2}$ (theor. calc. 451.1734 for $C_{58}H_{40}B_2N_8O_2$), **UV-Vis**: 284, 375 nm, **Extinction**: $1.7 \cdot 10^4$ $M^{-1}cm^{-1}$, **Emission**: 630 nm.

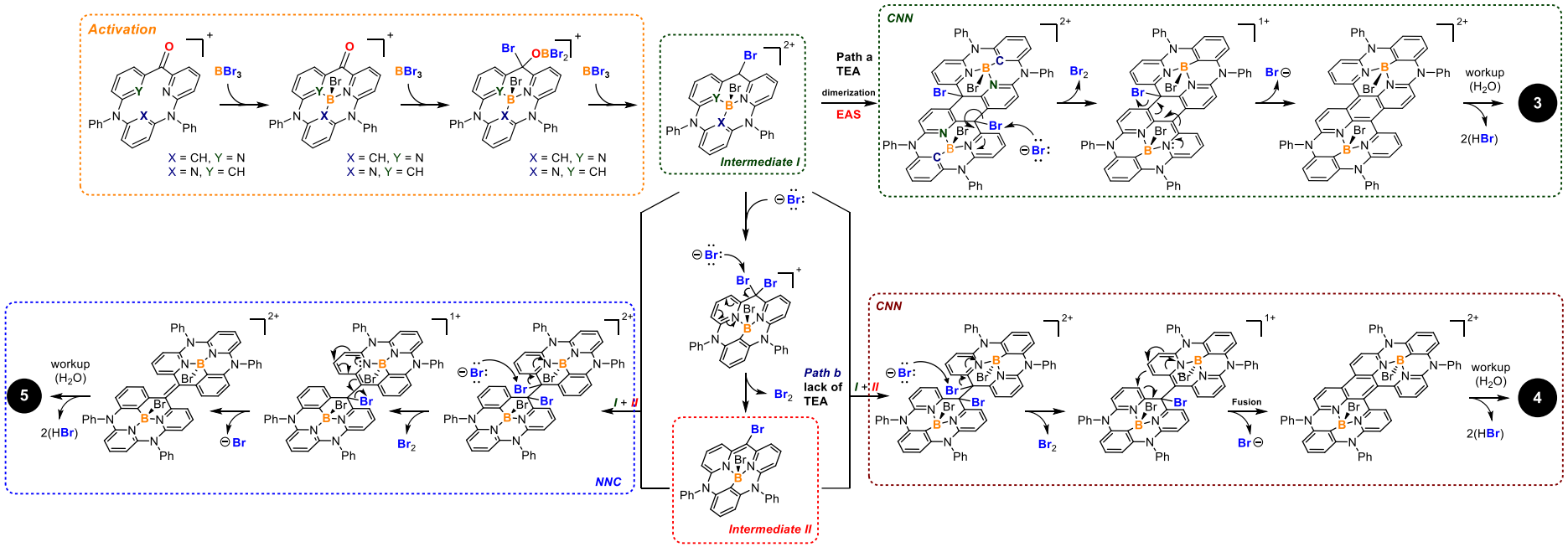

Scheme S5. Plausible mechanism.

3. NMR spectra

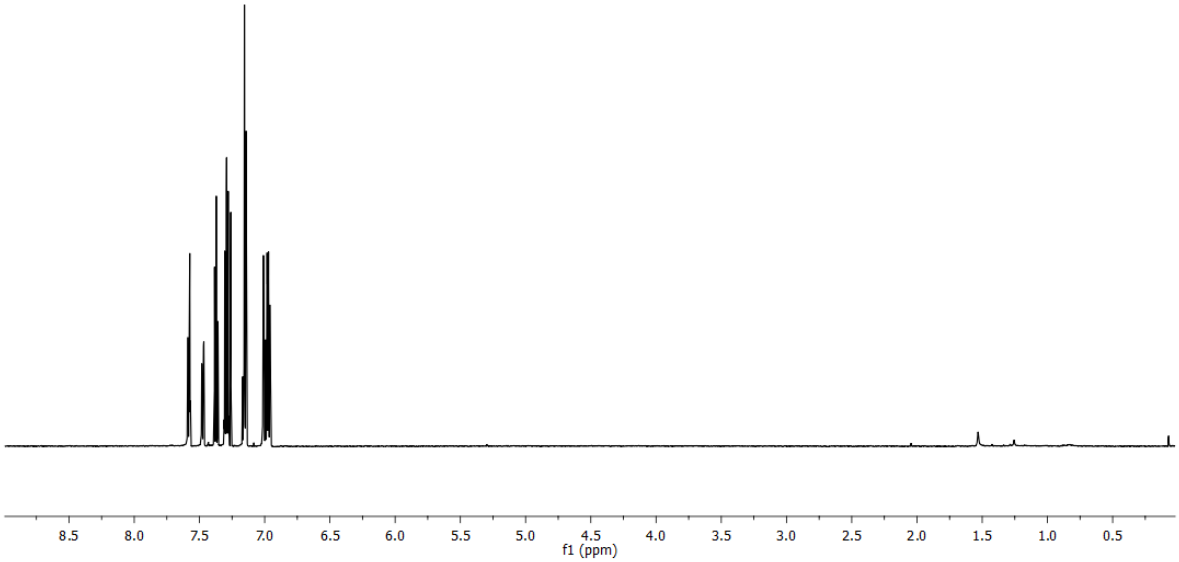

Figure S1. ^{1}H NMR spectrum of **1a** ($CDCl_3$, 300K, 600 MHz).

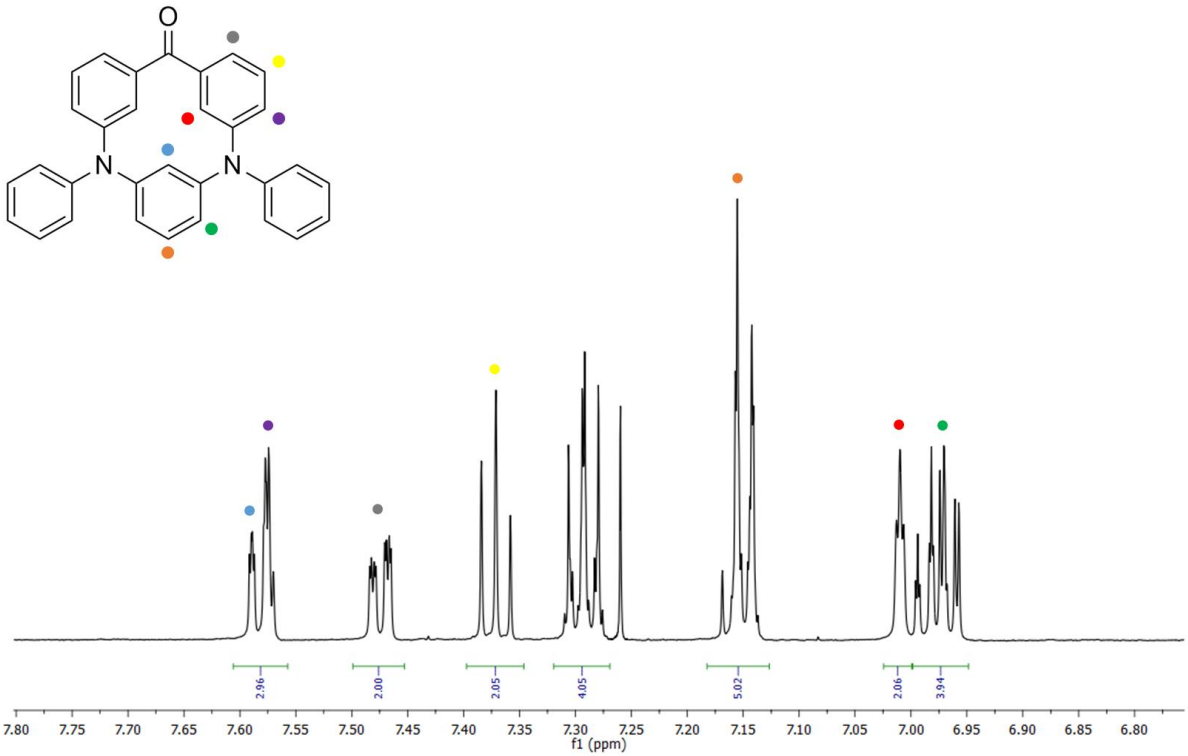

Figure S2. ^{1}H NMR spectrum (zoom, aromatic region) of **1a** ($CDCl_3$, 300K, 600 MHz).

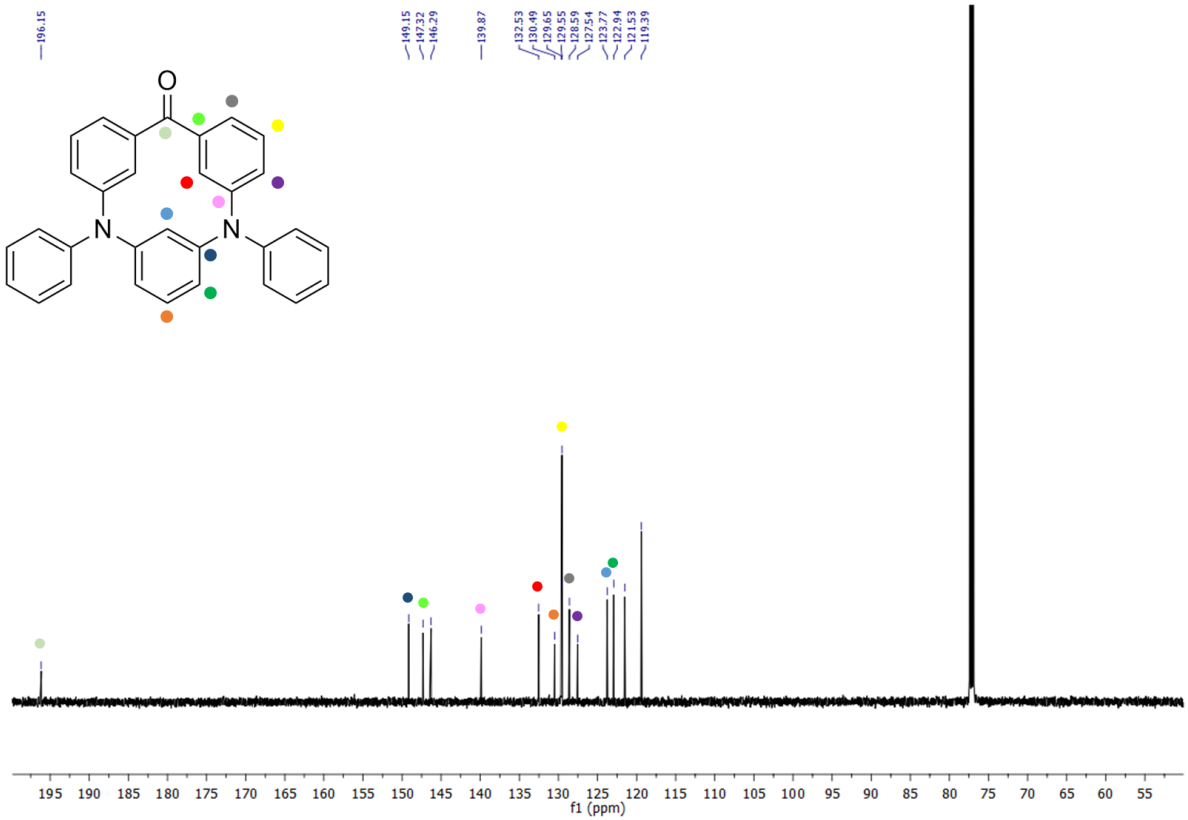

Figure S3. ^{13}C NMR spectrum of **1a** ($CDCl_3$, 300K, 151 MHz).

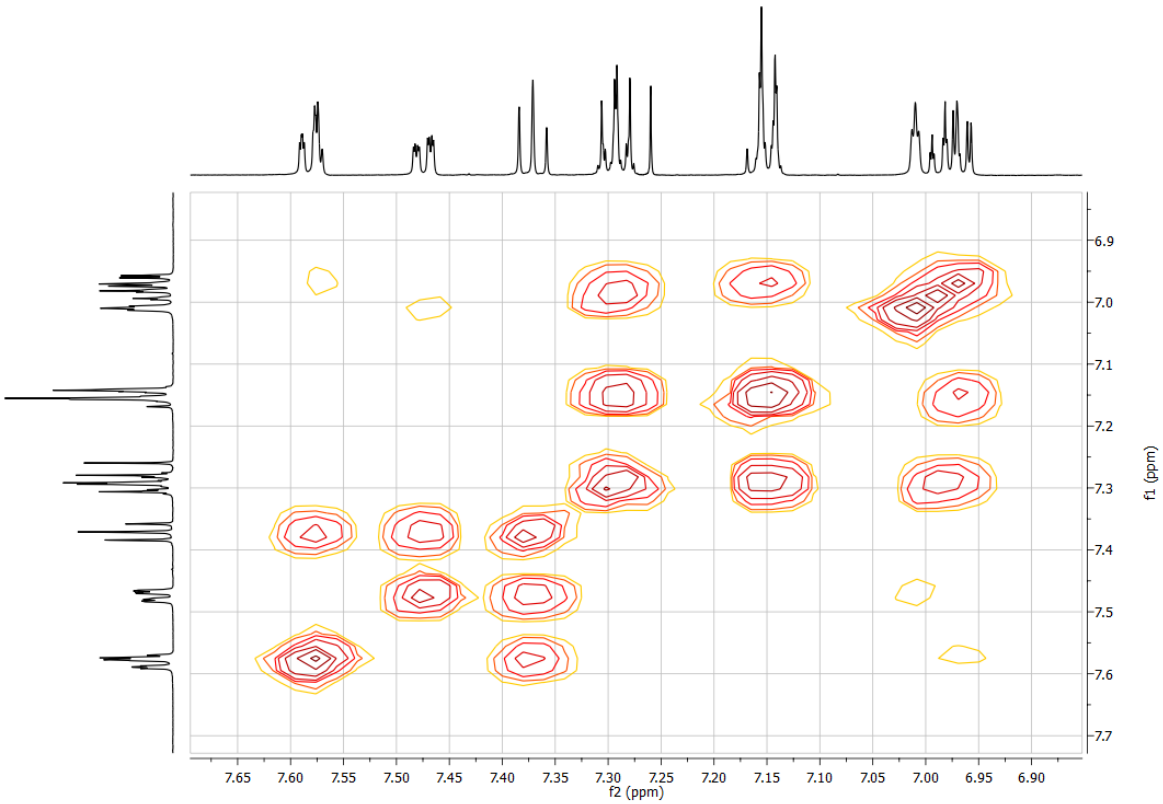

Figure S4. COSY NMR spectrum of **1a** ($CDCl_3$, 300K, 600 MHz).

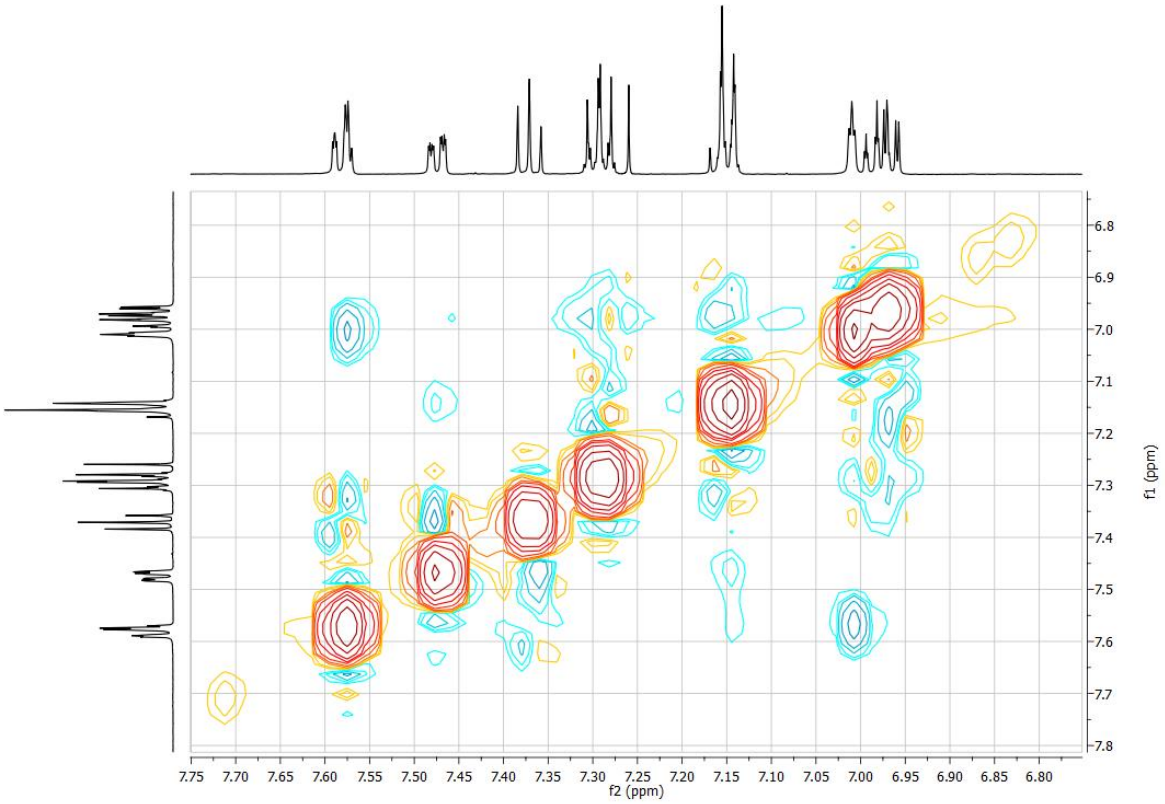

Figure S5. NOESY NMR spectrum of **1a** ($CDCl_3$, 300K, 600 MHz).

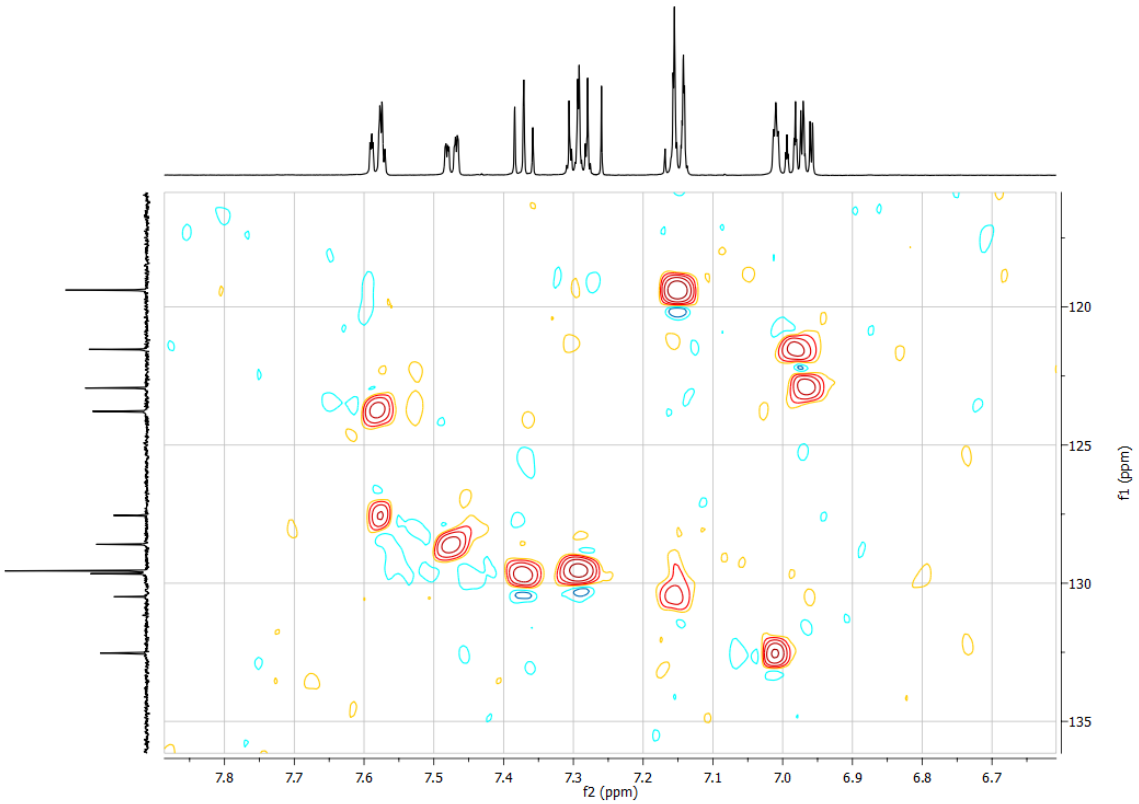

Figure S6. HSQC NMR spectrum of **1a** ($CDCl_3$, 300K, 600, 151 MHz).

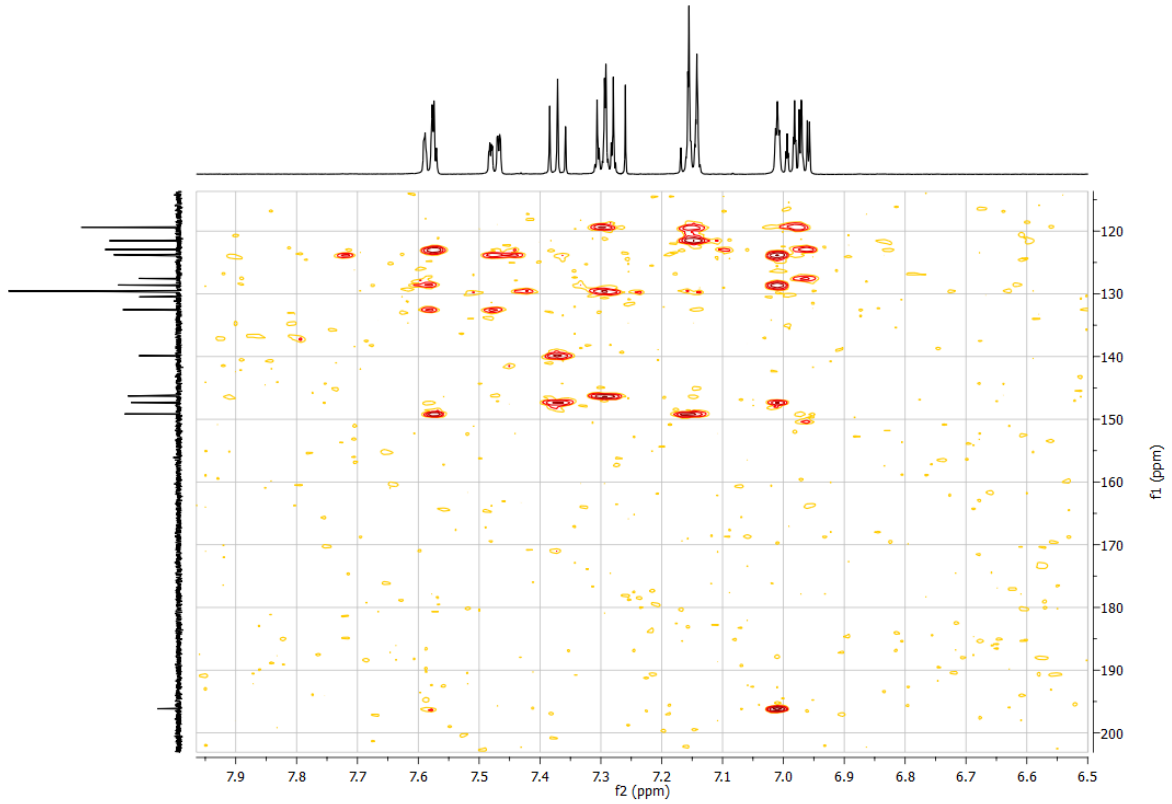

Figure S7. HMBC NMR spectrum of **1a** ($CDCl_3$, 300K, 600, 151 MHz).

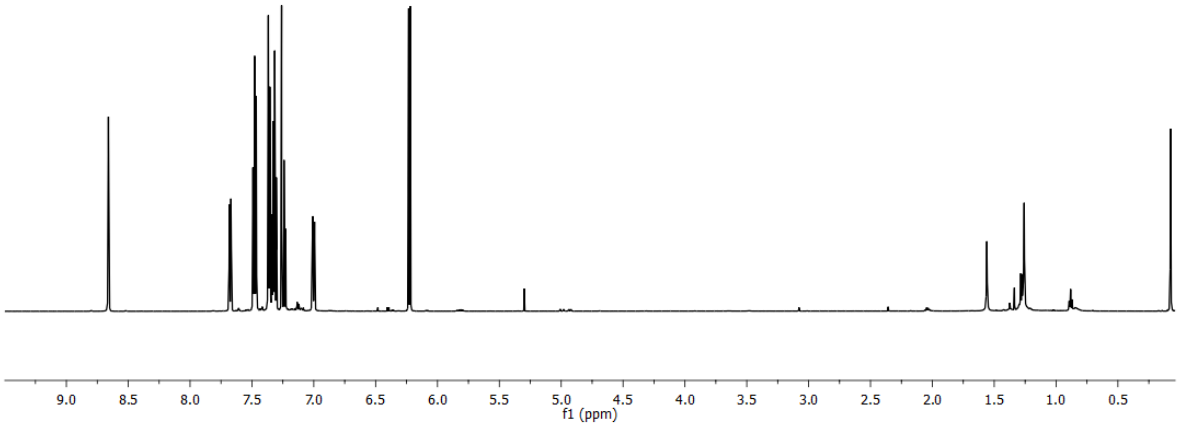

Figure S8. ^1H NMR spectrum of **1b** ($CDCl_3$, 300K, 600 MHz).

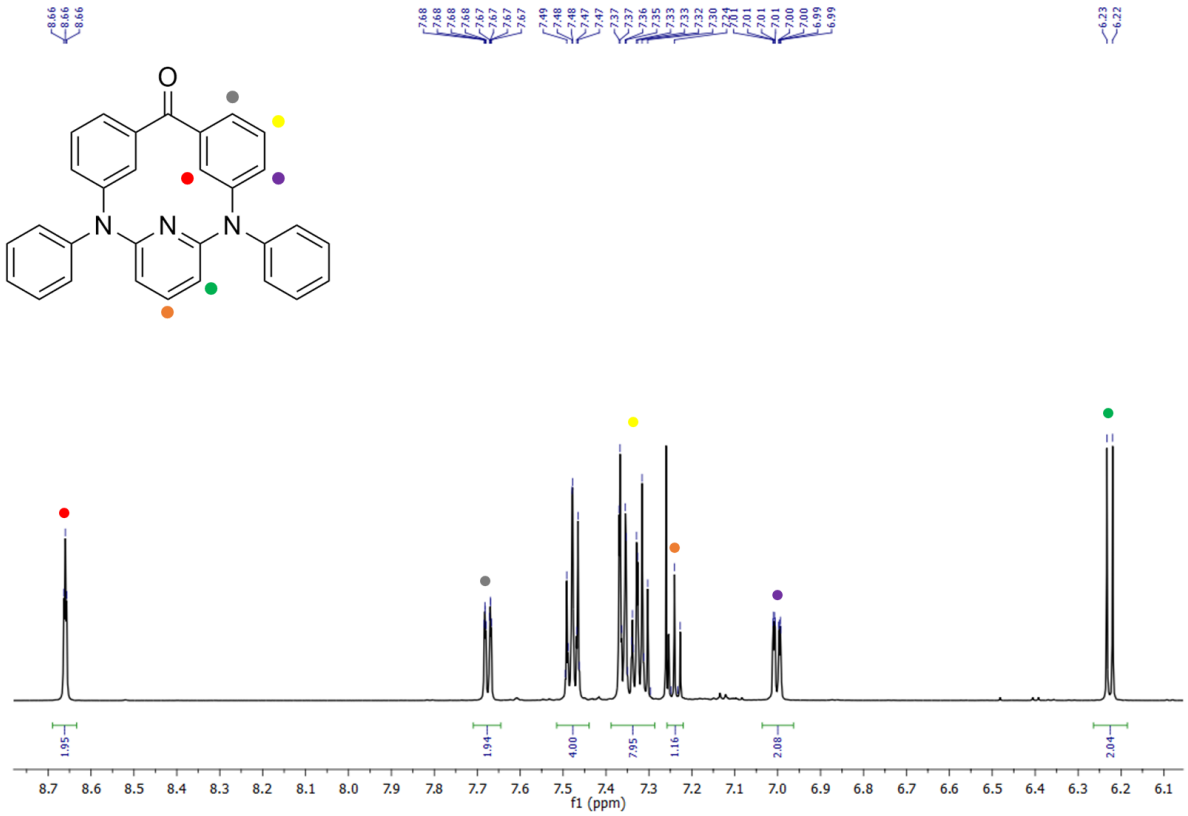

Figure S9. ^{1}H NMR spectrum (zoom, aromatic region) of **1b** ($CDCl_3$, 300K, 600 MHz).

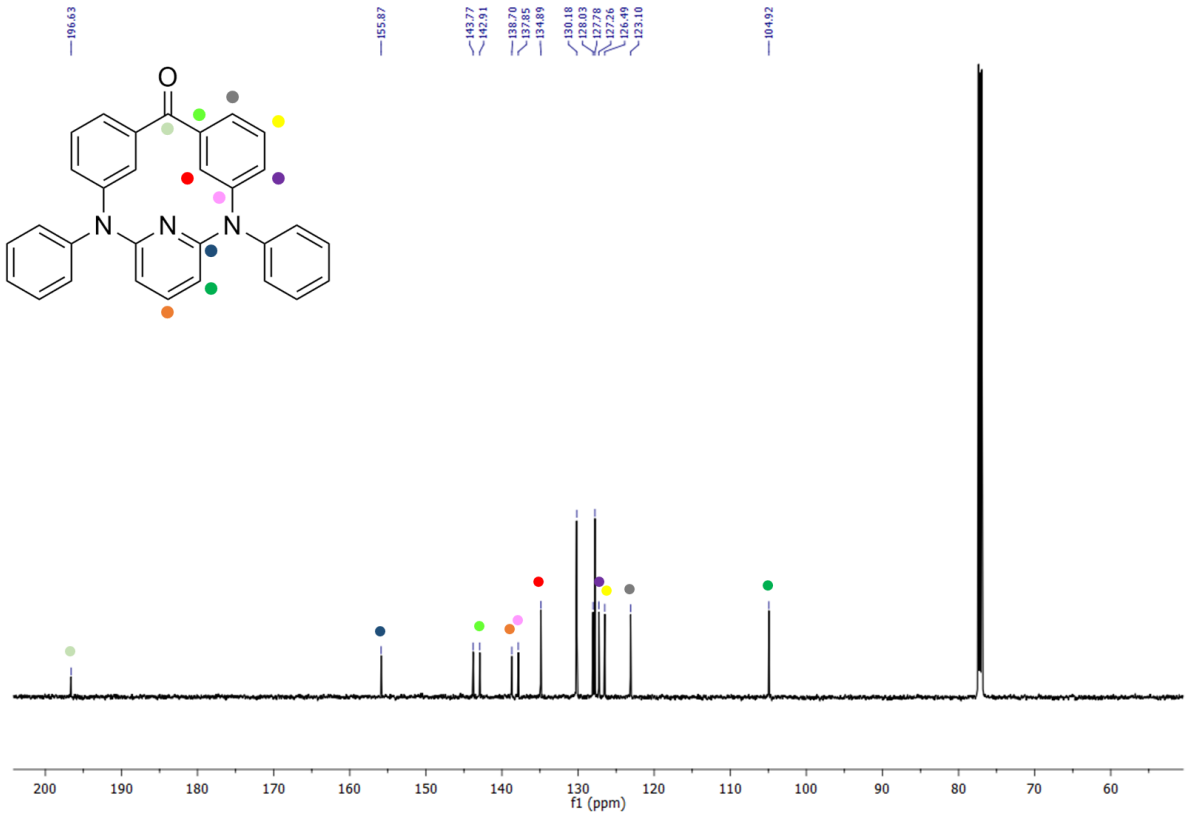

Figure S10. ^{13}C NMR spectrum of **1b** ($CDCl_3$, 300K, 151 MHz).

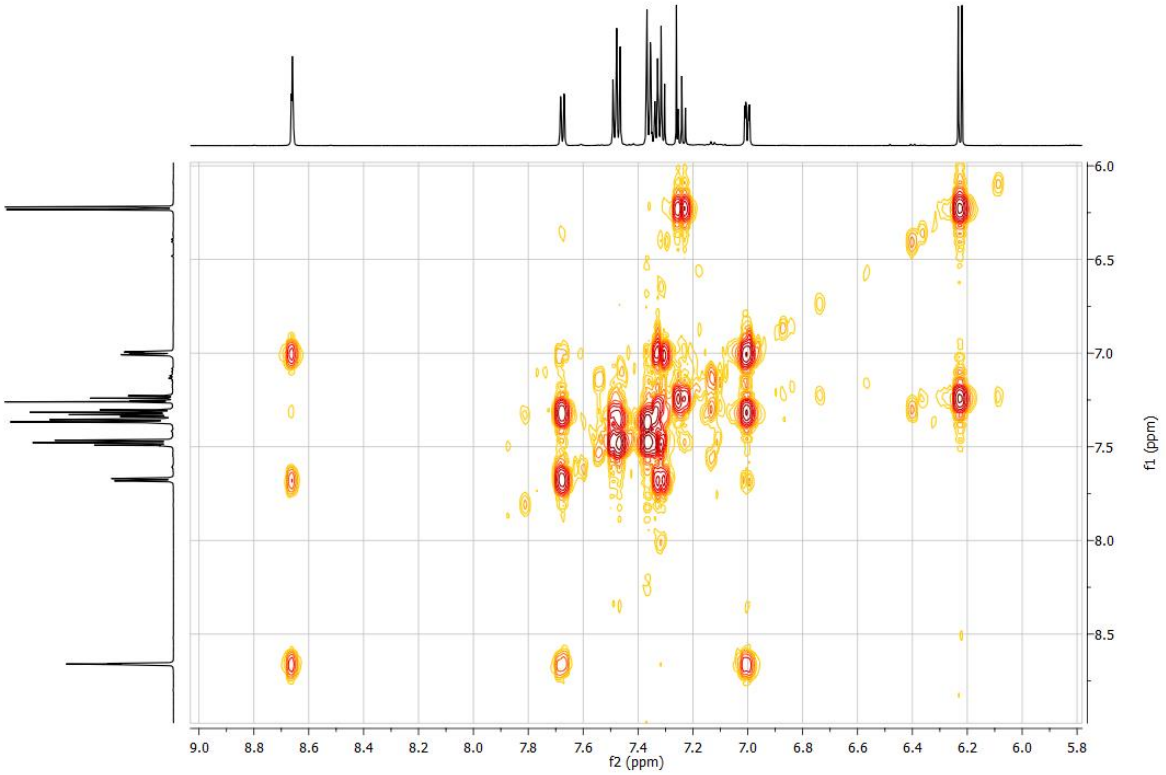

Figure S11. COSY NMR spectrum of **1b** ($CDCl_3$, 300K, 600 MHz).

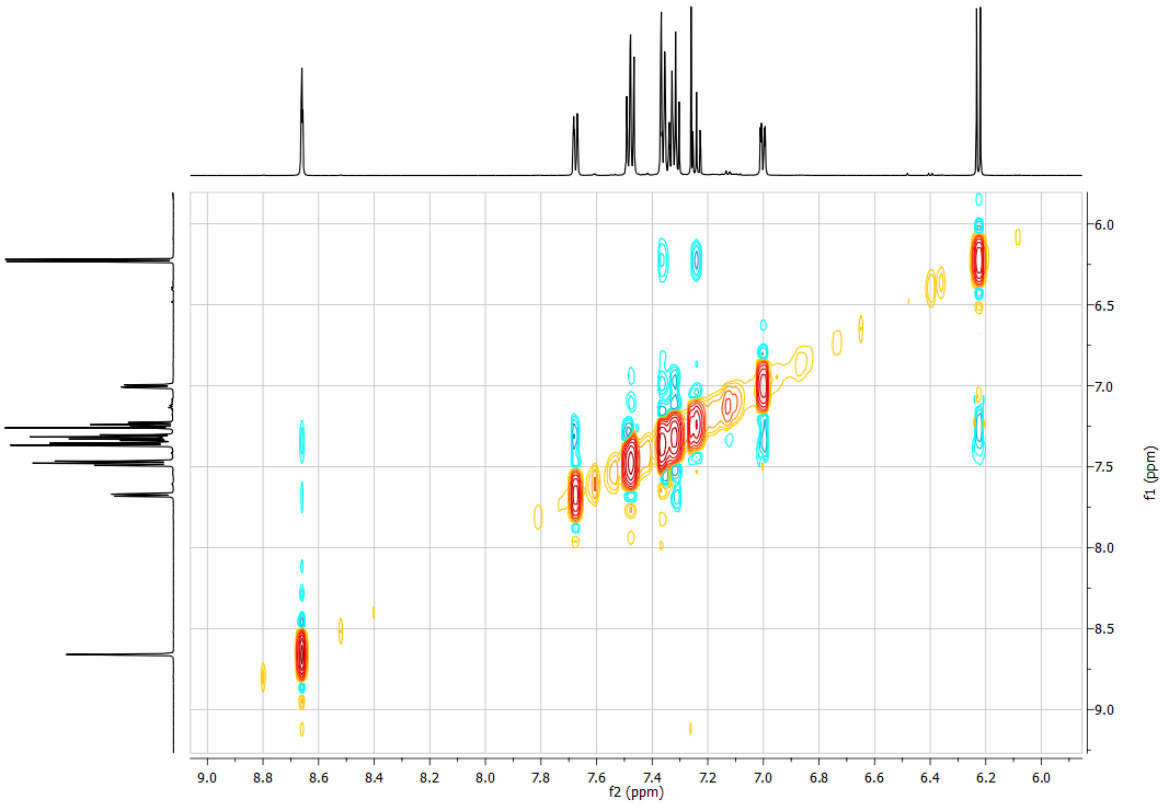

Figure S12. NOESY NMR spectrum of **1b** ($CDCl_3$, 300K, 600 MHz).

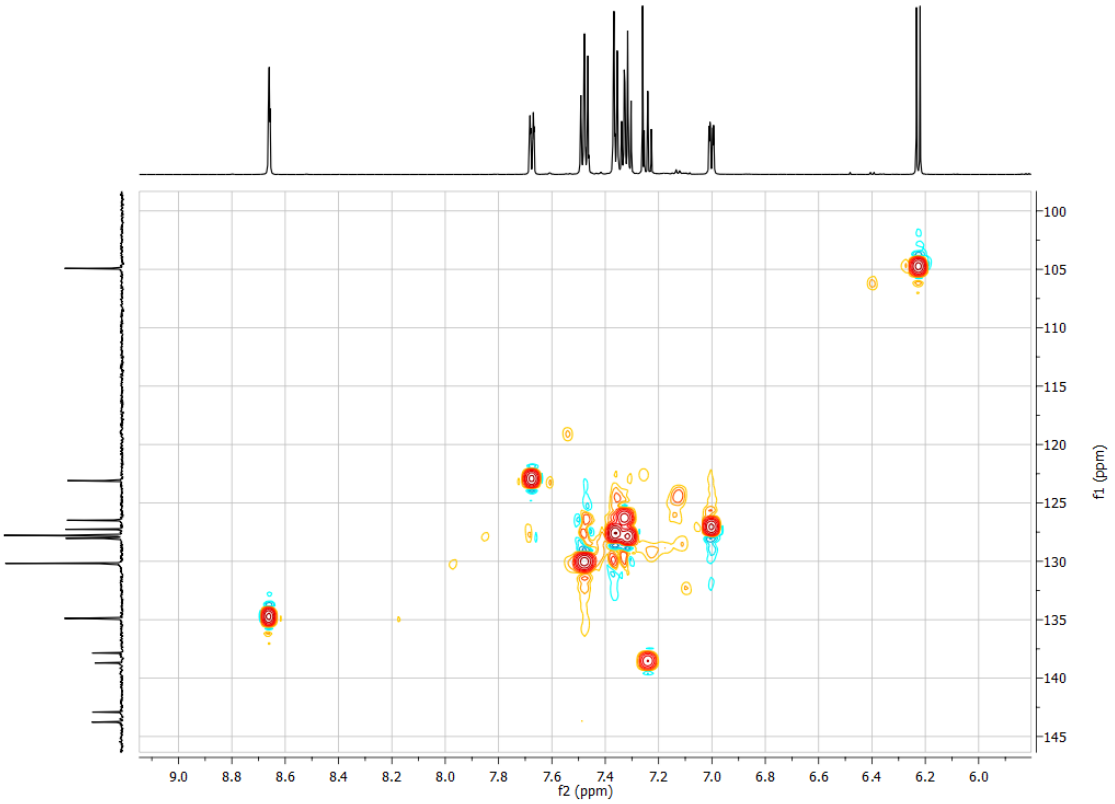

Figure S13. HSQC NMR spectrum of **1b** ($CDCl_3$, 300K, 600, 151 MHz).

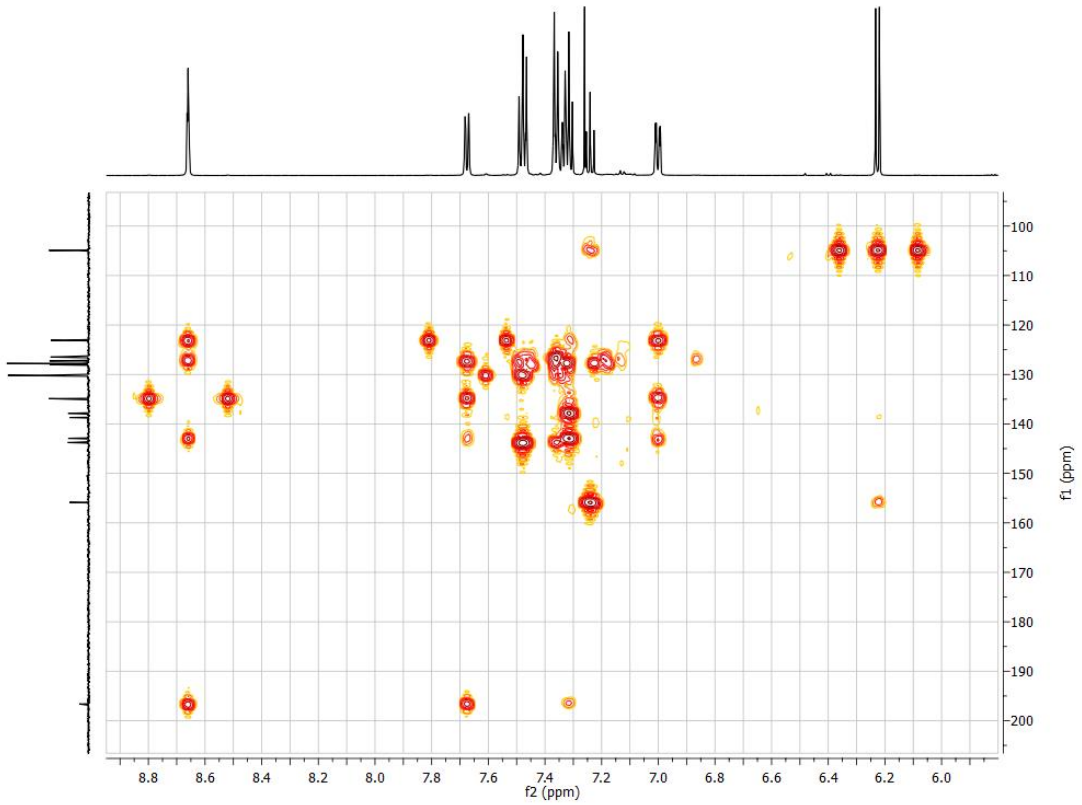

Figure S14. HMBC NMR spectrum of **1b** ($CDCl_3$, 300K, 600, 151 MHz).

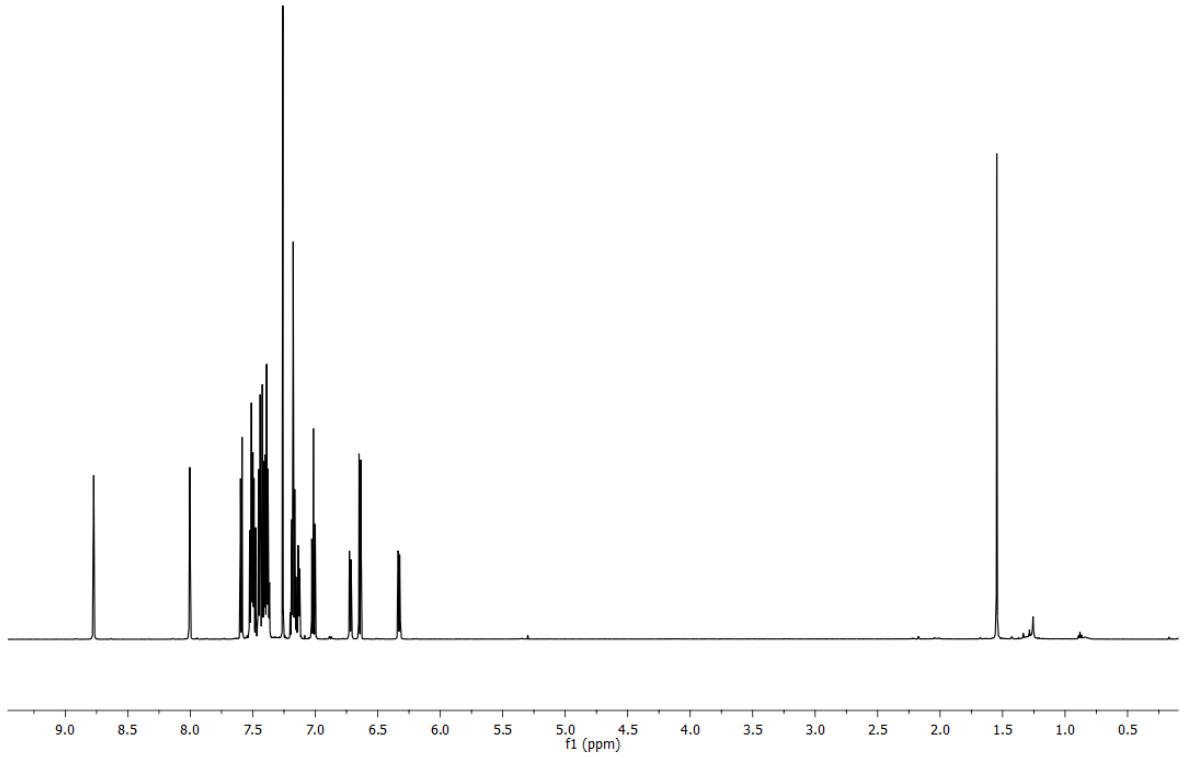

Figure S15. ^{1}H NMR spectrum of **1c** ($CDCl_3$, 300K, 600 MHz).

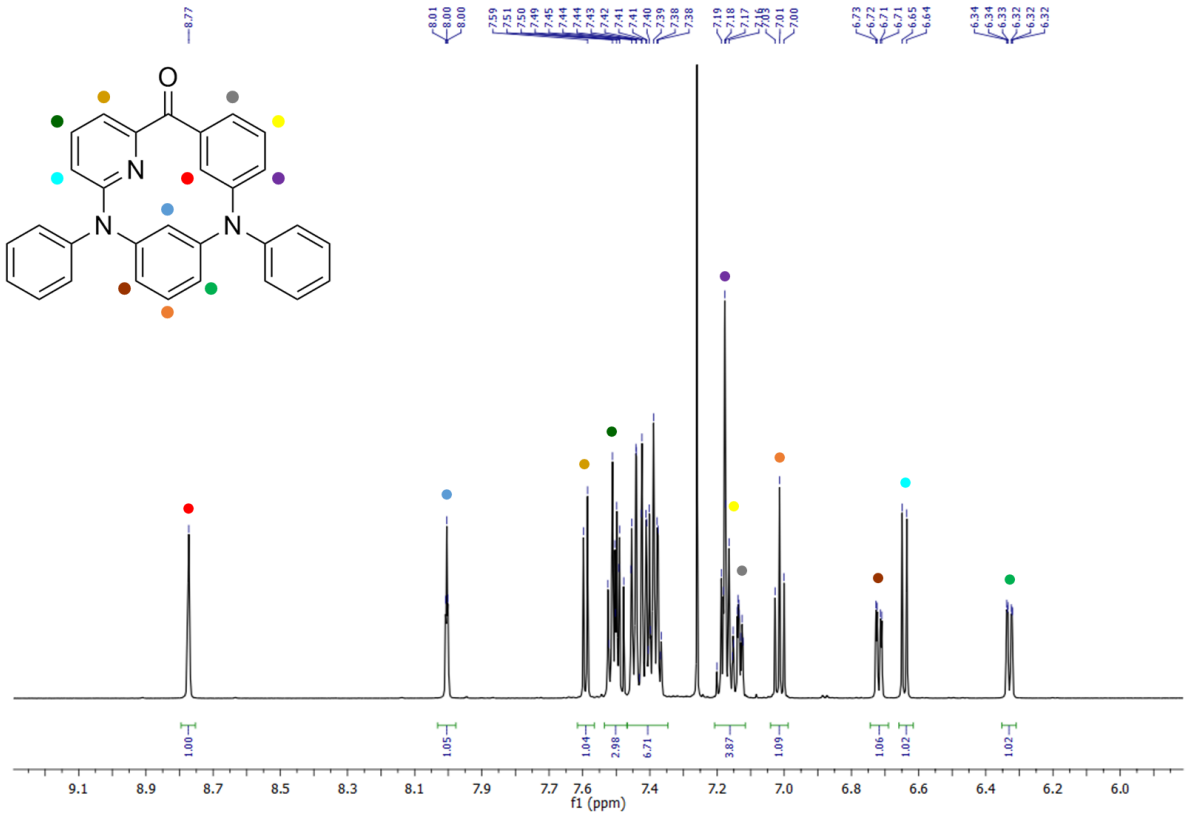

Figure S16. ^{1}H NMR spectrum (zoom, aromatic region) of **1c** ($CDCl_3$, 300K, 600 MHz).

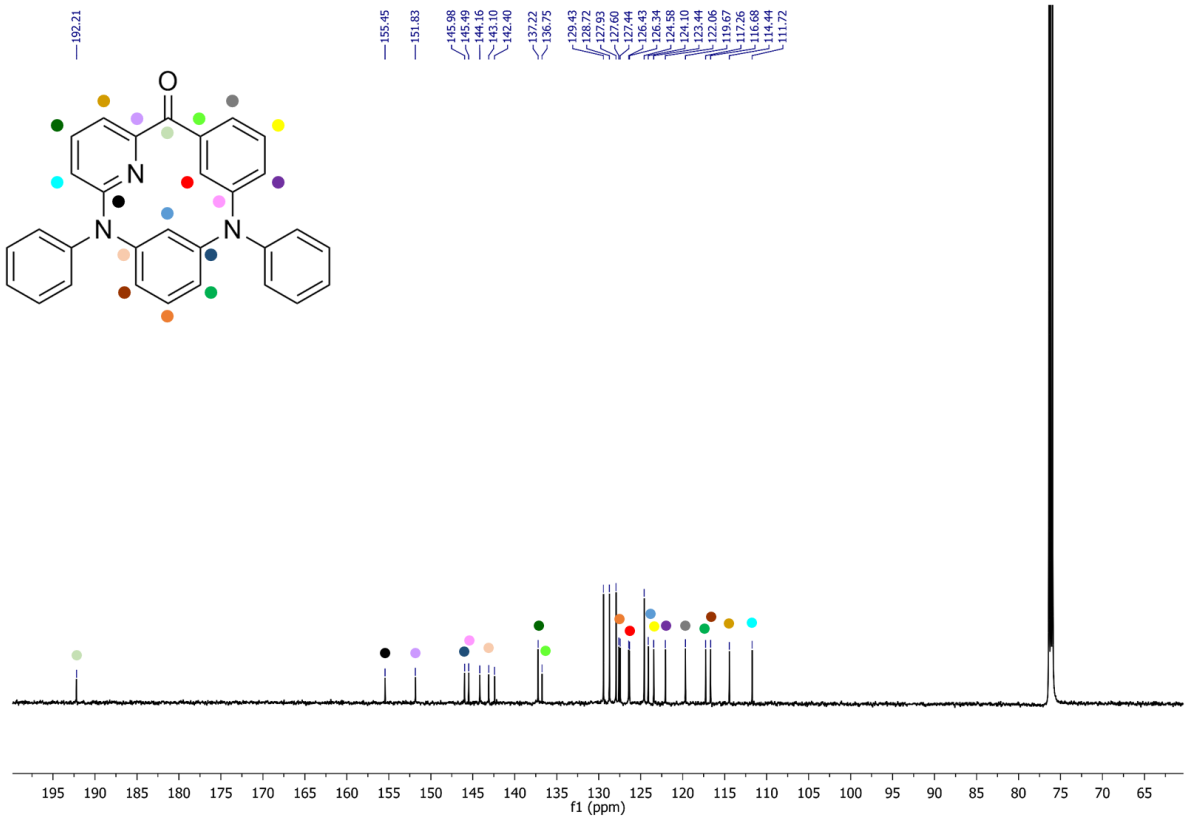

Figure S17. ^{13}C NMR spectrum of **1c** ($CDCl_3$, 300K, 151 MHz).

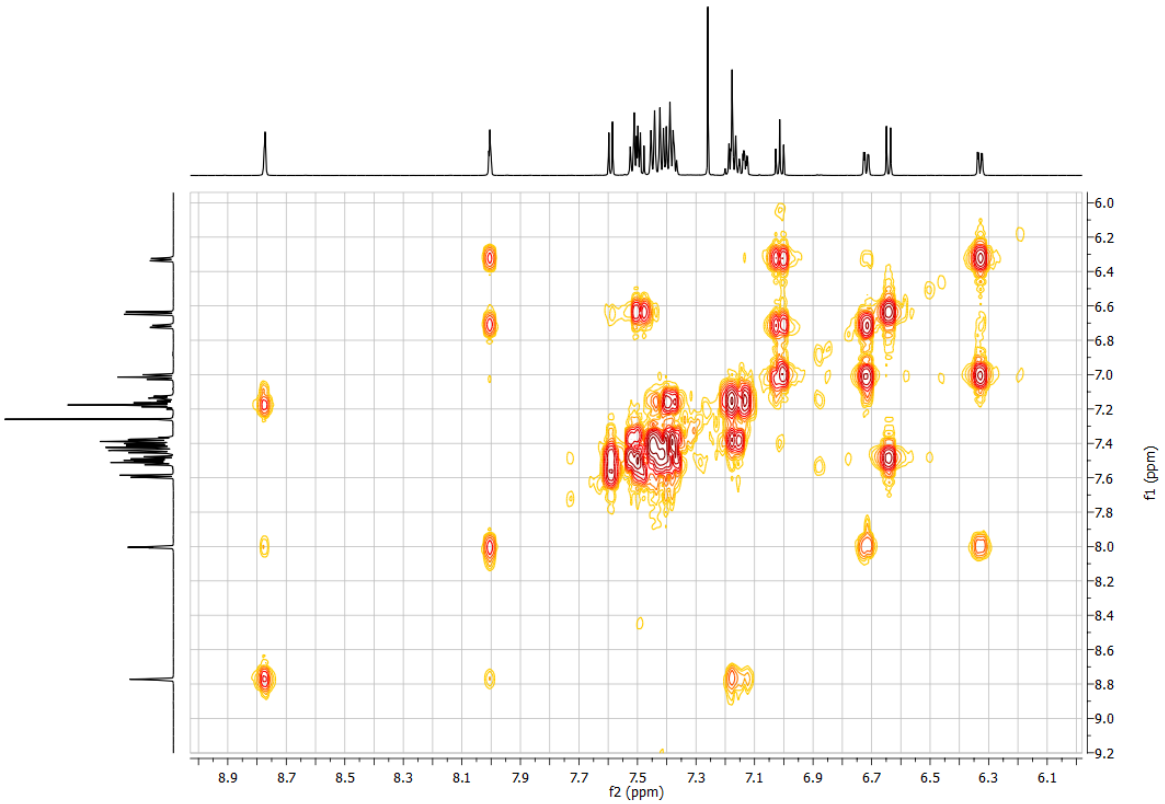

Figure S18. COSY NMR spectrum of **1c** ($CDCl_3$, 300K, 600 MHz).

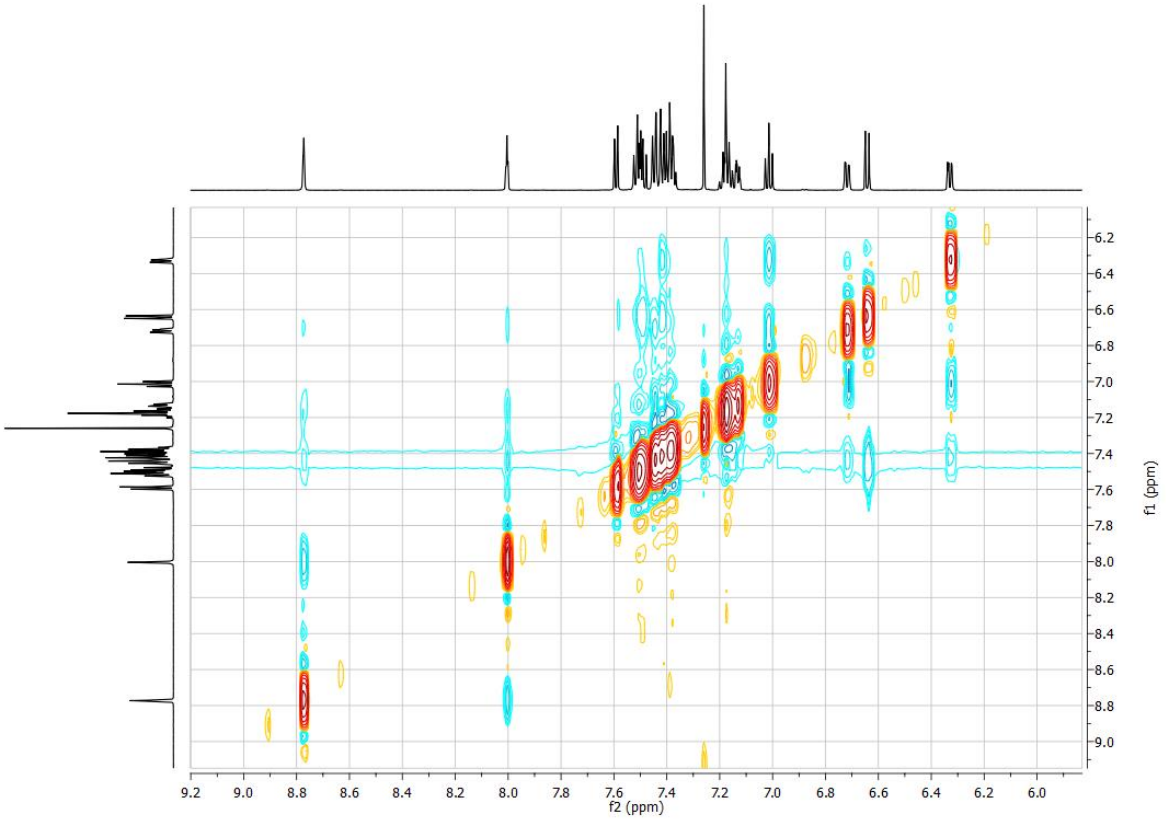

Figure S19. NOESY NMR spectrum of **1c** ($CDCl_3$, 300K, 600 MHz).

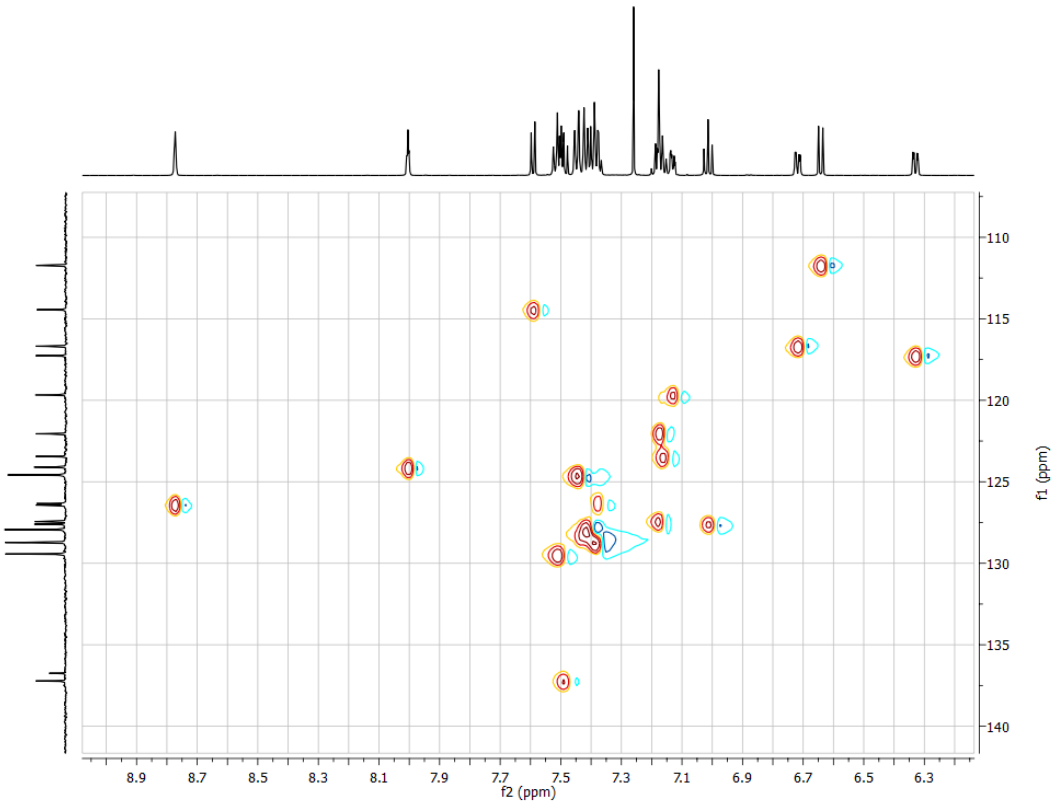

Figure S20. HSQC NMR spectrum of **1c** ($CDCl_3$, 300K, 600, 151 MHz).

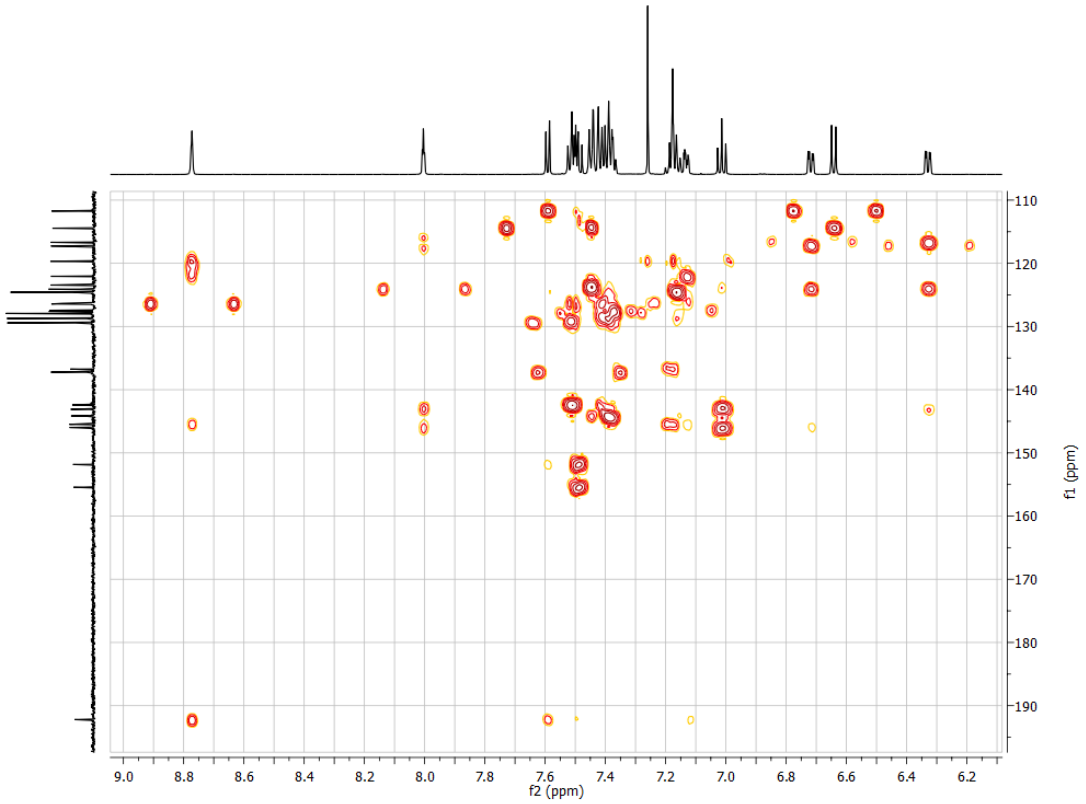

Figure S21. HMBC NMR spectrum of **1c** ($CDCl_3$, 300K, 600, 151 MHz).

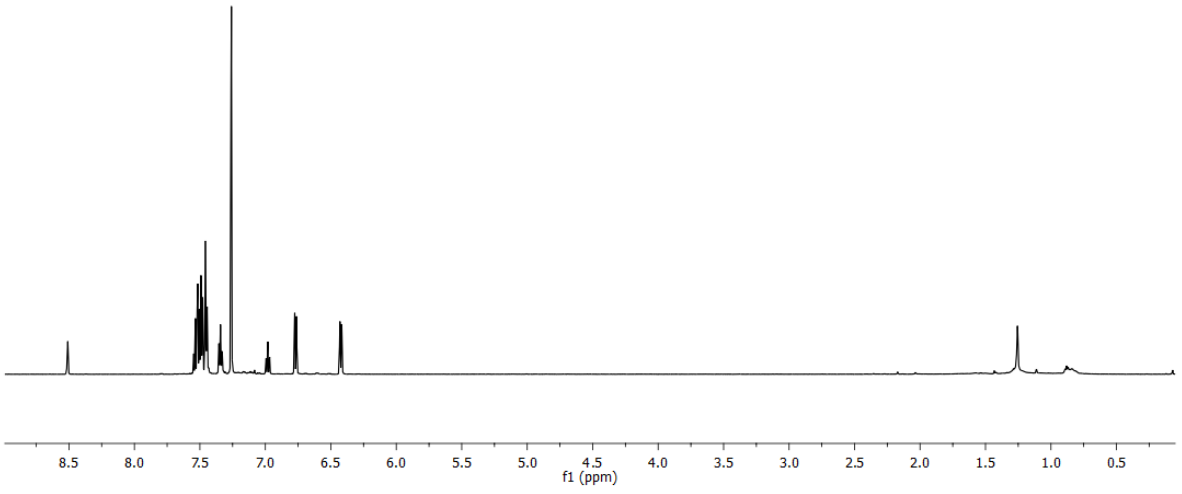

Figure S22. ^1H NMR spectrum of **1d** ($CDCl_3$, 300K, 600 MHz).

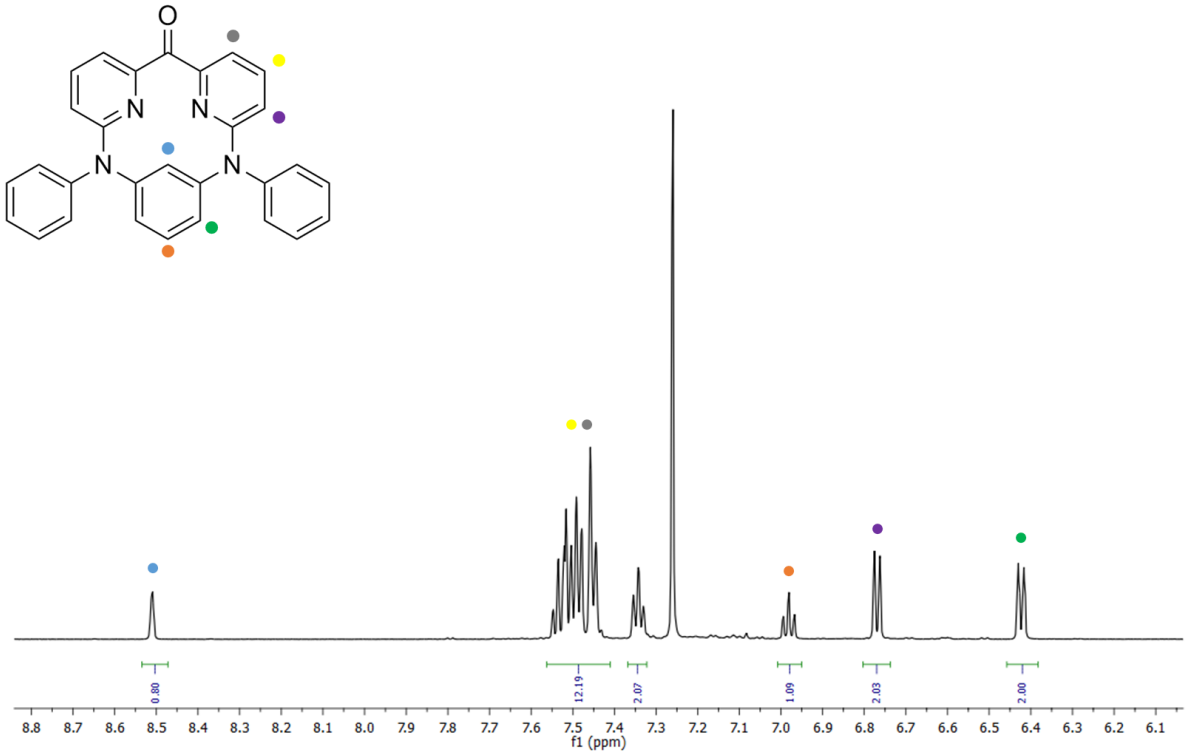

Figure S23. ^{1}H NMR spectrum (zoom, aromatic region) of **1d** ($CDCl_3$, 300K, 600 MHz).

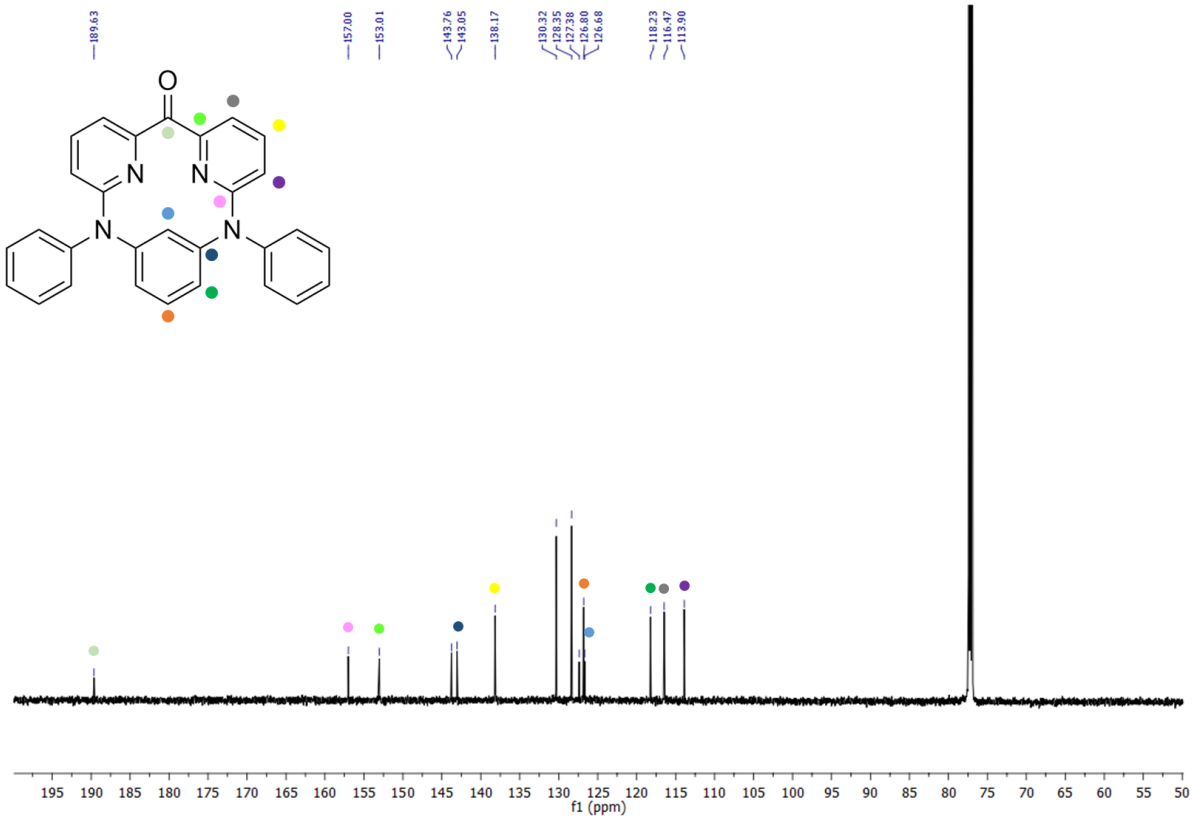

Figure S24. ^{13}C NMR spectrum of **1d** ($CDCl_3$, 300K, 151 MHz).

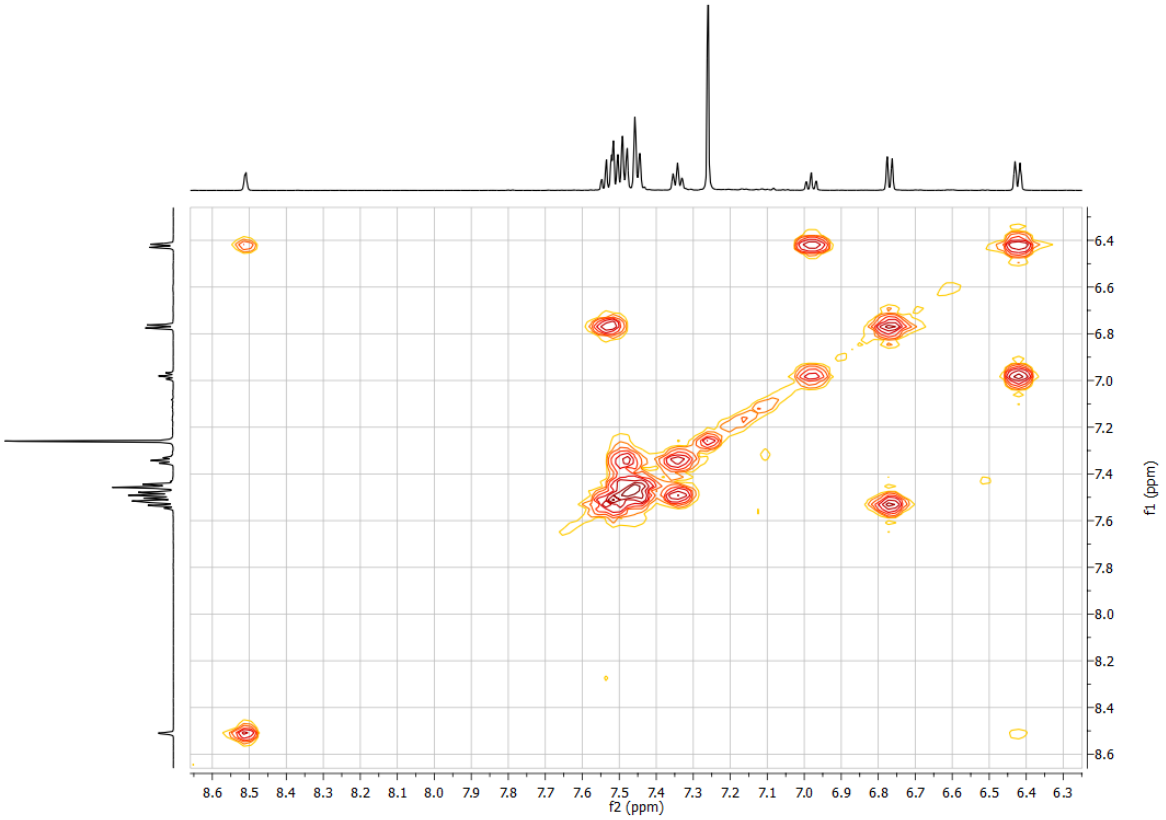

Figure S25. COSY NMR spectrum of **1d** ($CDCl_3$, 300K, 600 MHz).

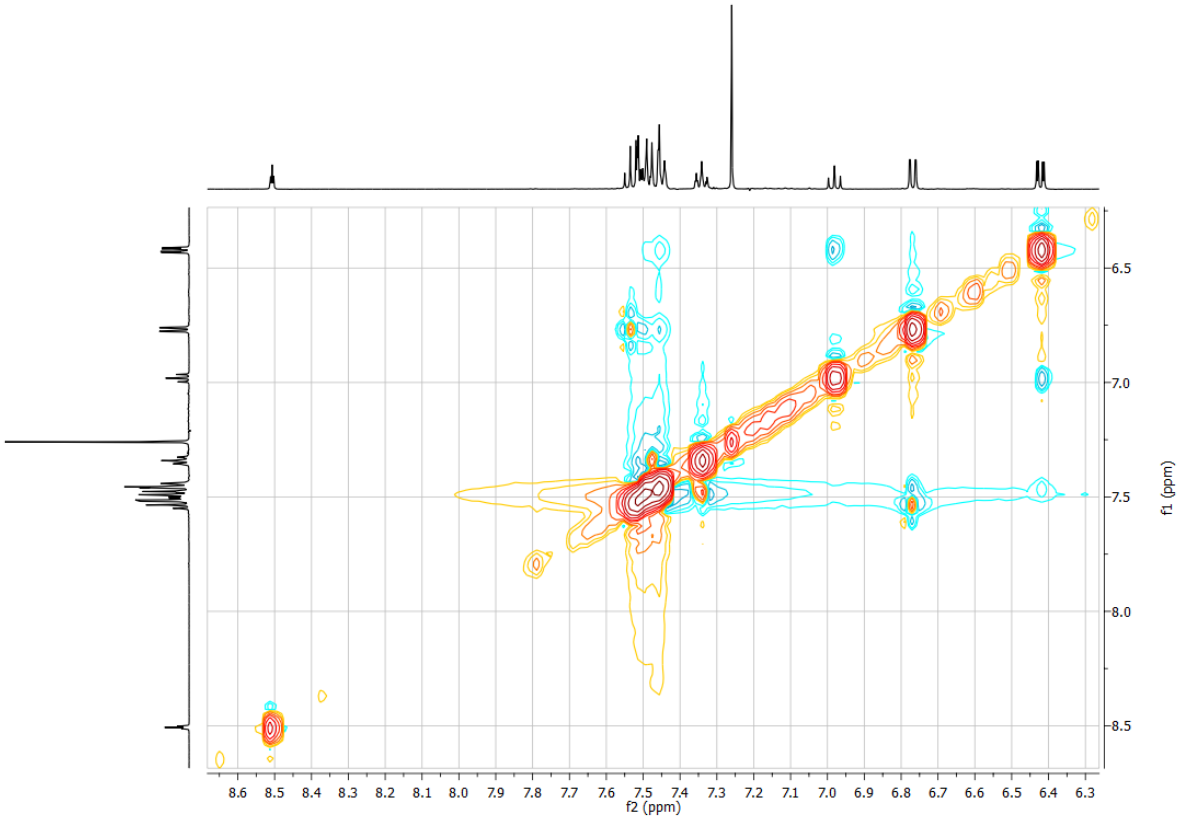

Figure S26. NOESY NMR spectrum of **1d** ($CDCl_3$, 300K, 600 MHz).

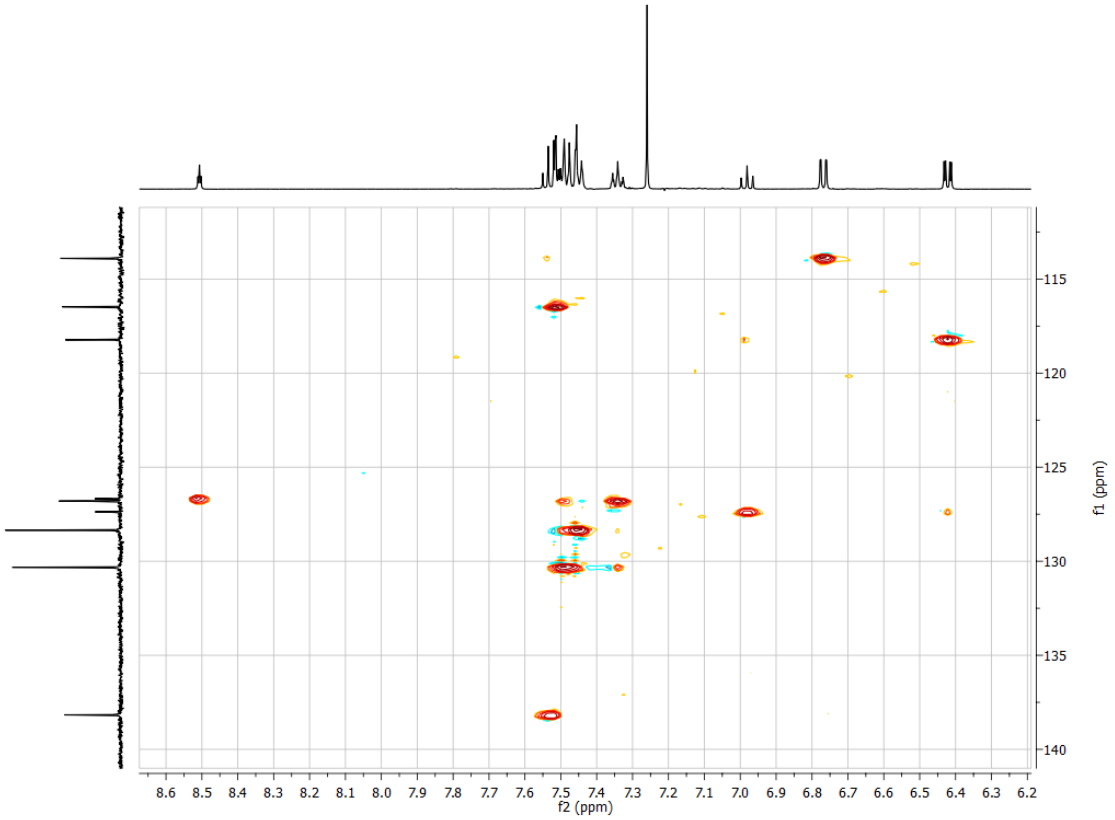

Figure S27. HSQC NMR spectrum of **1d** ($CDCl_3$, 300K, 600, 151 MHz).

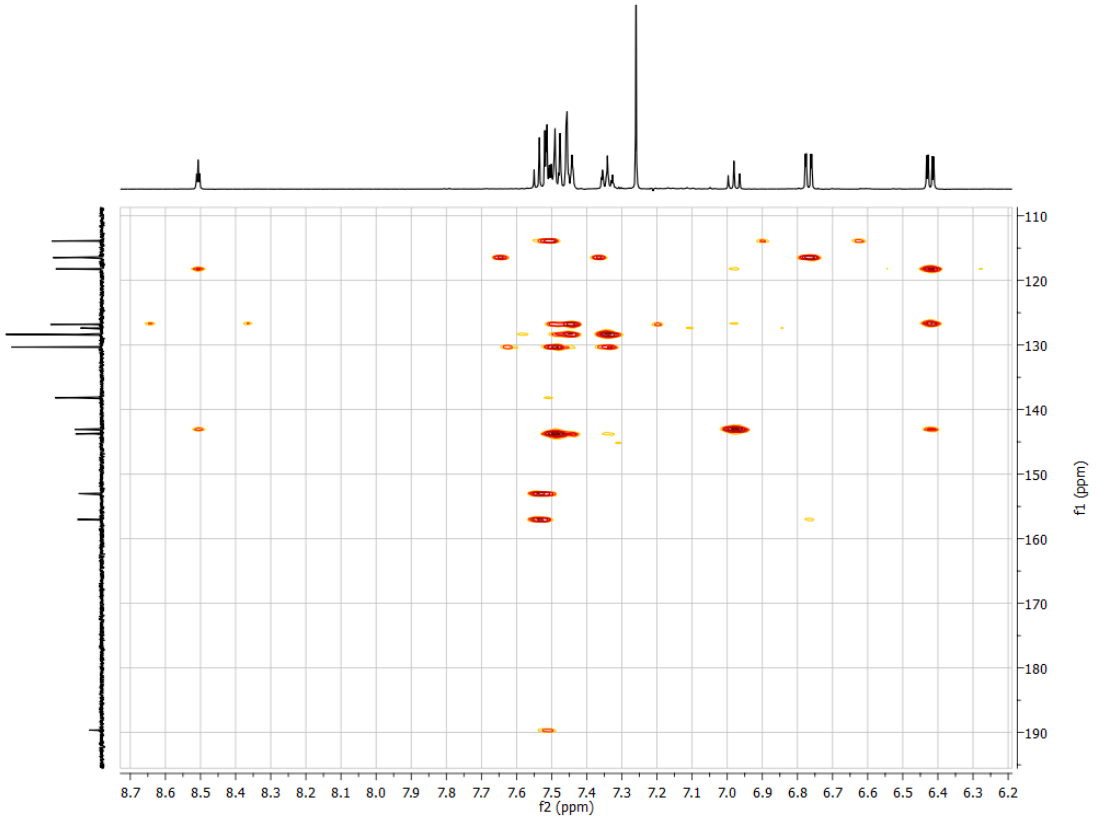

Figure S28. HMBC NMR spectrum of **1d** ($CDCl_3$, 300K, 600, 151 MHz).

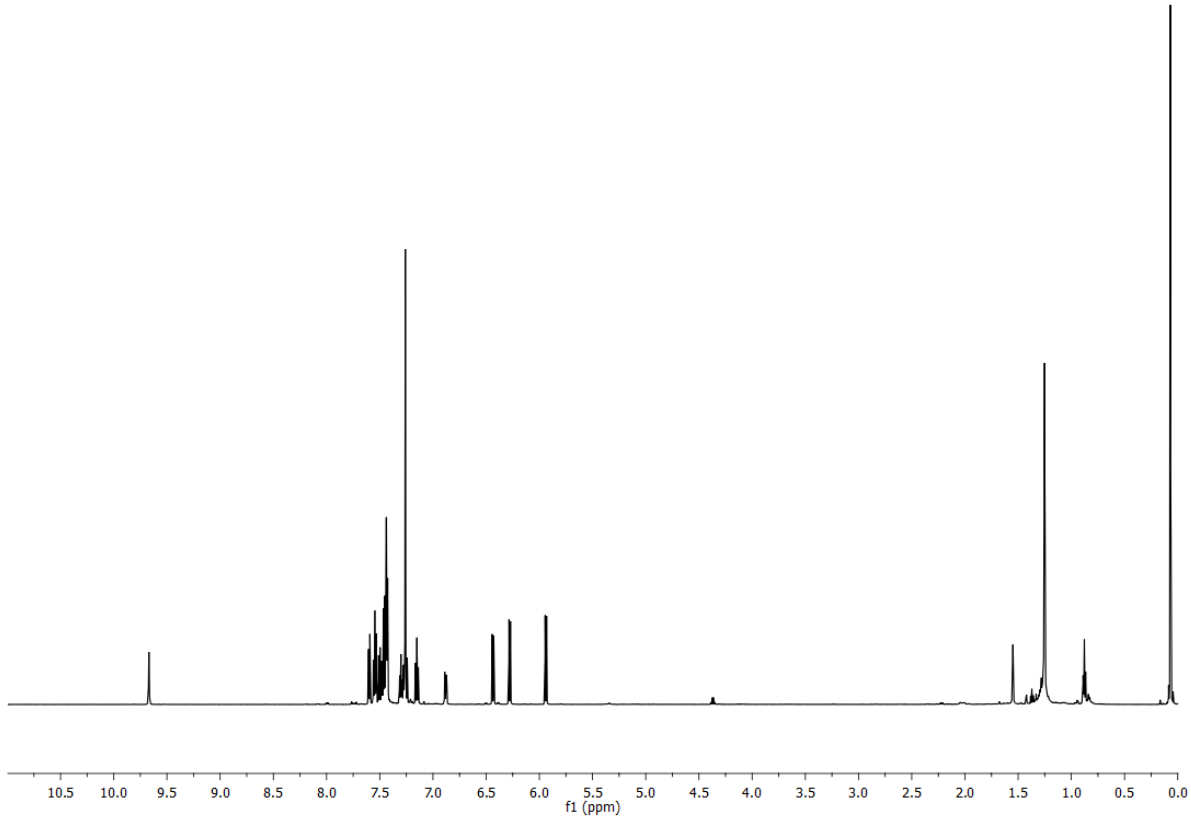

Figure S29. ^{1}H NMR spectrum of **1e** ($CDCl_3$, 300K, 600 MHz).

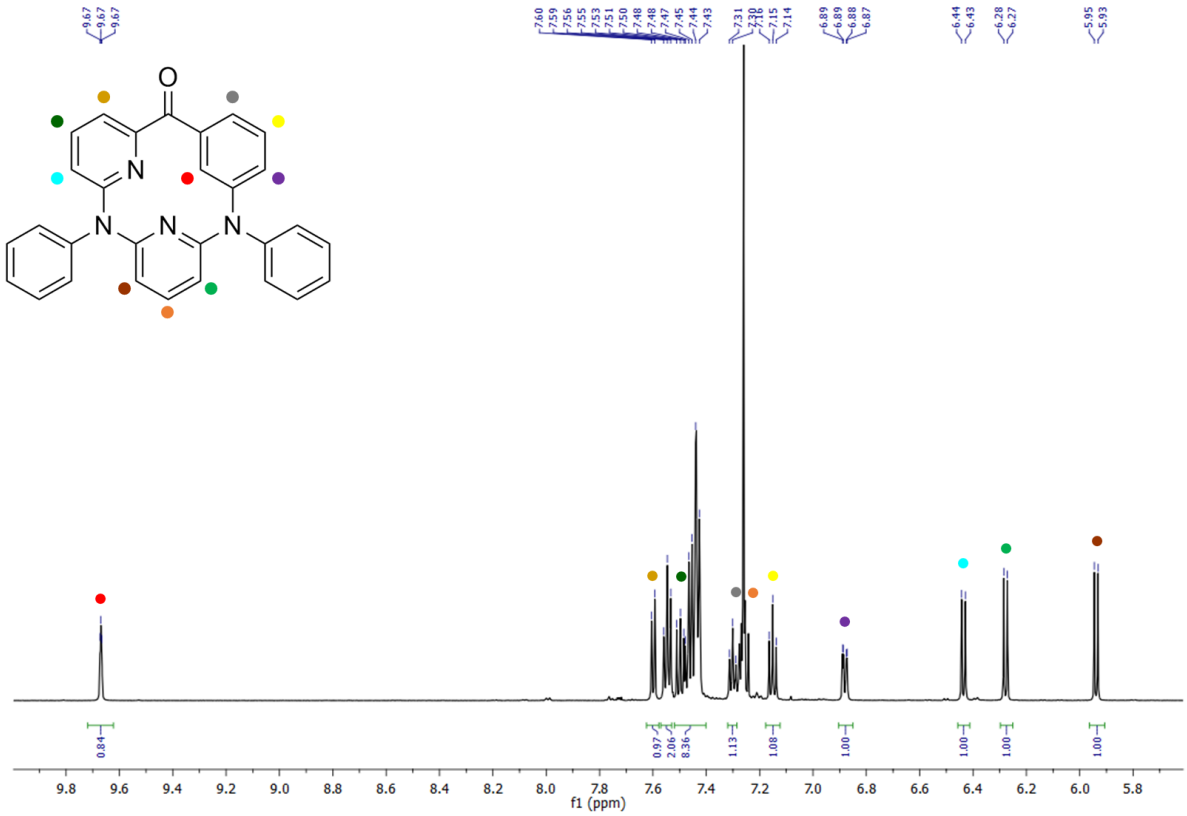

Figure S30. ^{1}H NMR spectrum (zoom, aromatic region) of **1e** ($CDCl_3$, 300K, 600 MHz).

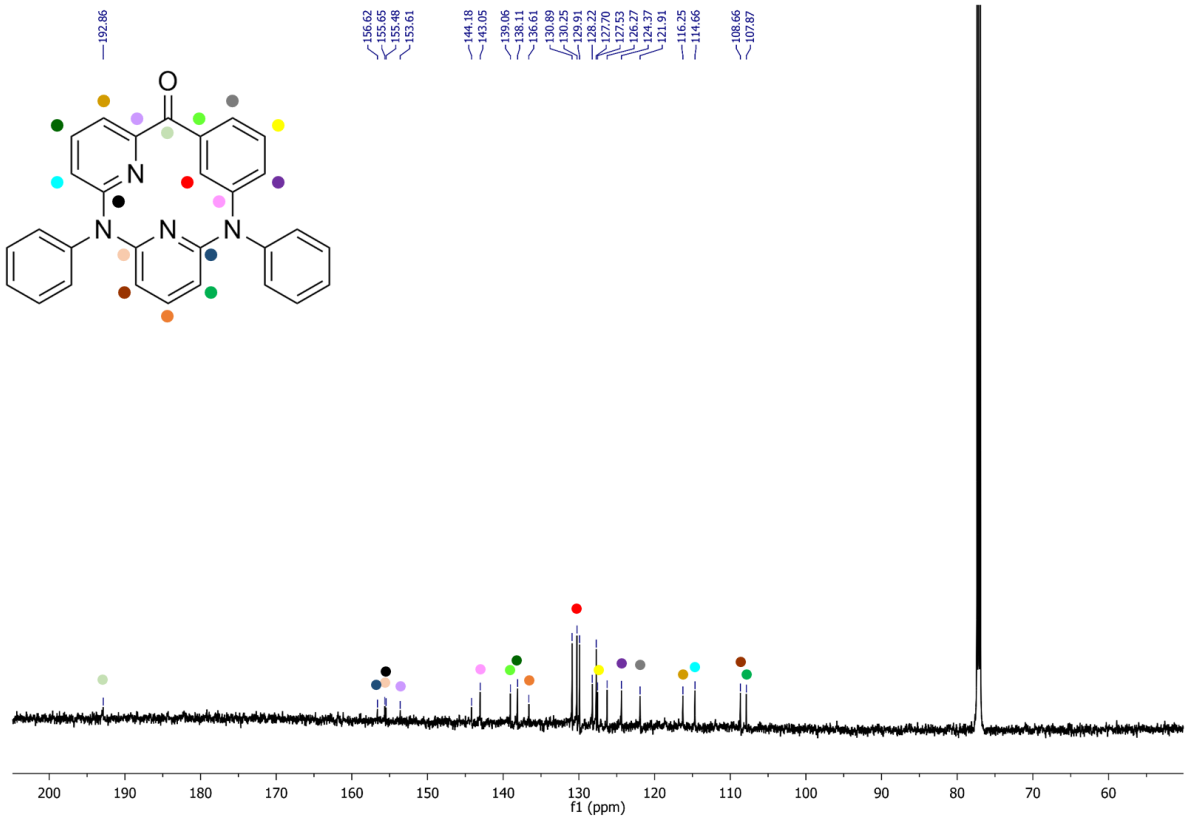

Figure S31. ^{13}C NMR spectrum of **1e** ($CDCl_3$, 300K, 151 MHz).

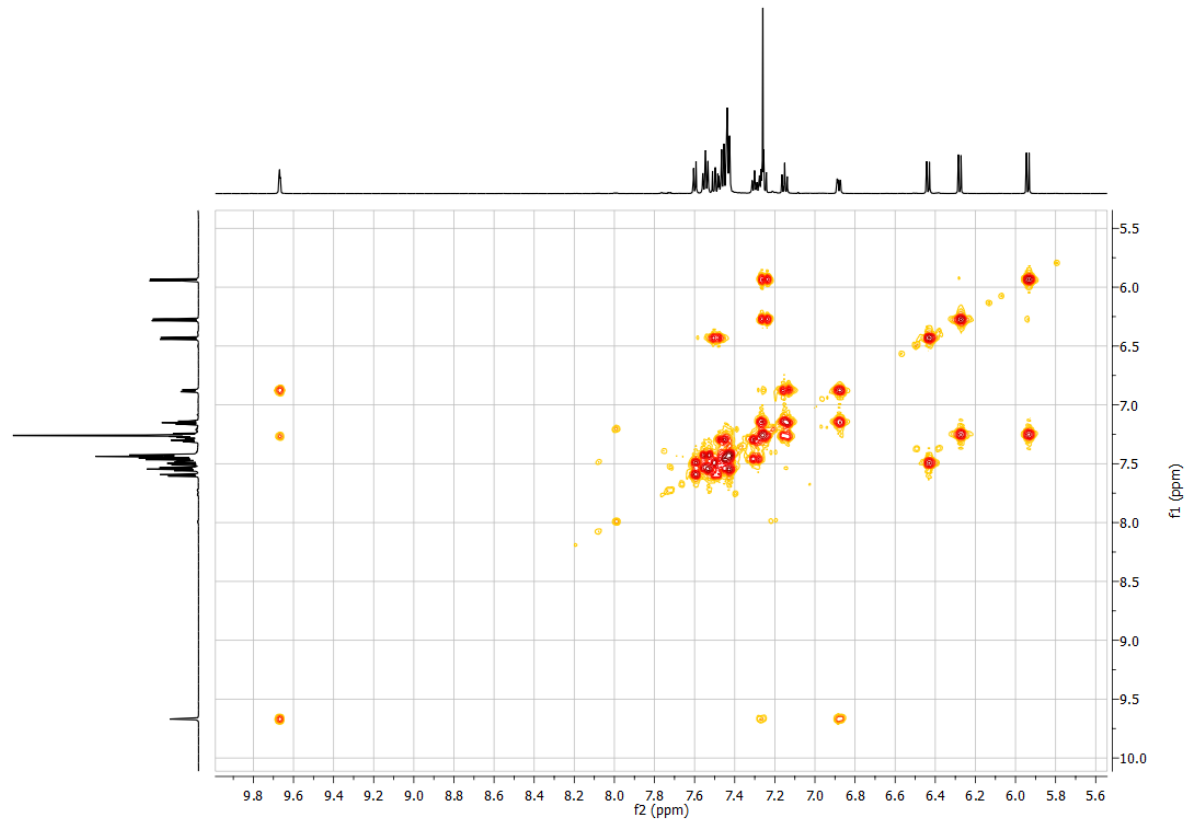

Figure S32. COSY NMR spectrum of **1e** ($CDCl_3$, 300K, 600 MHz).

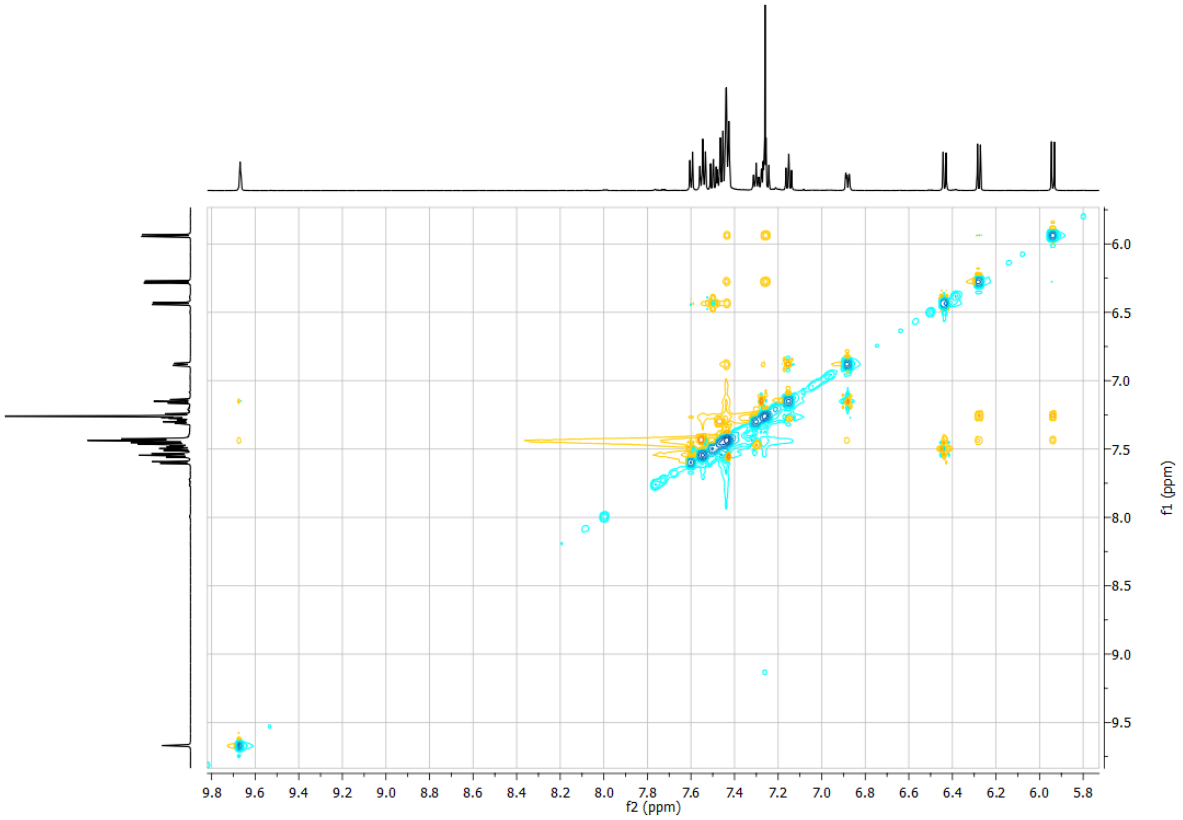

Figure S33. NOESY NMR spectrum of **1e** ($CDCl_3$, 300K, 600 MHz).

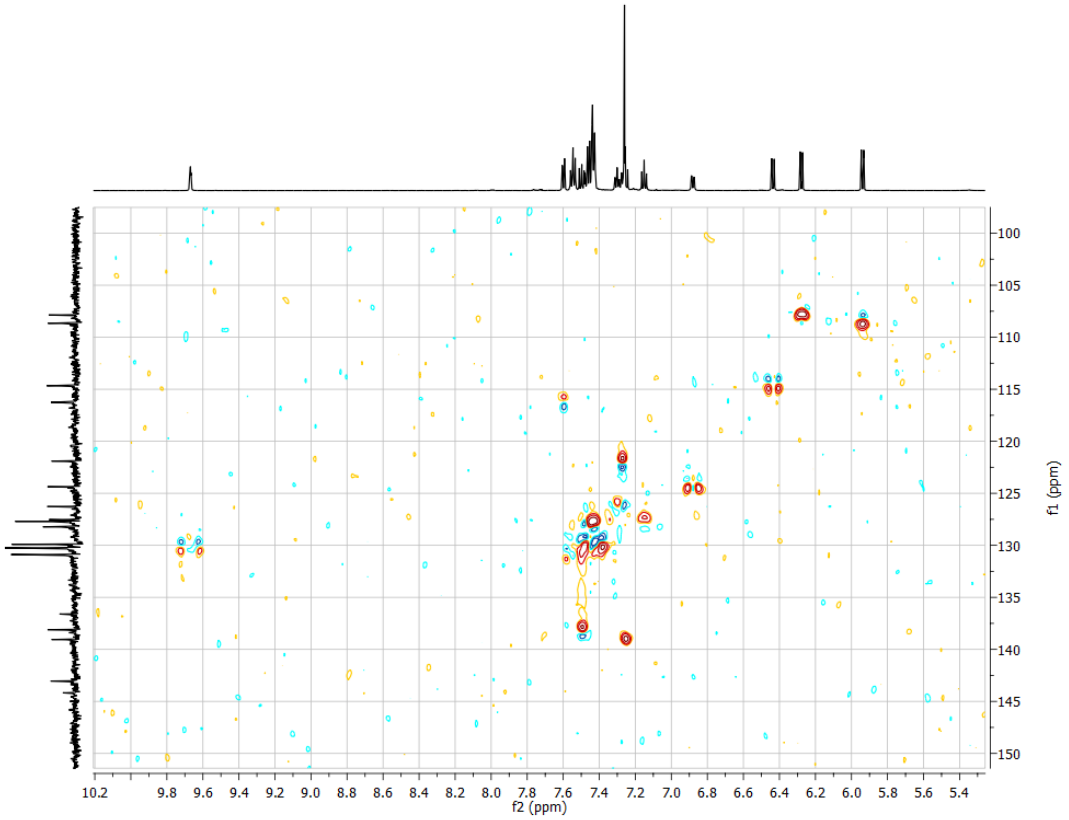

Figure S34. HSQC NMR spectrum of **1e** ($CDCl_3$, 300K, 600, 151 MHz).

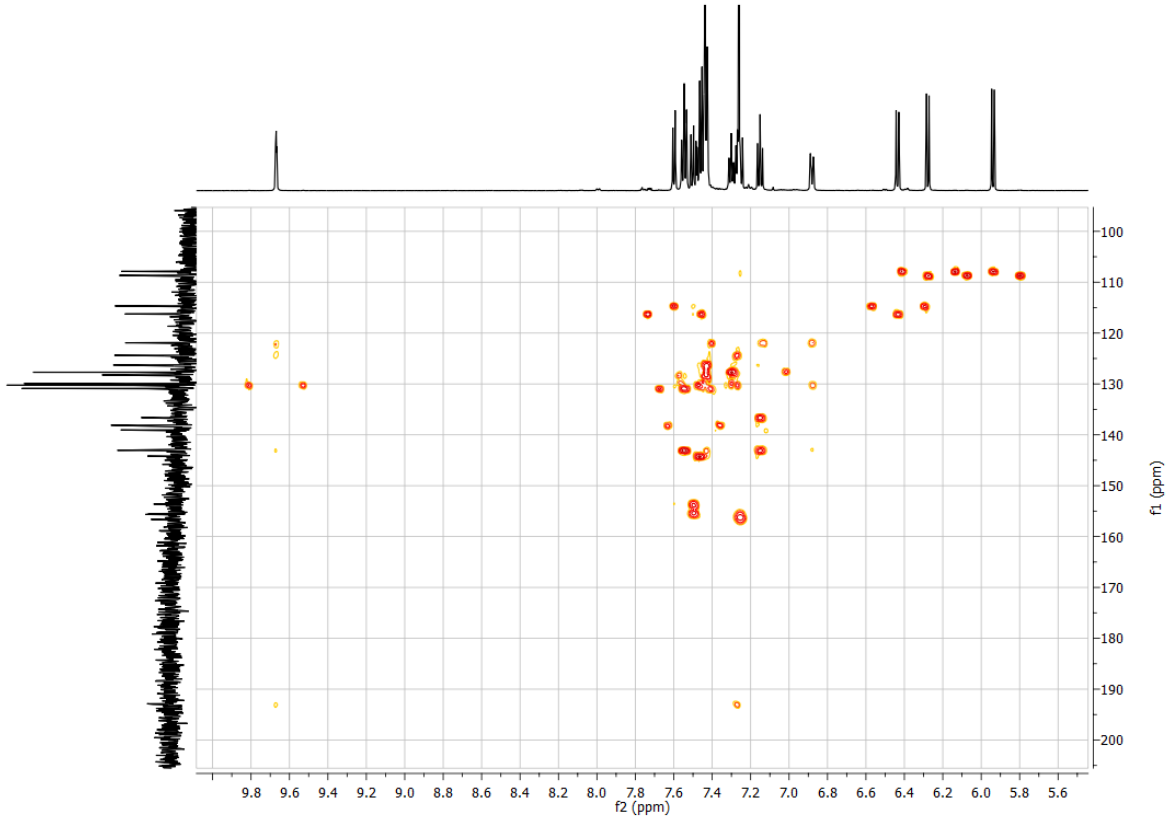

Figure S35. HMBC NMR spectrum of **1e** ($CDCl_3$, 300K, 600, 151 MHz).

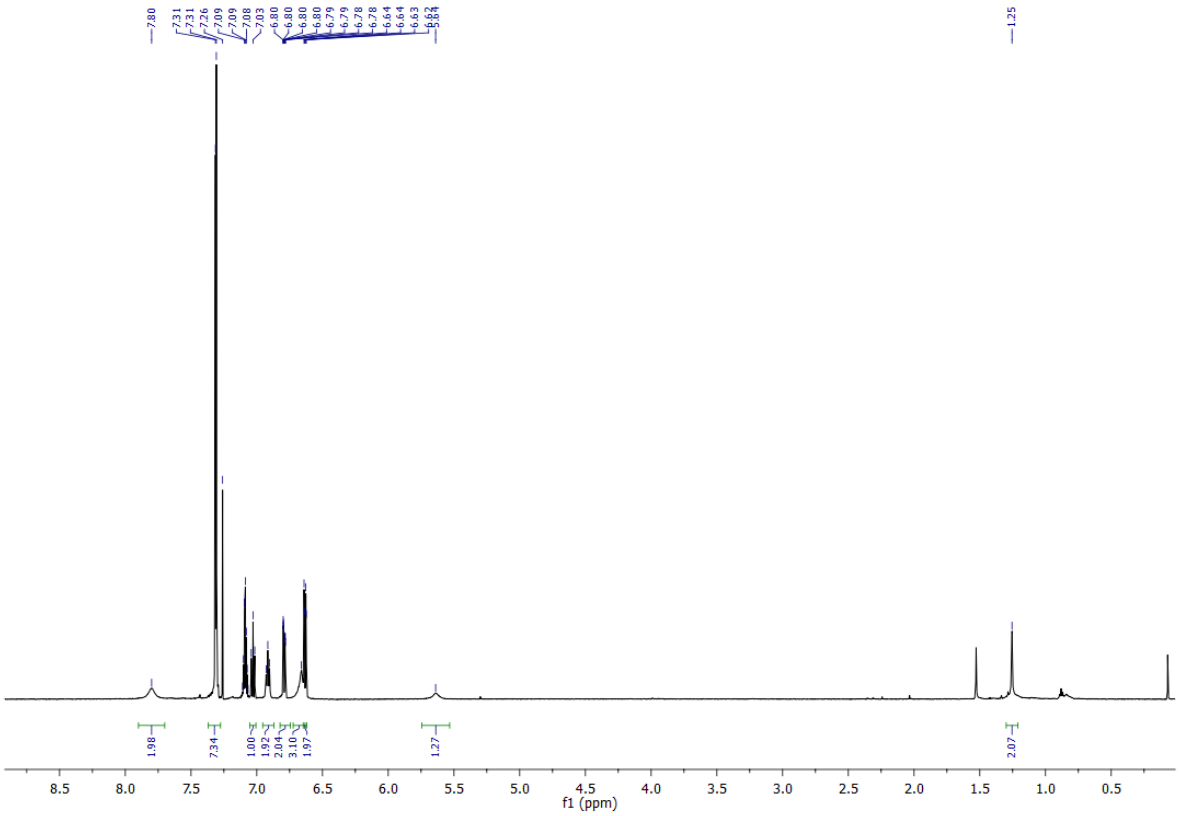

Figure S36. ^1H NMR spectrum of **2a** ($CDCl_3$, 300K, 600 MHz).

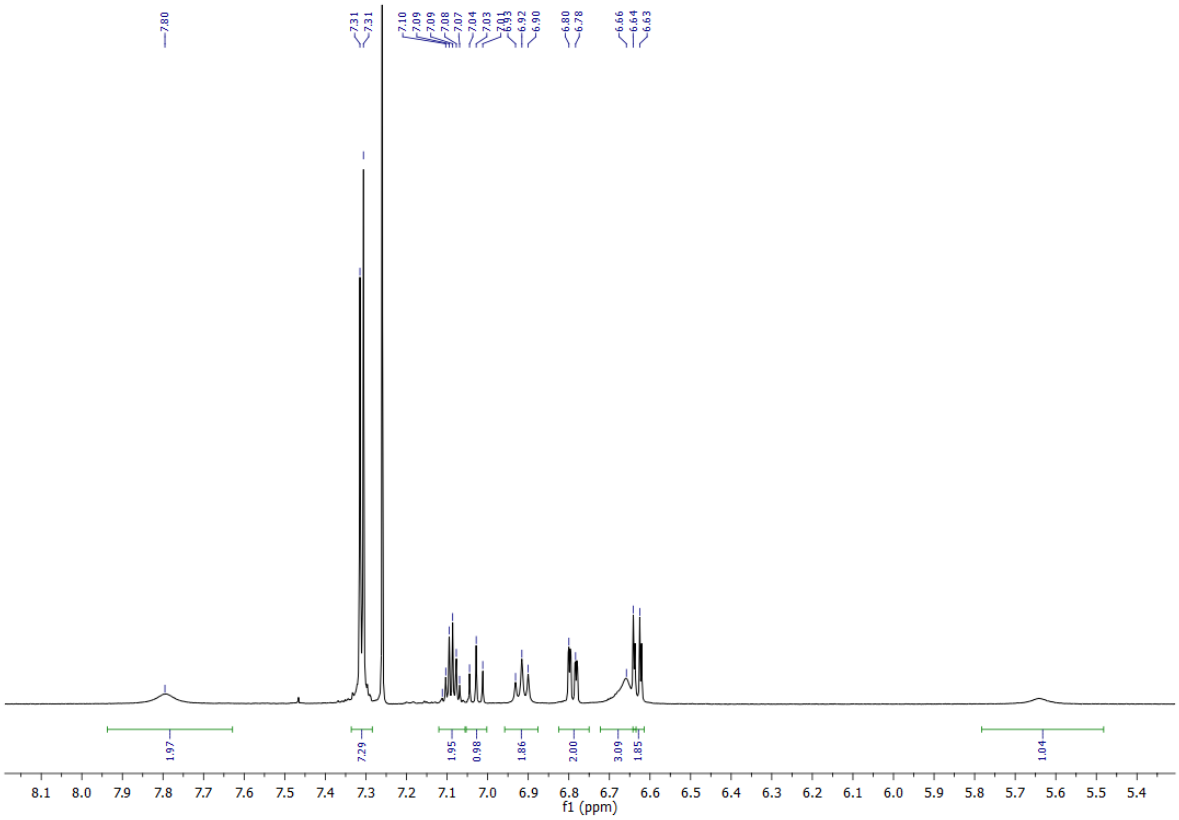

Figure S37. ^{1}H NMR spectrum (zoom, aromatic region) of **2a** ($CDCl_3$, 300K, 600 MHz).

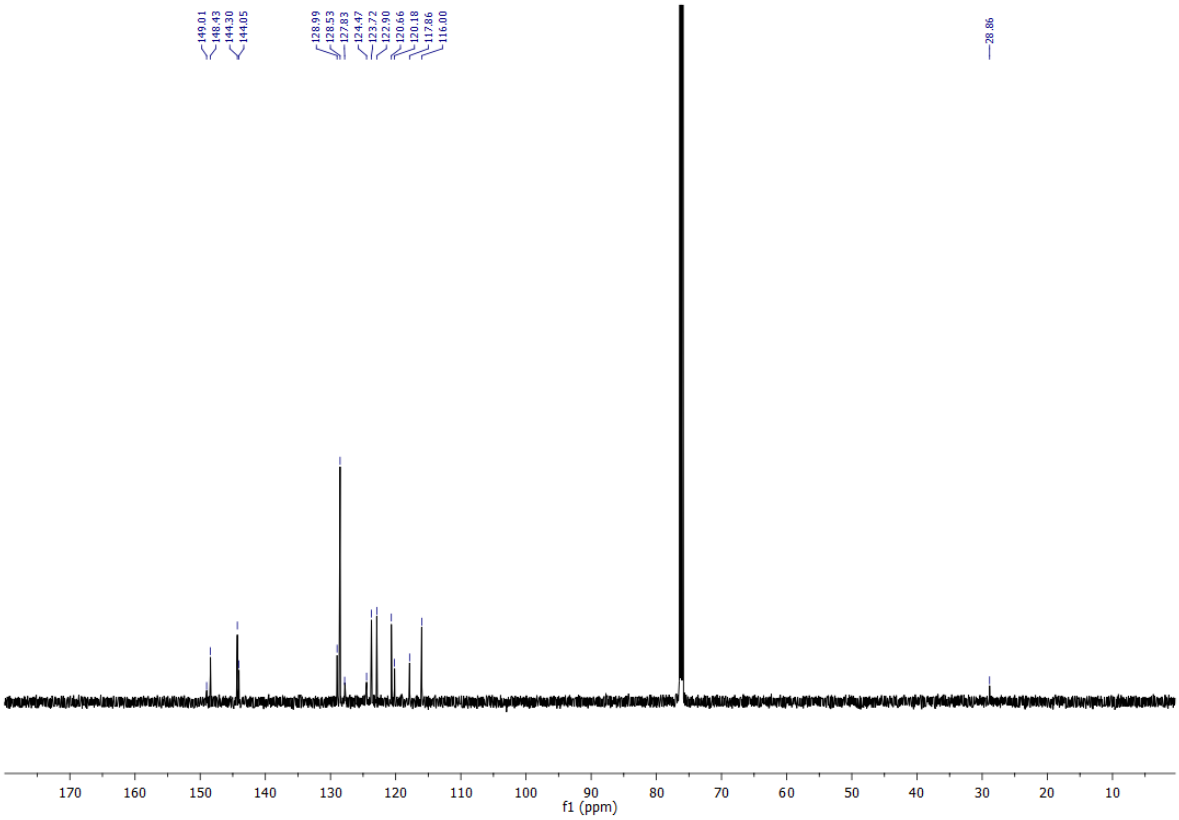

Figure S38. ^{13}C NMR spectrum of **2a** ($CDCl_3$, 300K, 151 MHz).

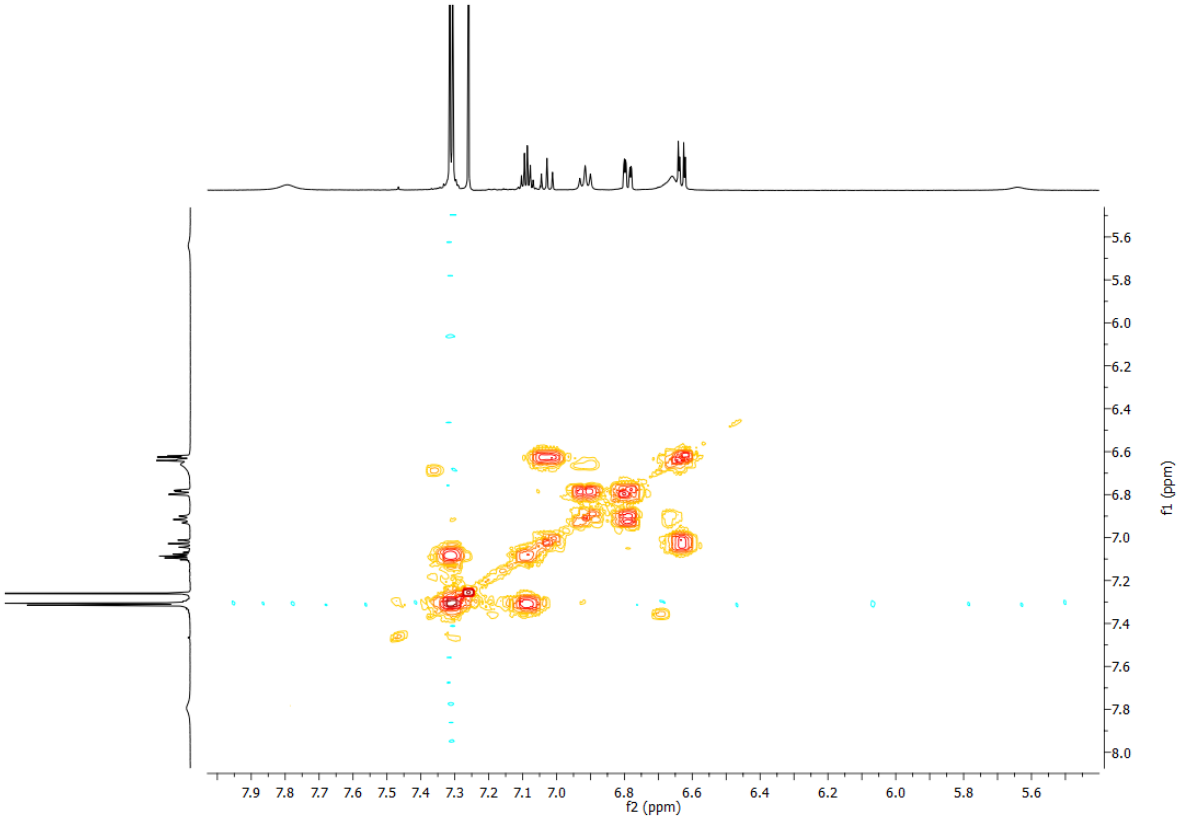

Figure S39. COSY NMR spectrum of **2a** ($CDCl_3$, 300K, 600 MHz).

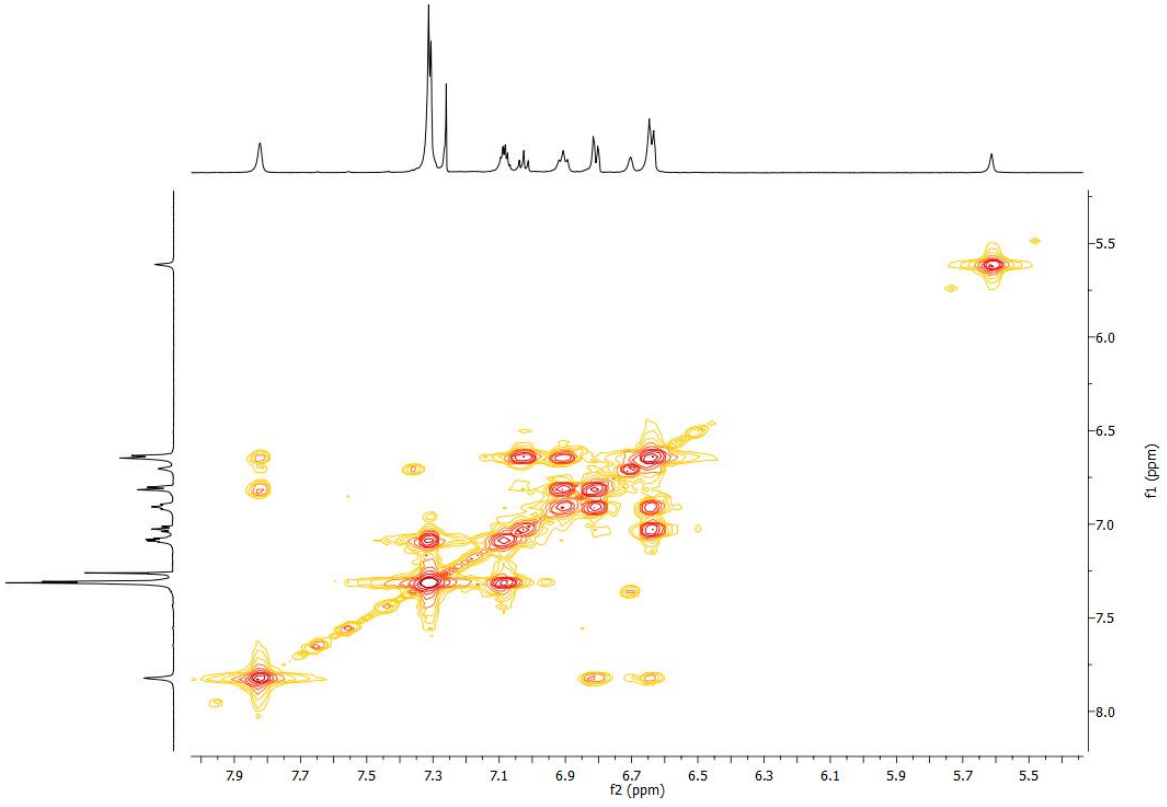

Figure S40. COSY NMR spectrum of **2a** ($CDCl_3$, 270K, 600 MHz).

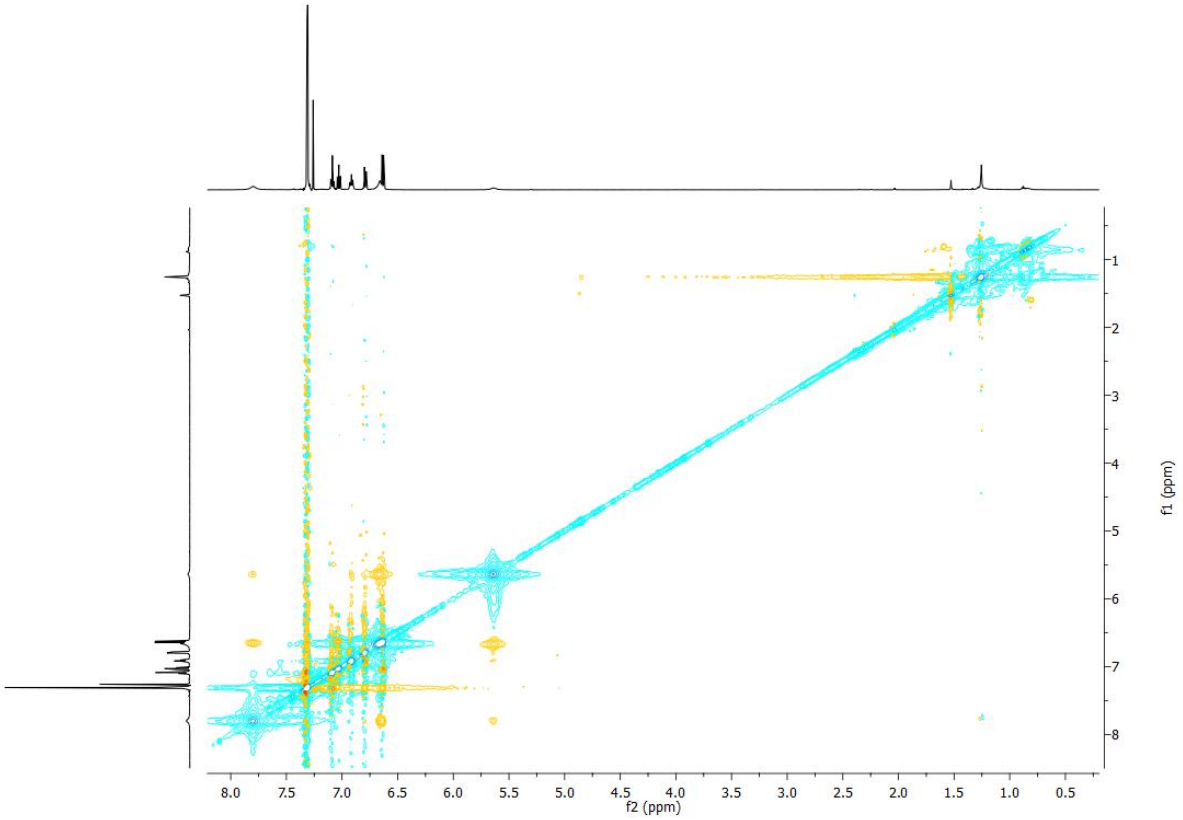

Figure S41. ROESY NMR spectrum of **2a** ($CDCl_3$, 300K, 600 MHz).

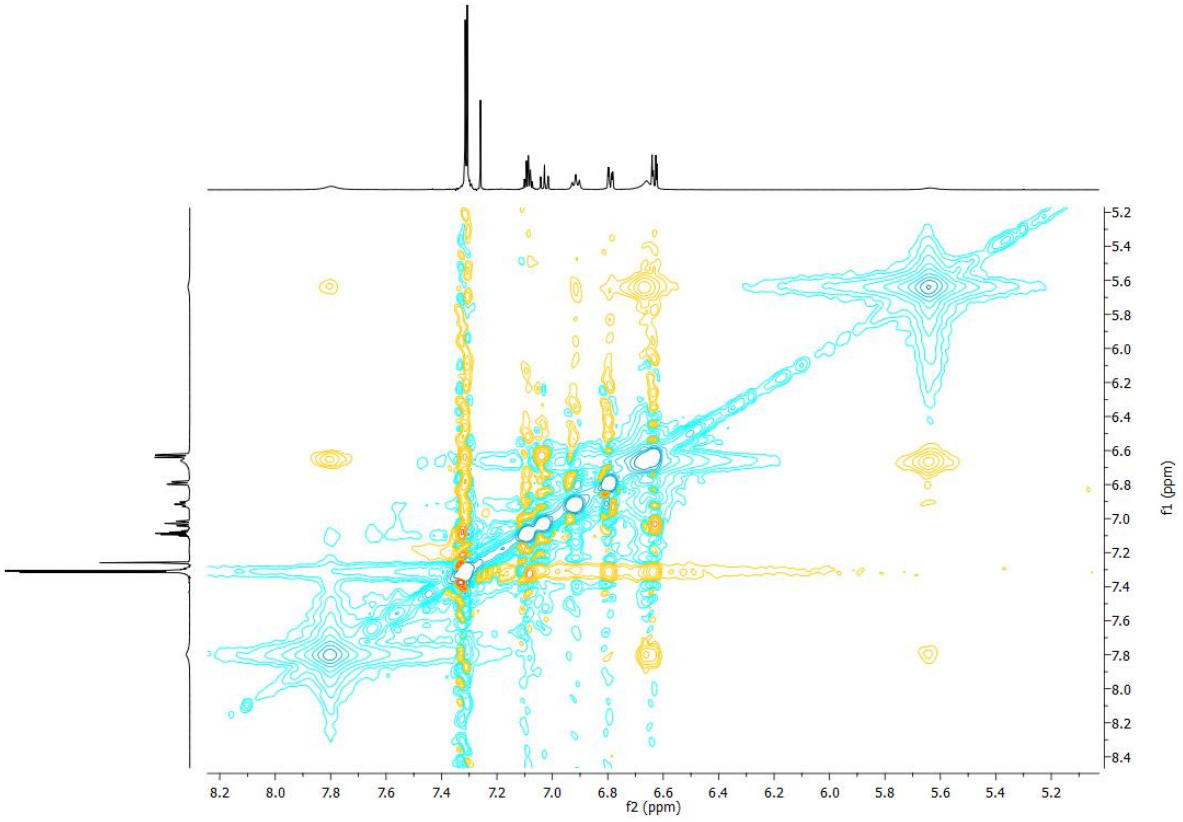

Figure S42. ROESY NMR (zoom, aromatic region) spectrum of **2a** ($CDCl_3$, 300K, 600 MHz).

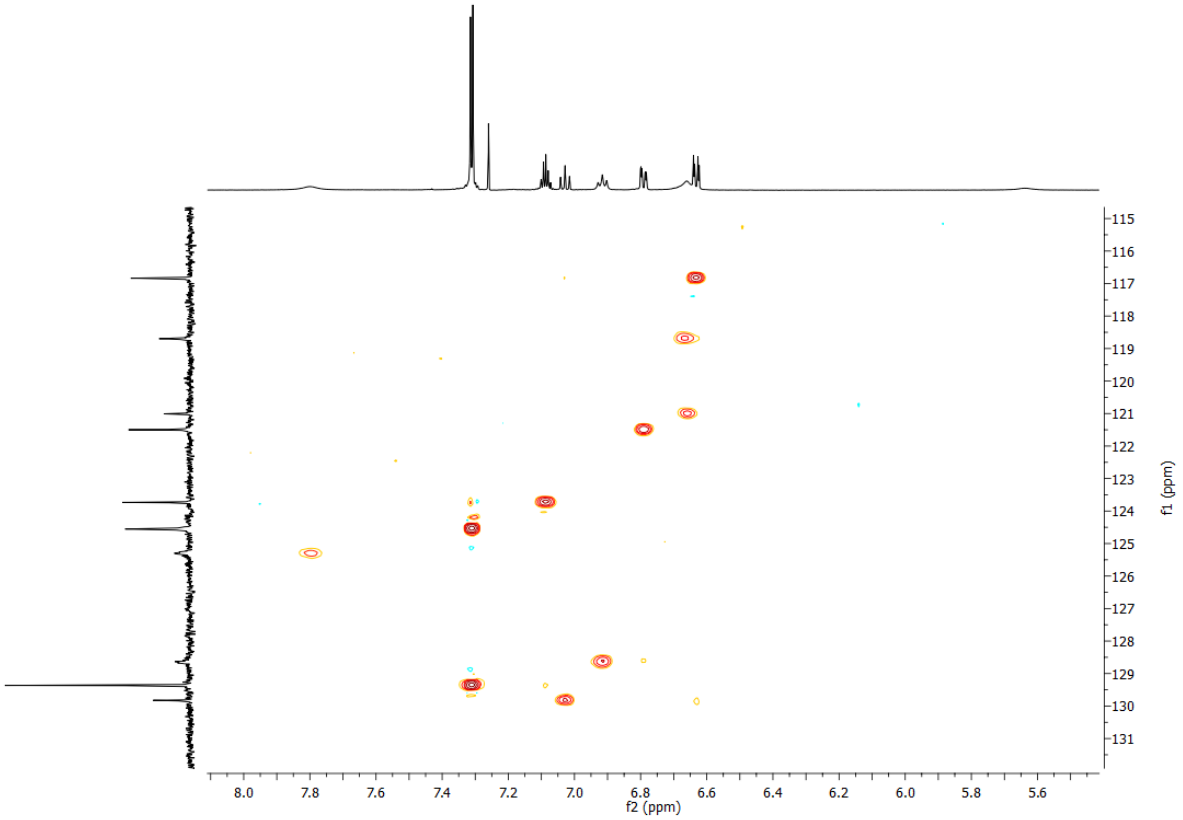

Figure S43. HSQC NMR spectrum of **2a** ($CDCl_3$, 300K, 600, 151 MHz).

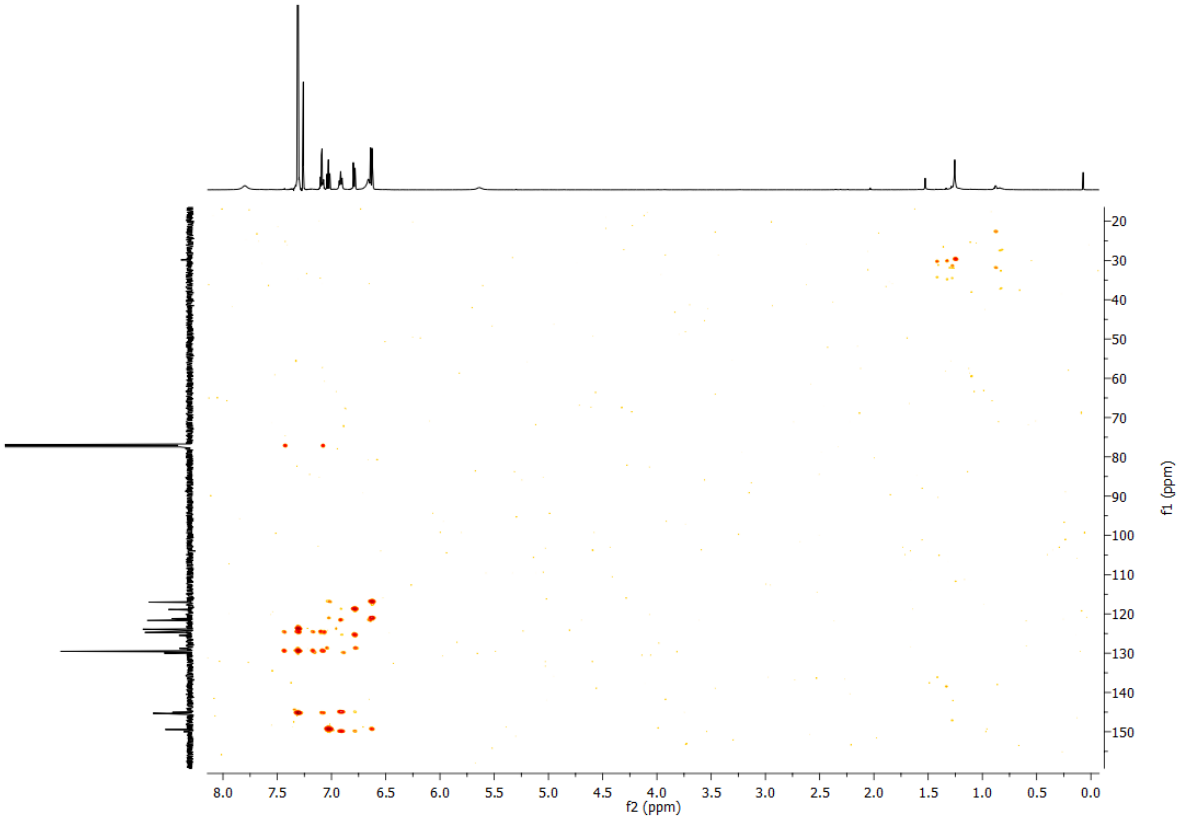

Figure S44. HMBC NMR spectrum of **2a** ($CDCl_3$, 300K, 600, 151 MHz).

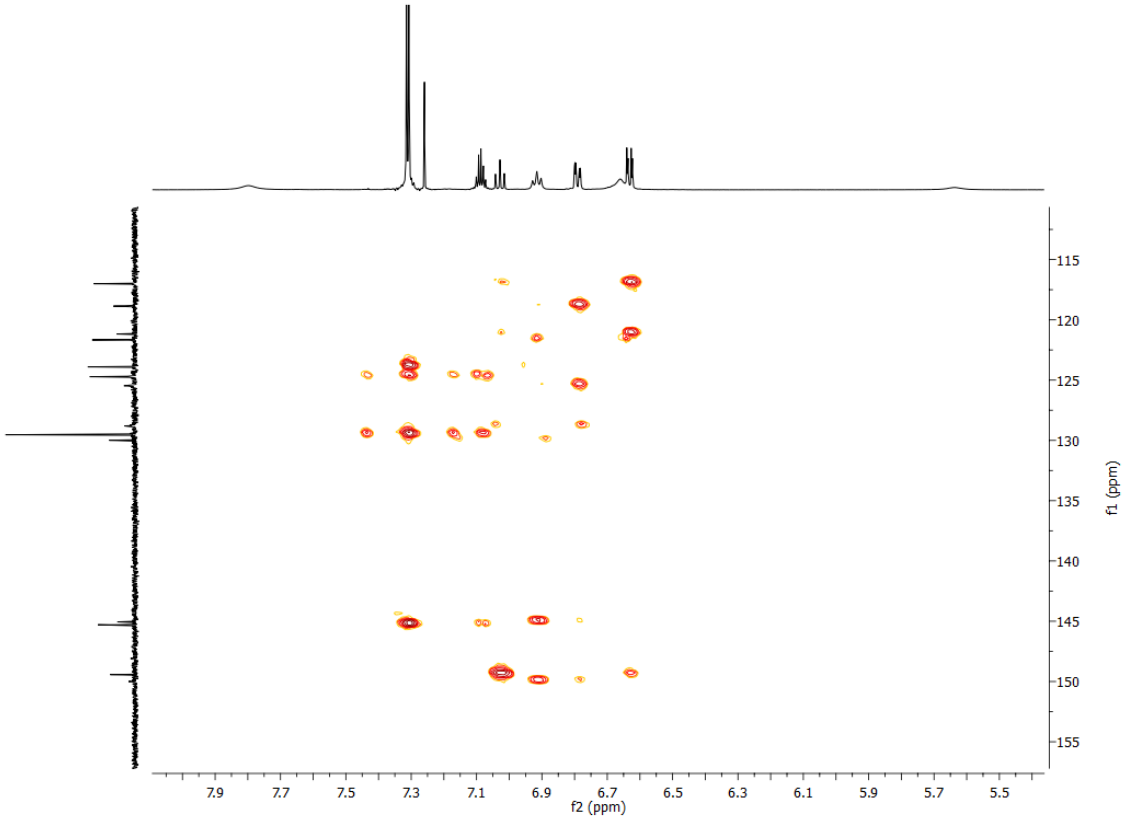

Figure S45. HMBC NMR spectrum (zoom, aromatic region) of **2a** ($CDCl_3$, 300K, 600, 151 MHz).

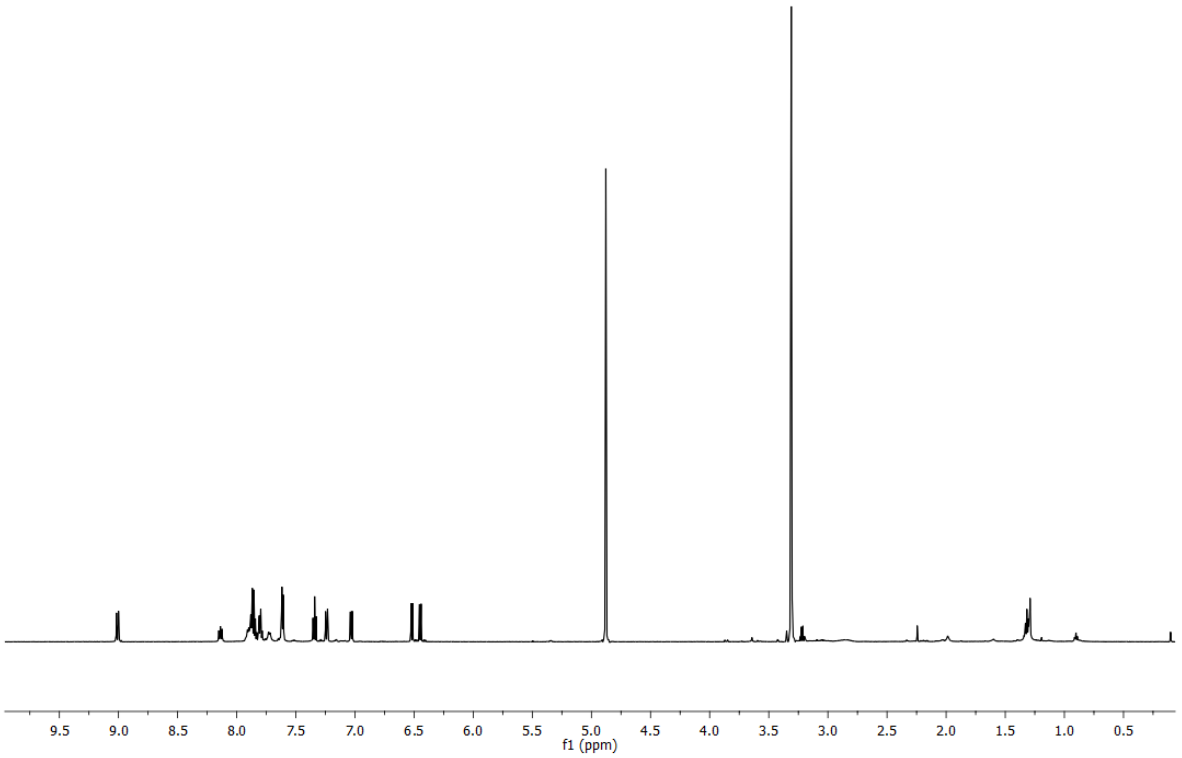

Figure S46. ^1H NMR spectrum of **3** (CD_3OD, 300K, 600 MHz).

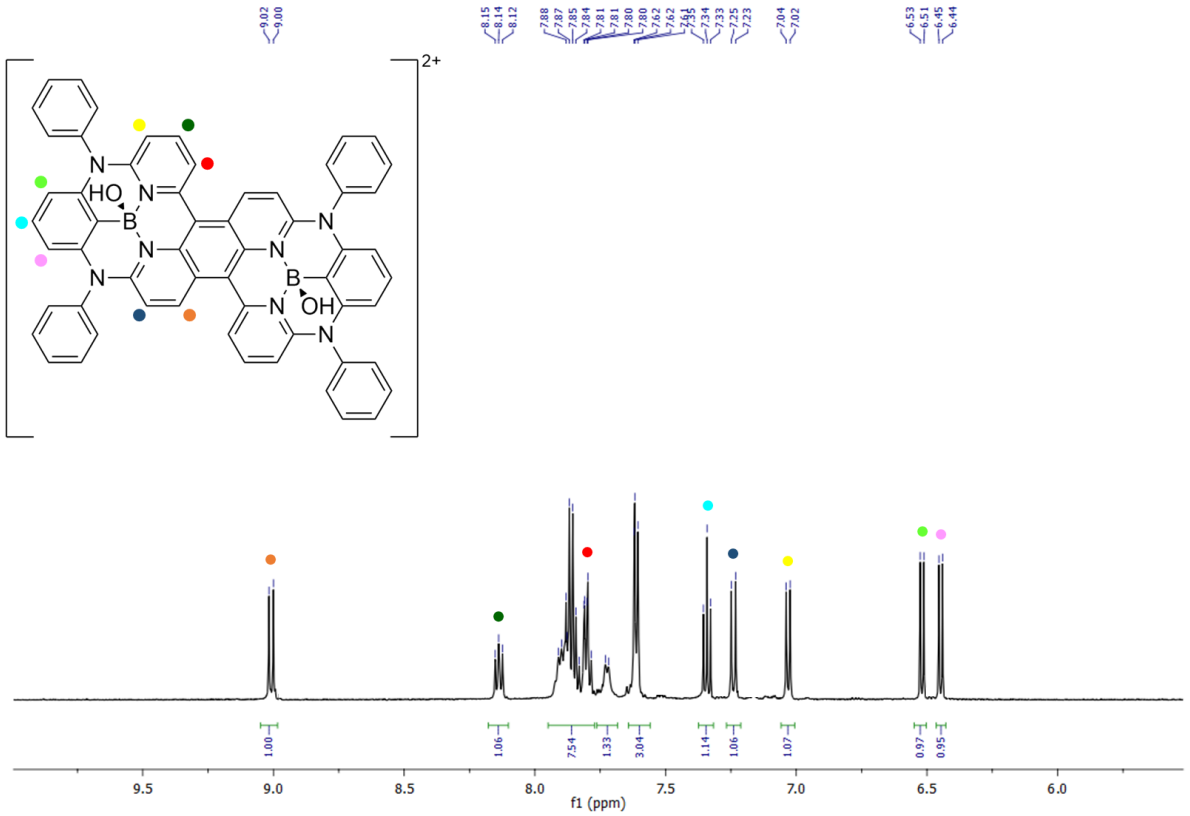

Figure S47. ^{1}H NMR spectrum (zoom, aromatic region) of **3** (CD_3OD, 300K, 600 MHz).

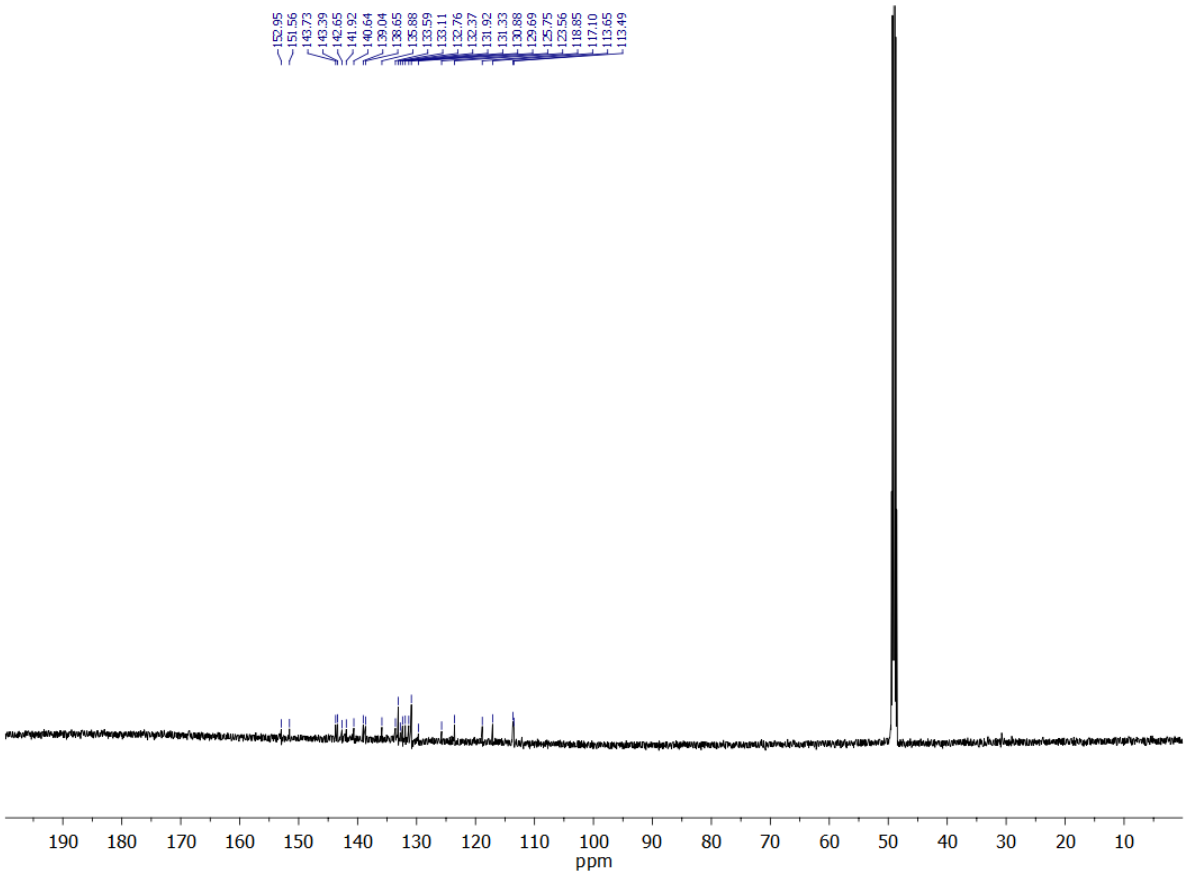

Figure S48. ^{13}C NMR spectrum of **3** (CD_3OD, 300K, 151 MHz).

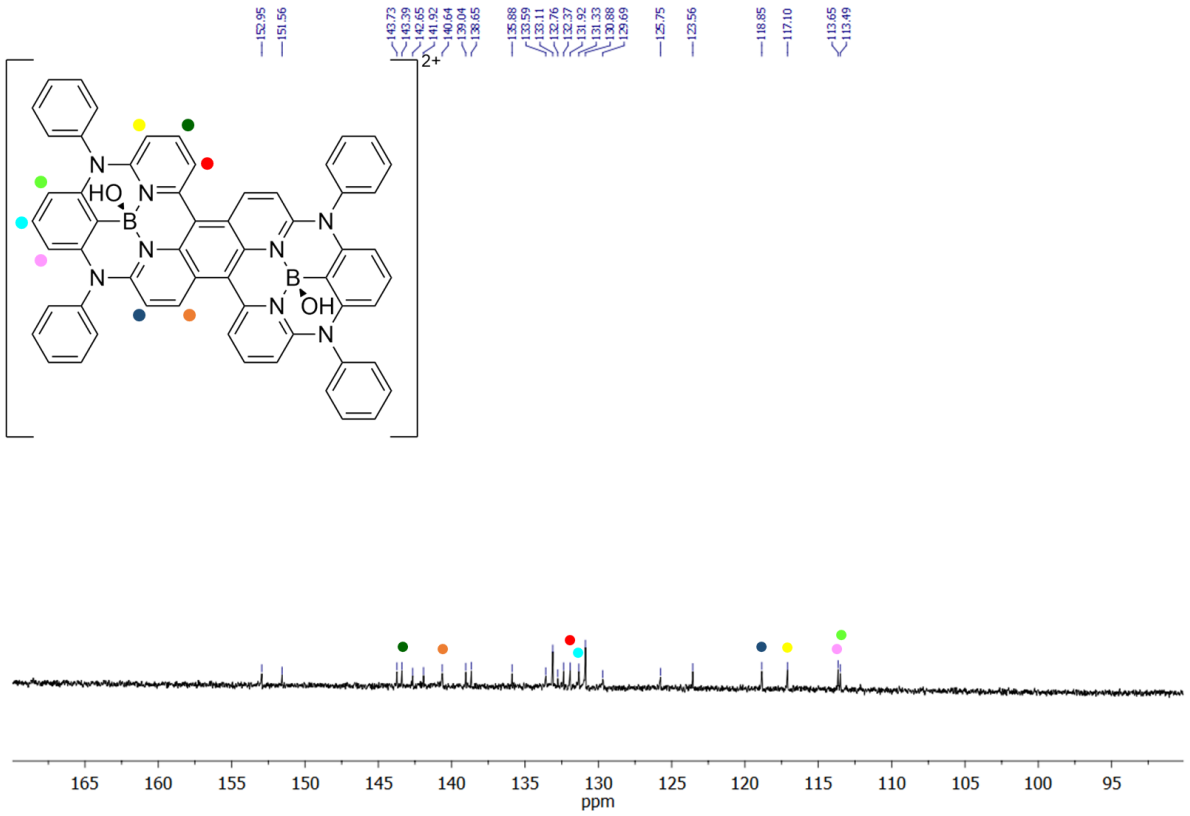

Figure S49. ^{13}C NMR spectrum (zoom) of **3** (CD_3OD, 300K, 151 MHz).

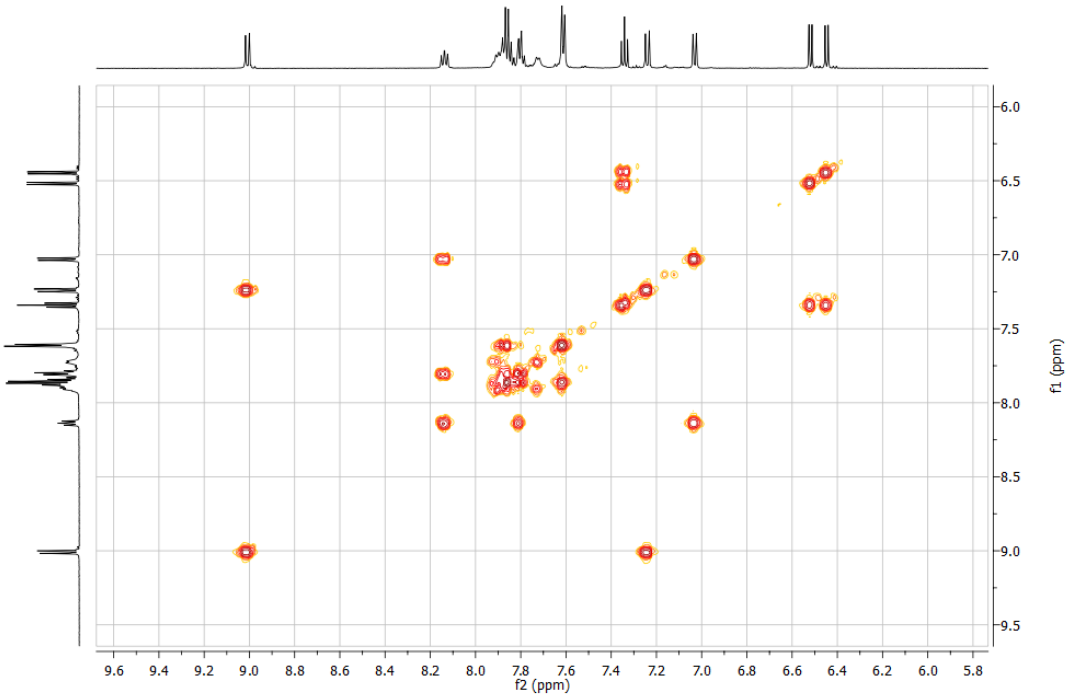

Figure S50. COSY NMR spectrum of **3** (CD_3OD, 300K, 600 MHz).

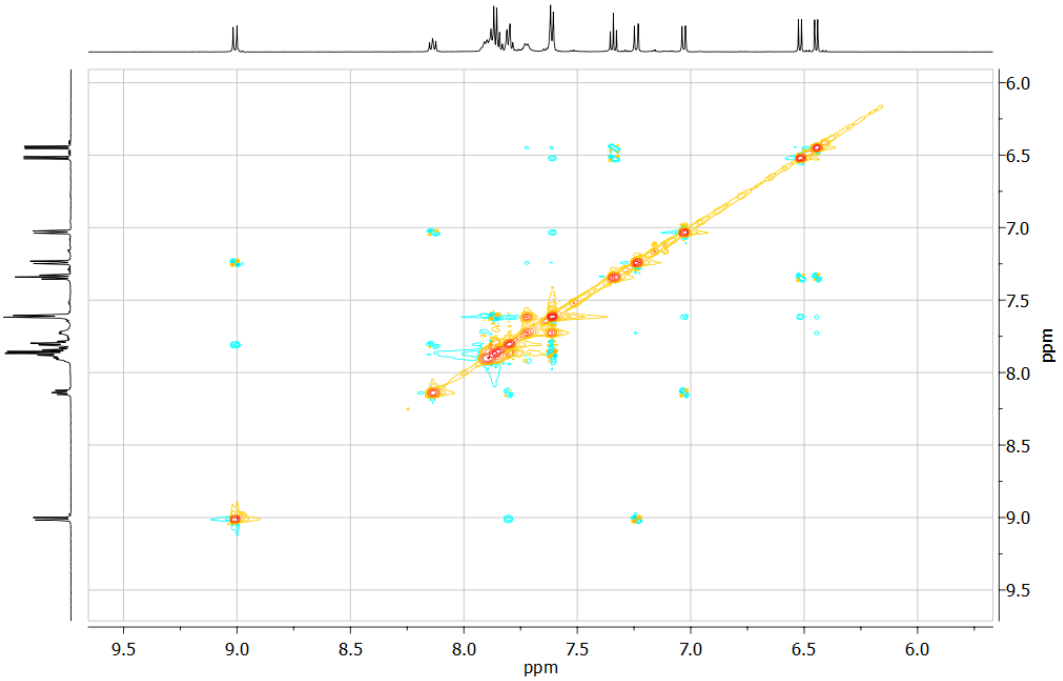

Figure S51. NOESY NMR spectrum of **3** (CD_3OD, 300K, 600 MHz).

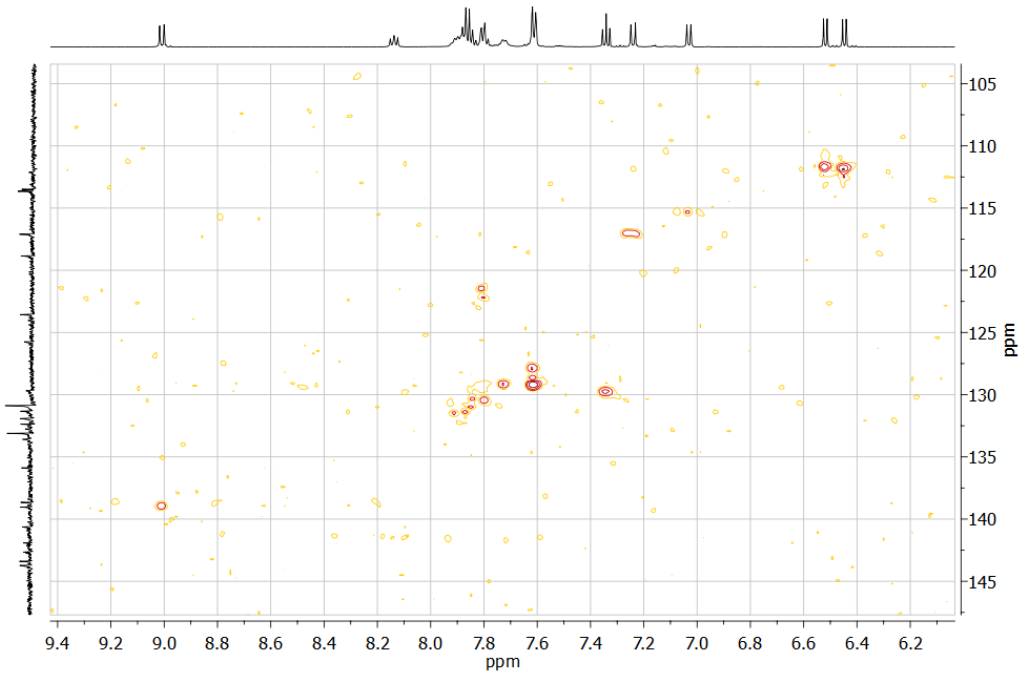

Figure S52. HSQC NMR spectrum of **3** (CD_3OD, 300K, 600, 151 MHz).

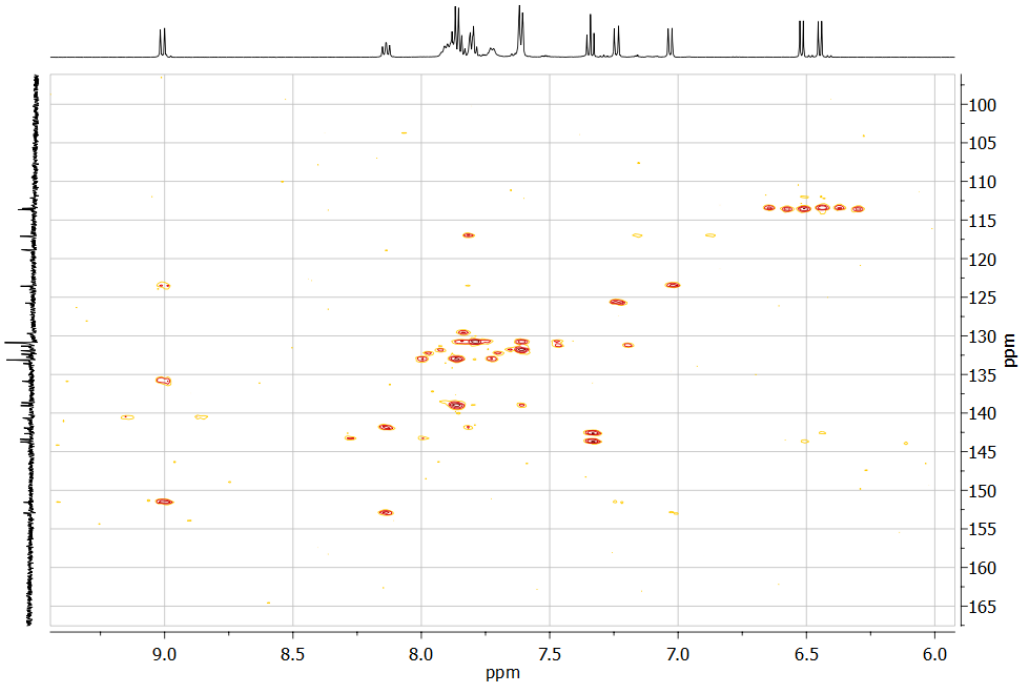

Figure S53. HMBC NMR spectrum of **3** (CD_3OD, 300K, 600, 151 MHz).

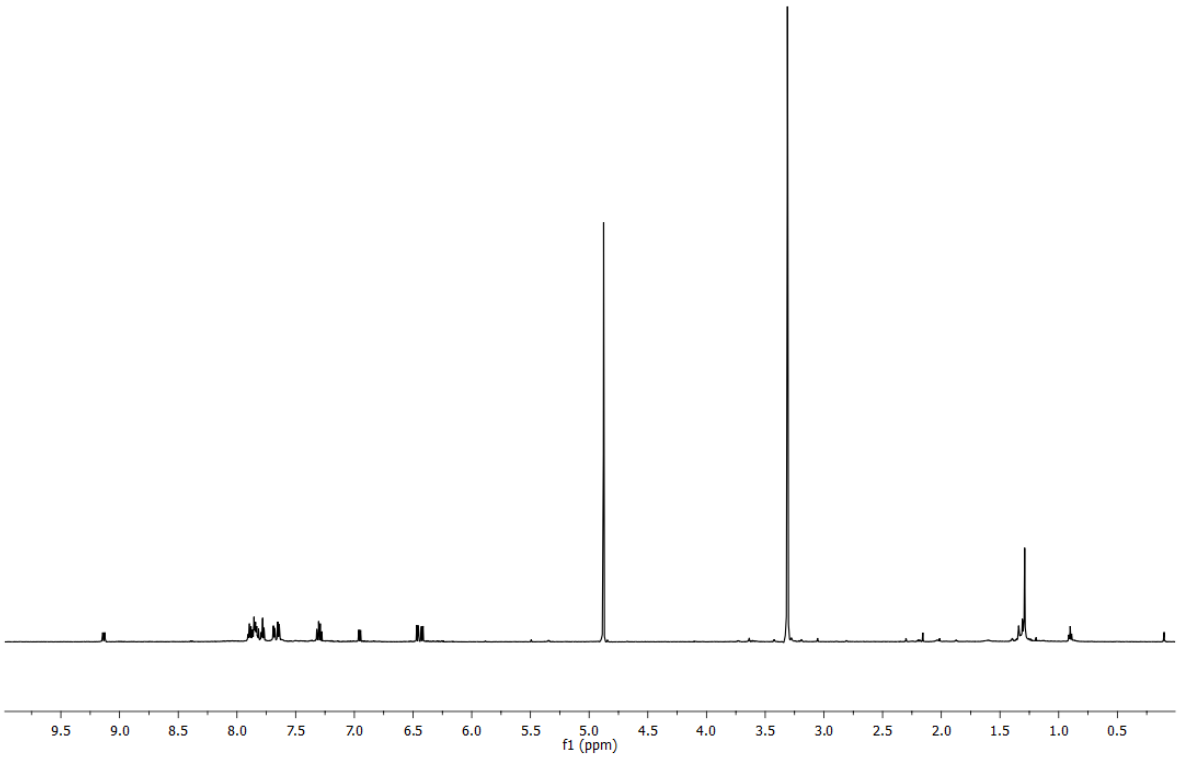

Figure S54. ^1H NMR spectrum of **4** (CD_3OD, 300K, 600 MHz).

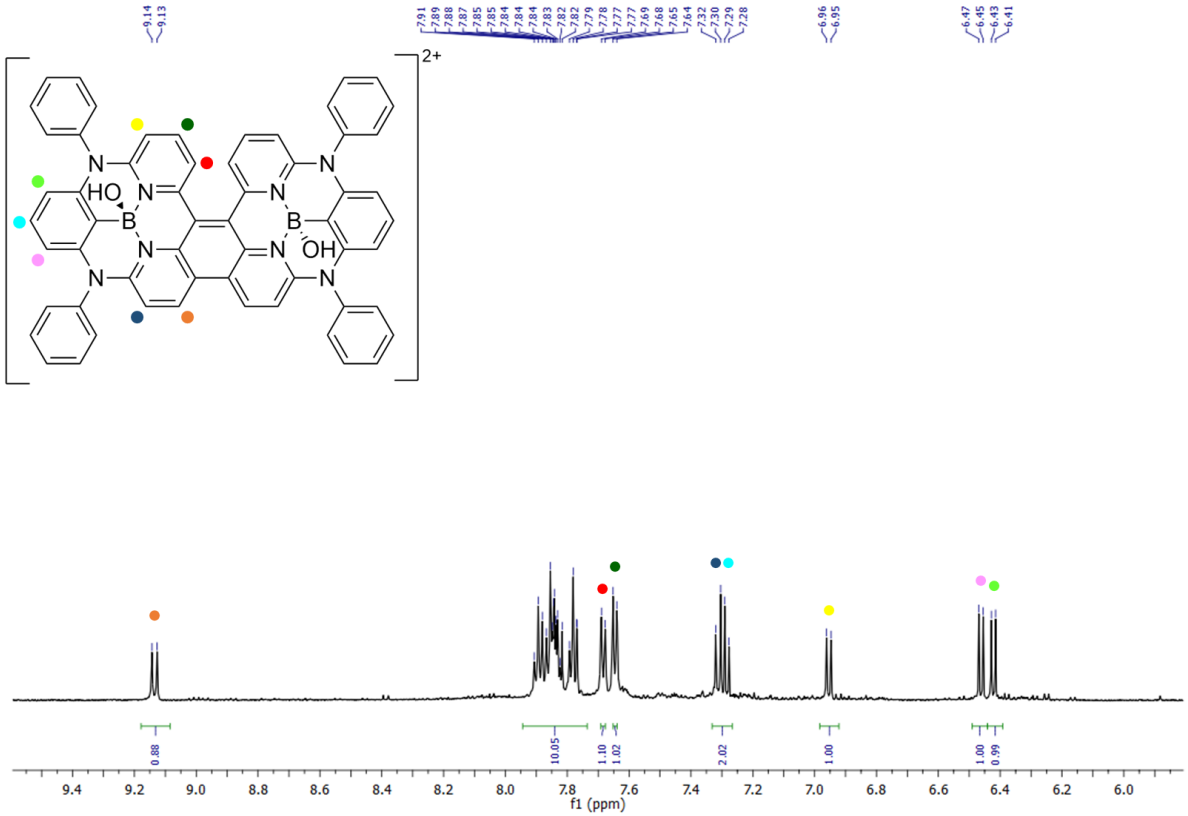

Figure S55. ^{1}H NMR spectrum (zoom, aromatic region) of **4** (CD_3OD, 300K, 600 MHz).

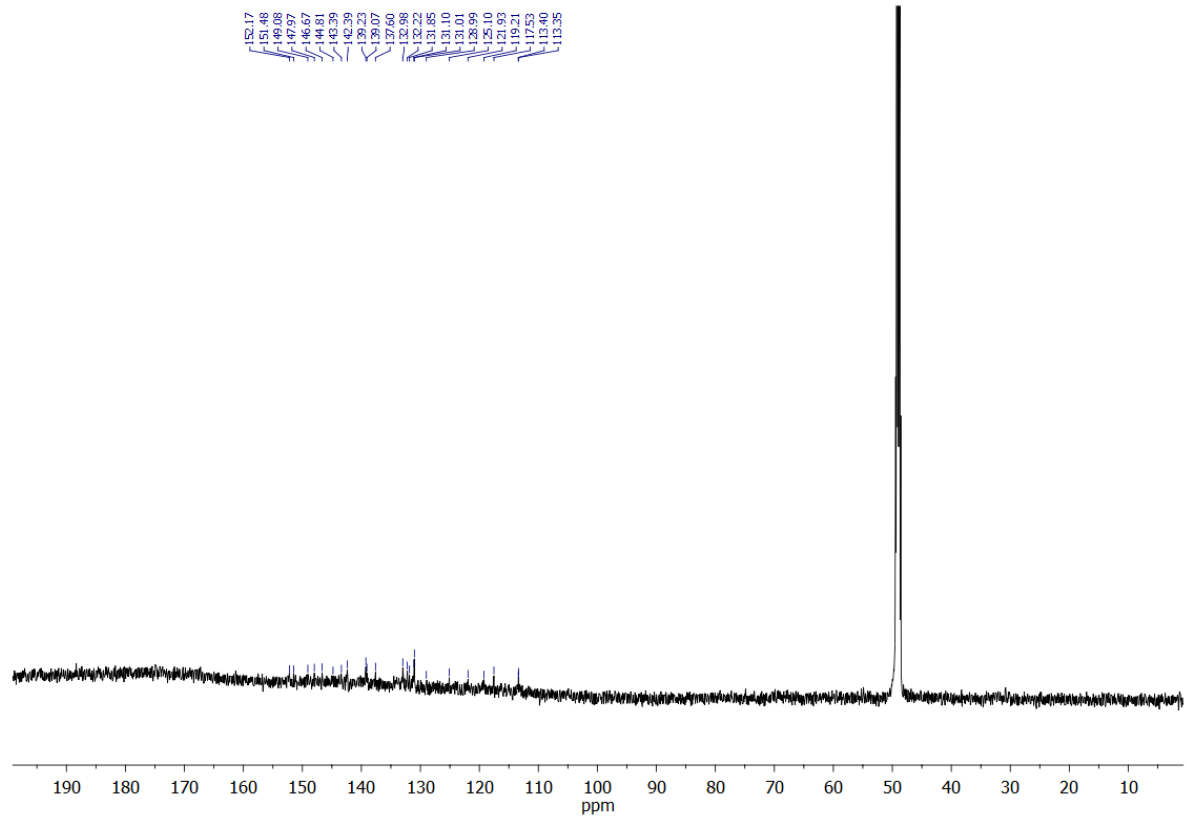

Figure S56. ^{13}C NMR spectrum of **4** (CD_3OD, 300K, 151 MHz).

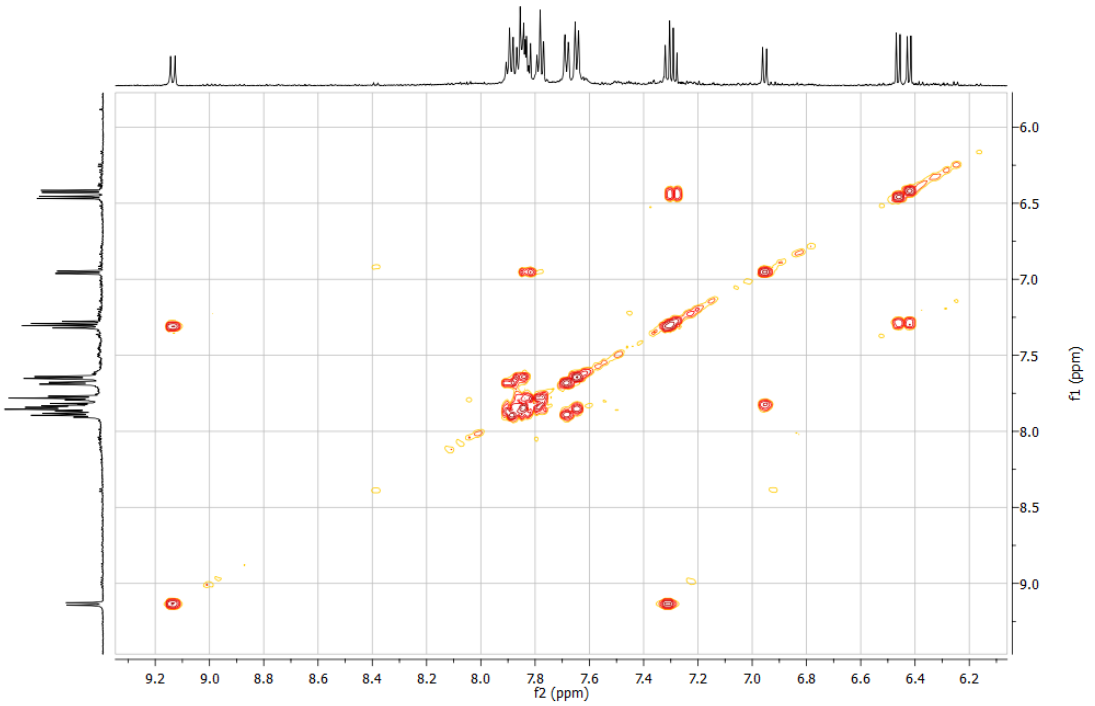

Figure S57. COSY NMR spectrum of **4** (CD_3OD, 300K, 600 MHz).

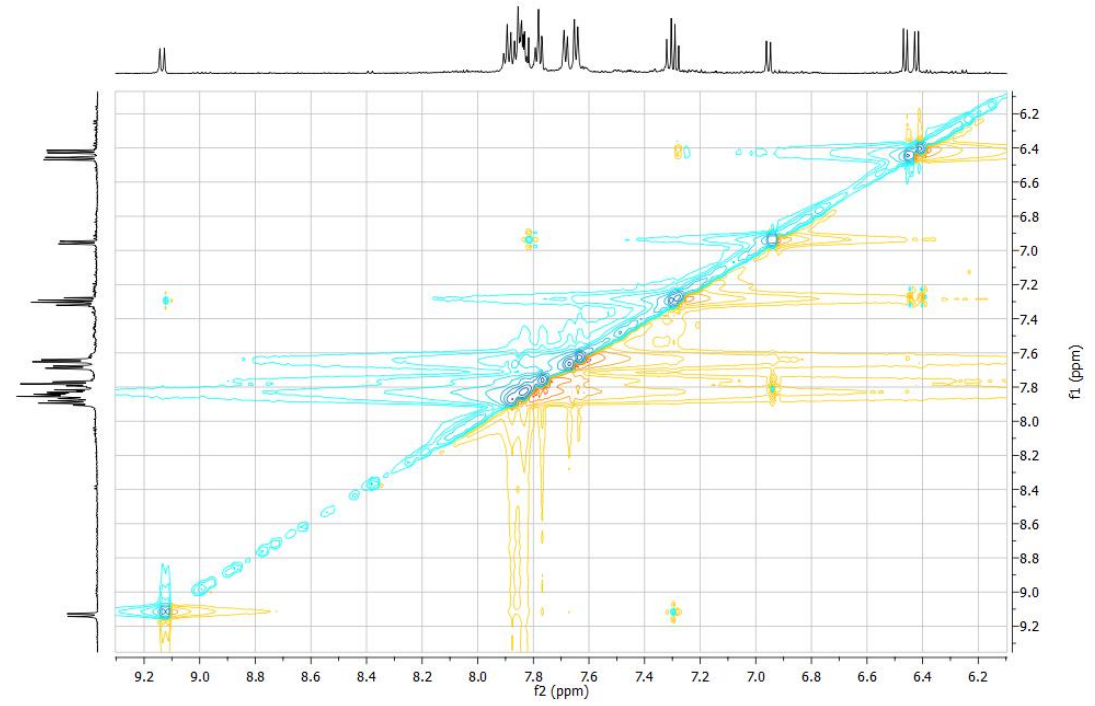

Figure S58. NOESY NMR spectrum of **4** (CD_3OD, 300K, 600 MHz).

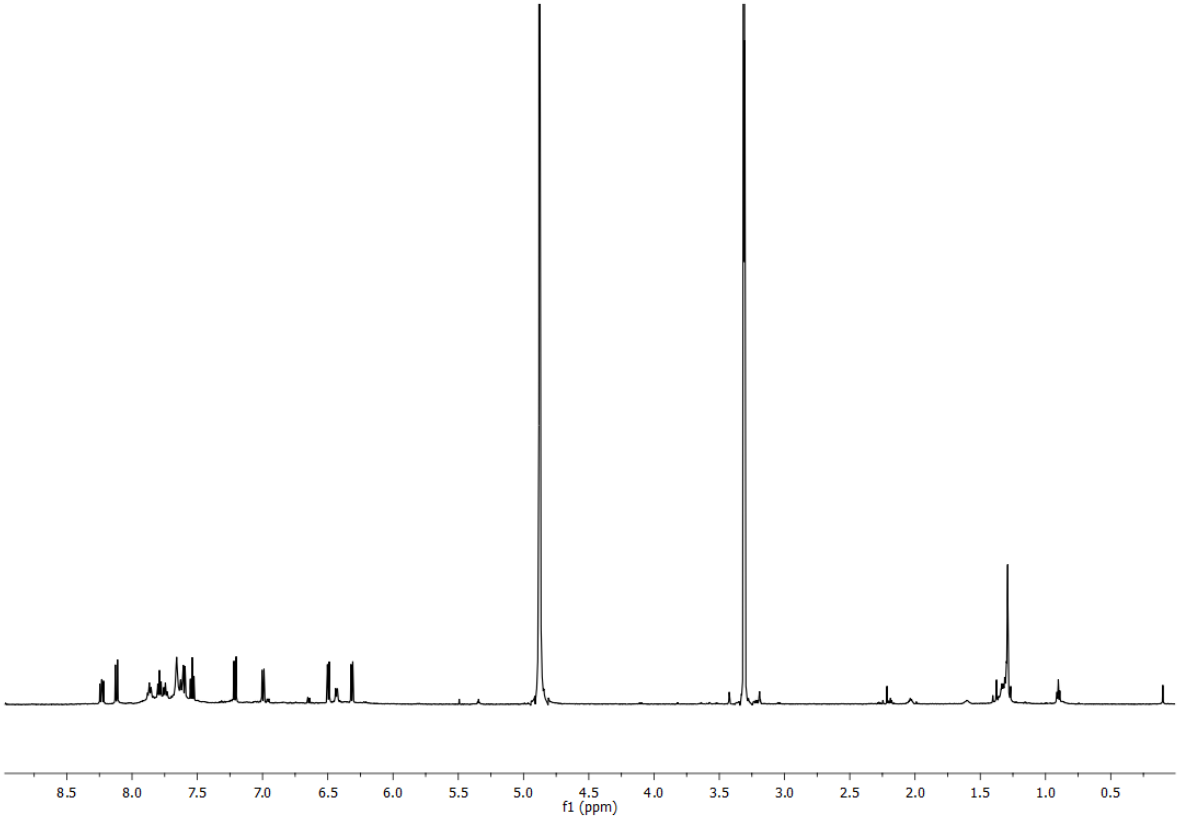

Figure S59 ^{1}H NMR spectrum of **3**-*O*-**3** (CD_3OD, 300K, 600 MHz).

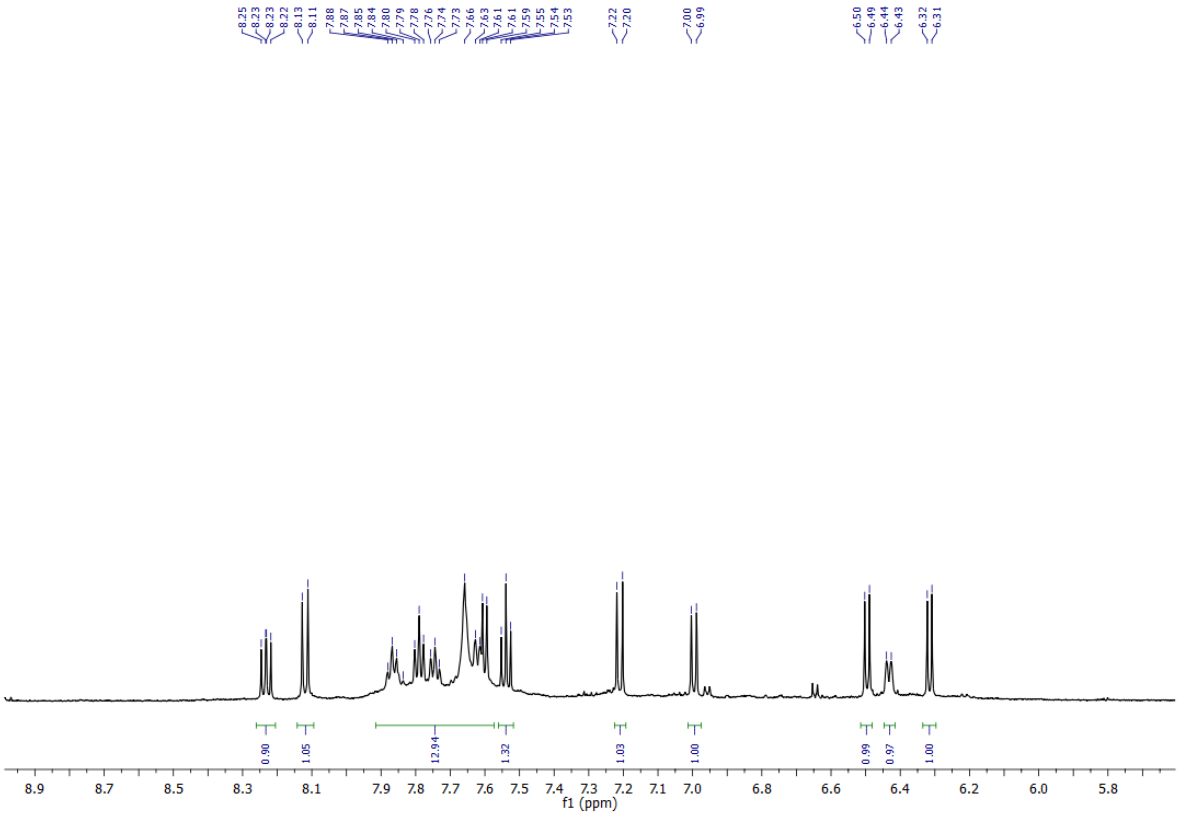

Figure S60. ^{1}H NMR spectrum (zoom, aromatic region) of **3**-*O*-**3** (CD_3OD, 300K, 600 MHz).

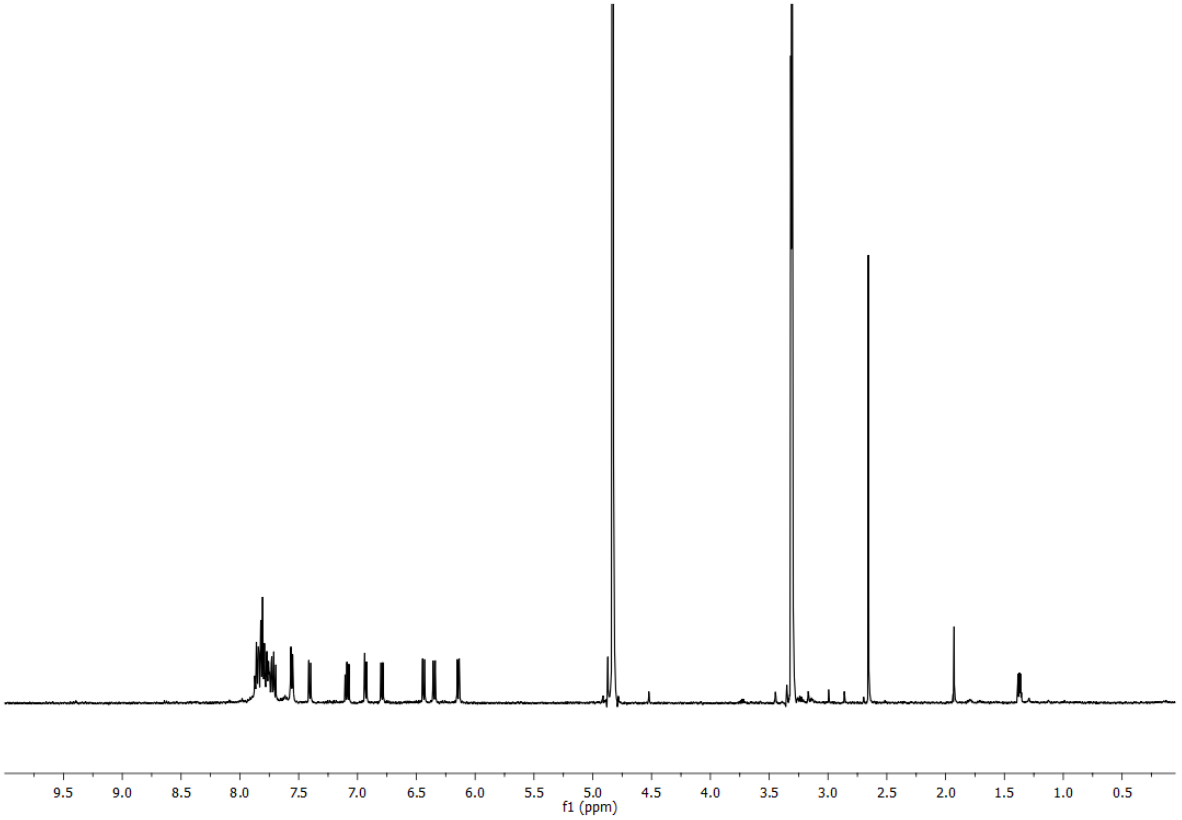

Figure S61. ^{1}H NMR spectrum of **5** (CD_3OD, 300K, 500 MHz).

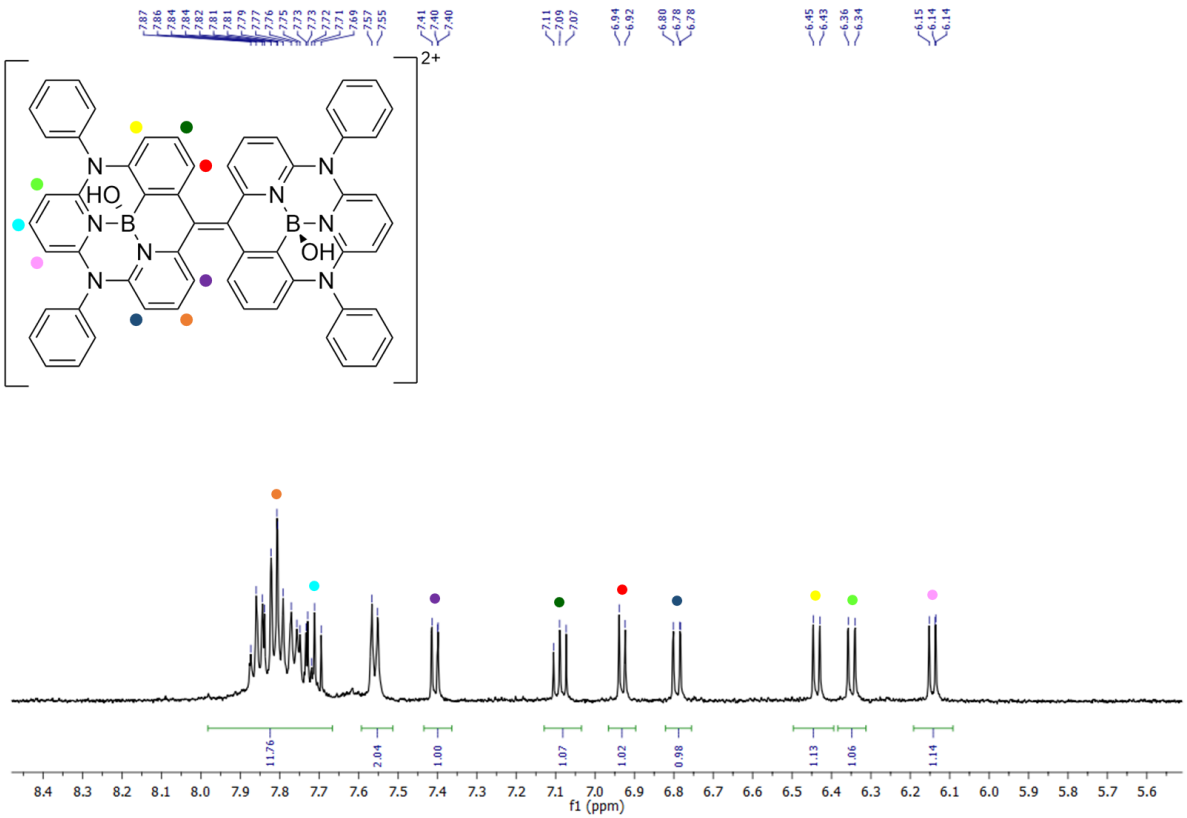

Figure S62 ^{1}H NMR spectrum (zoom, aromatic region) of **5** (CD_3OD, 300K, 500 MHz).

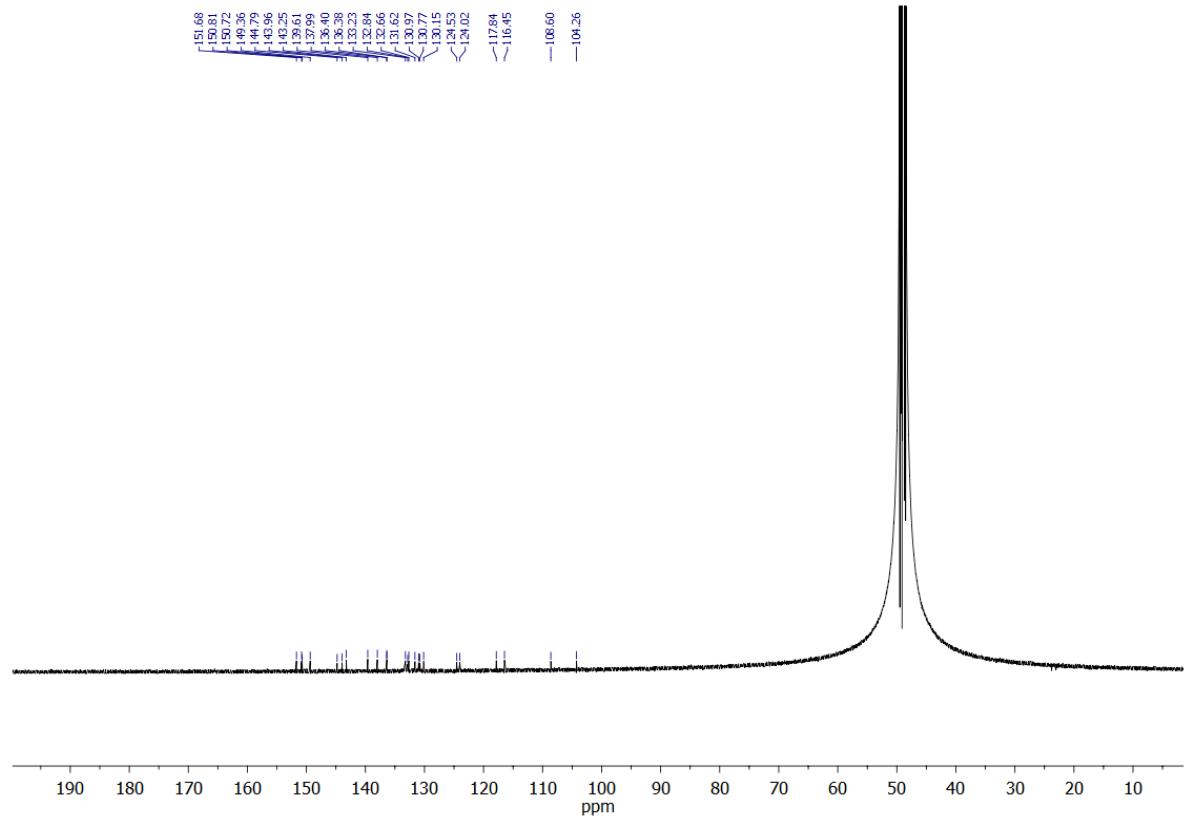

Figure S63. ^{13}C NMR spectrum of **5** (CD_3OD, 300K, 126 MHz).

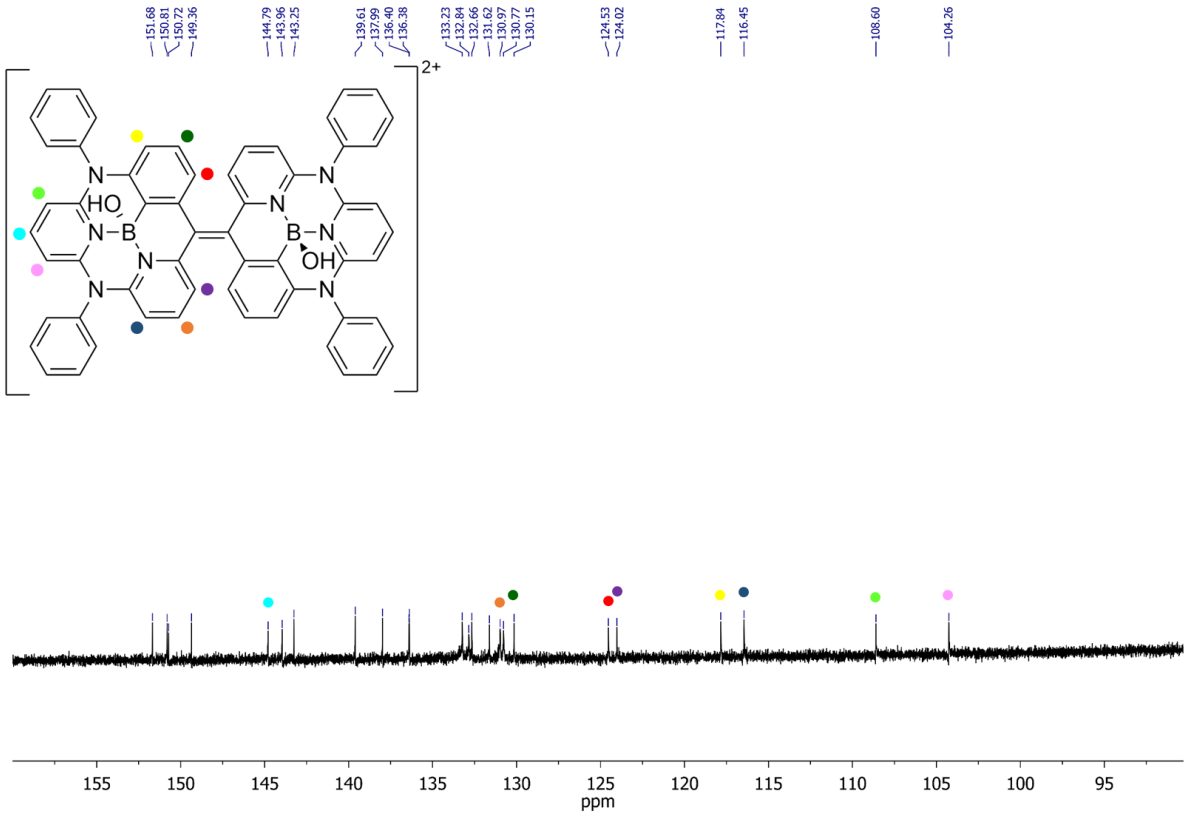

Figure S64. ^{13}C NMR spectrum (zoom) of **5** (CD_3OD, 300K, 126 MHz).

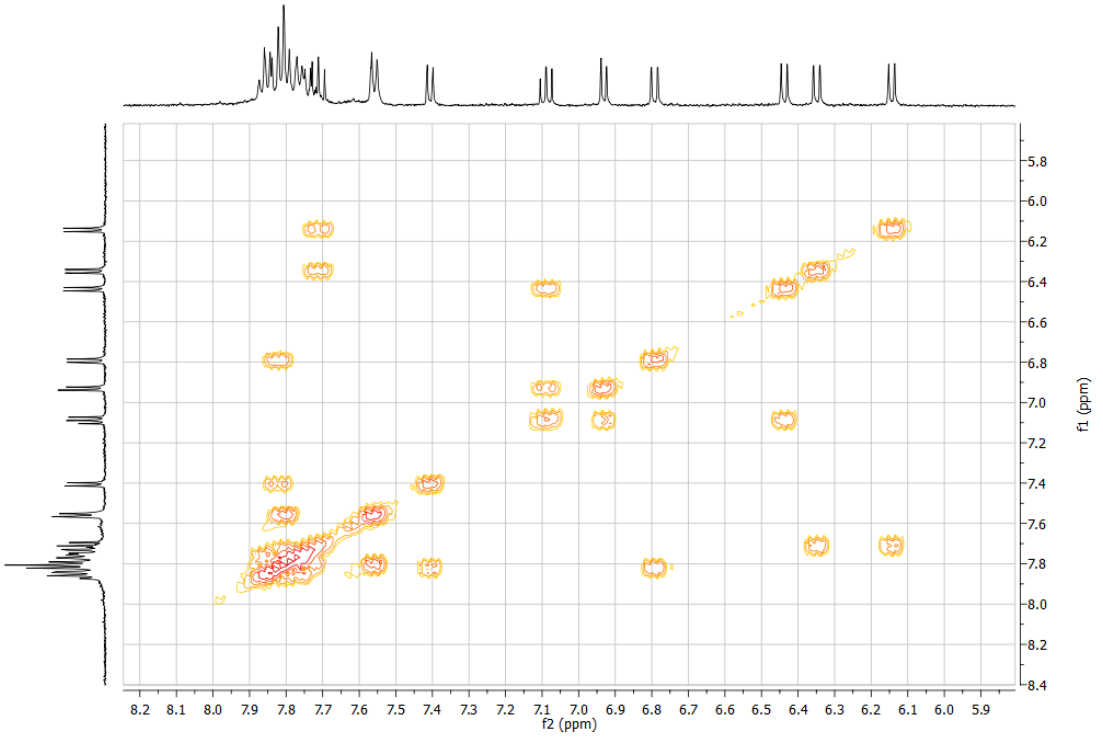

Figure S65. COSY NMR spectrum of **5** (CD_3OD, 300K, 500 MHz).

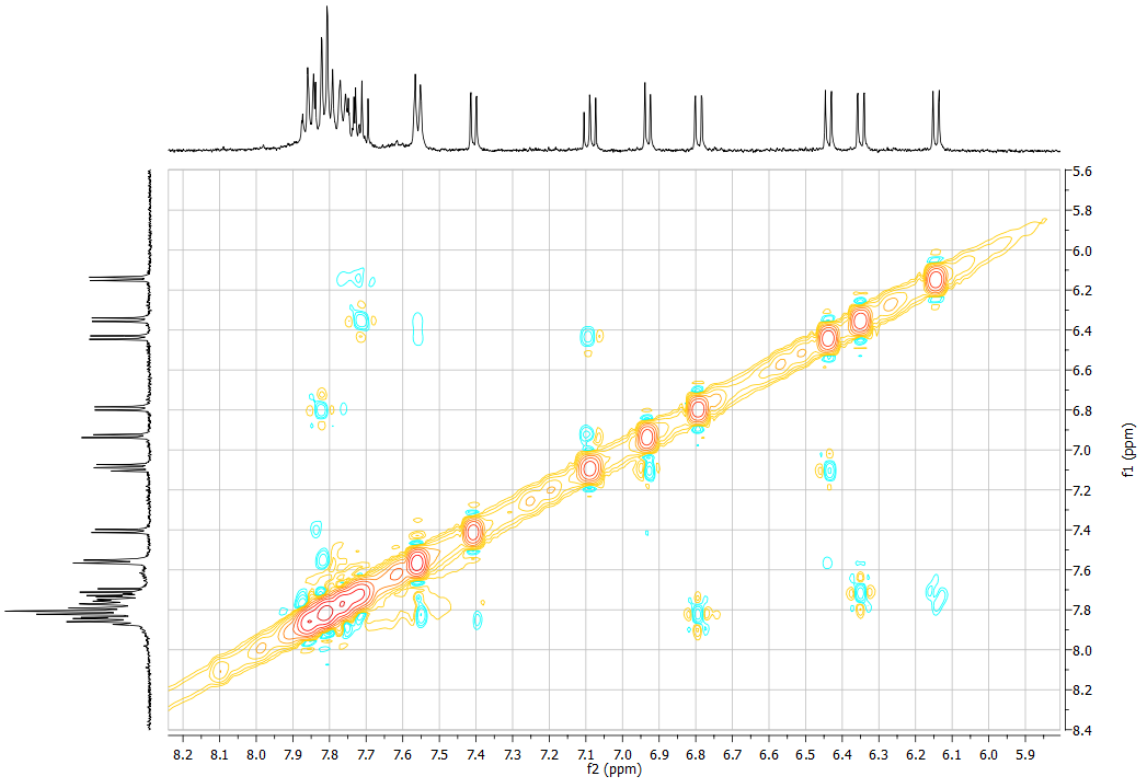

Figure S66. NOESY NMR spectrum of **5** (CD_3OD, 300K, 500 MHz).

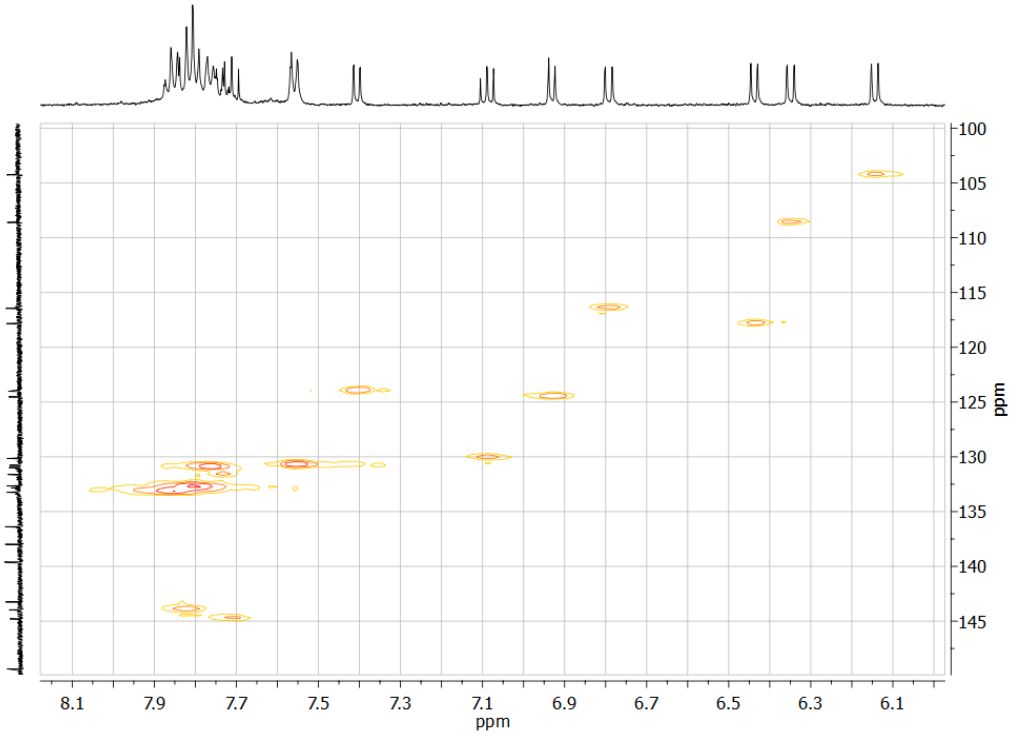

Figure S67. HSQC NMR spectrum of **5** (CD_3OD, 300K, 500, 126 MHz).

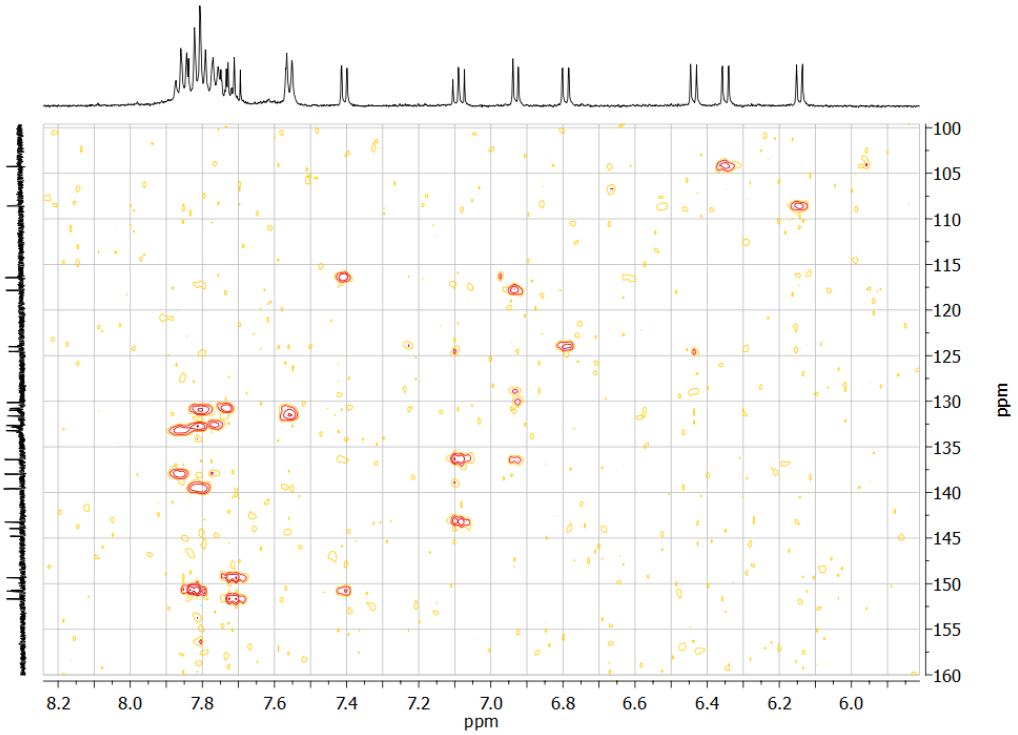

Figure S68. HMBC NMR spectrum of **5** (CD_3OD, 300K, 500, 126 MHz).

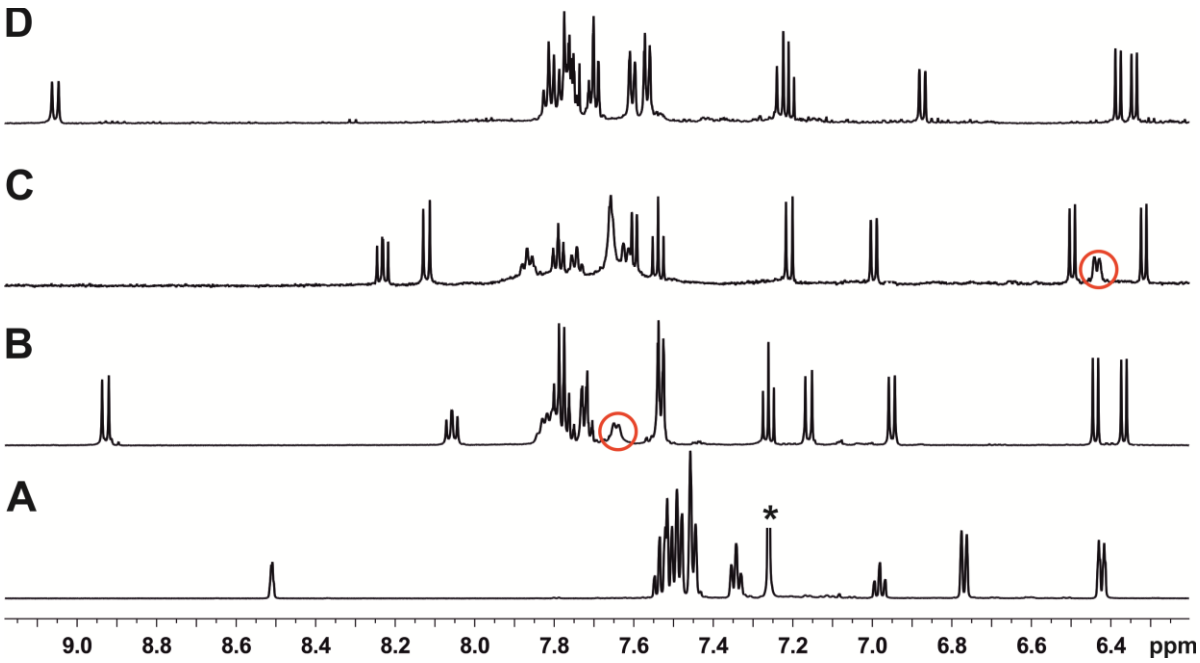

Figure S69. NMR stacking of NMR spectra; A: **1d**, B: **3**, C: **3**-*O*-**3**, D: **4**. * peak was suppressed, solvent peak. All spectra were recorded at 300 K, 600 MHz. Solvent in spectrum A: $CDCl_3$, solvent in spectra B, C and D: CD_3OD.

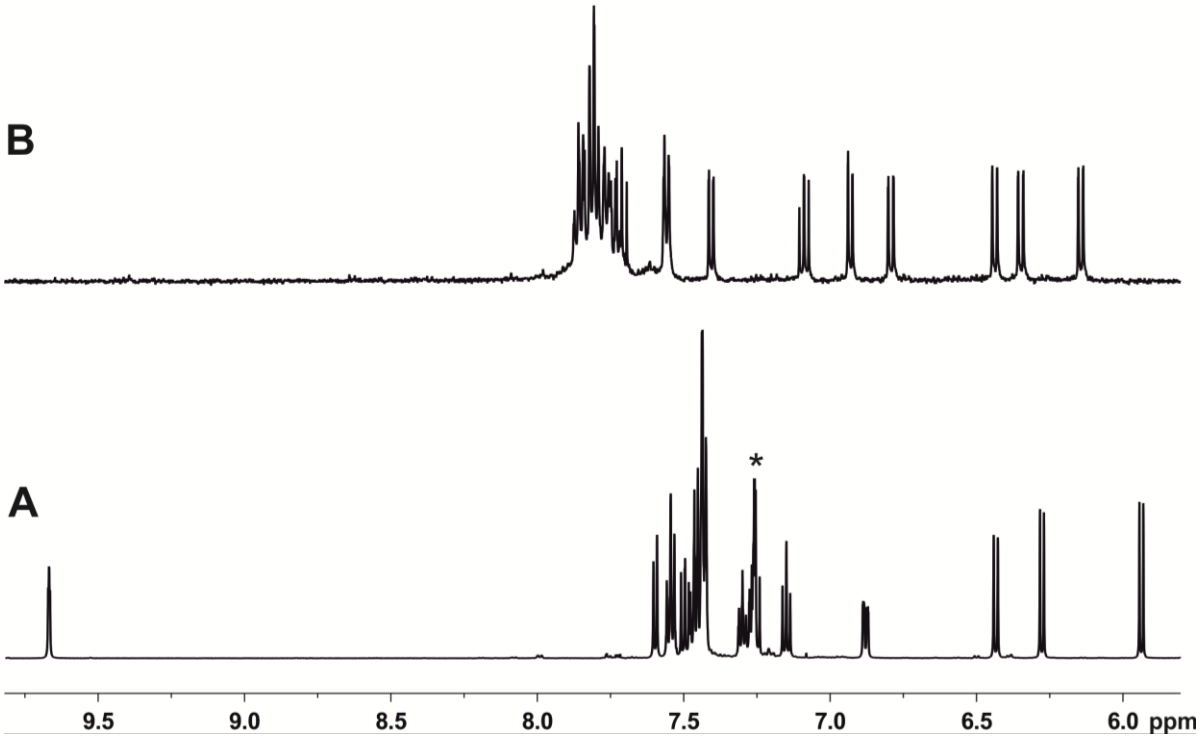

Figure S70. NMR stacking of NMR spectra; A: **1e**, B: **5**. * peak was suppressed, solvent peak. All spectra were recorded at 300 K, 600 MHz. Solvent in spectrum A: $CDCl_3$, solvent in spectra B: CD_3OD.

4. Mass spectra.

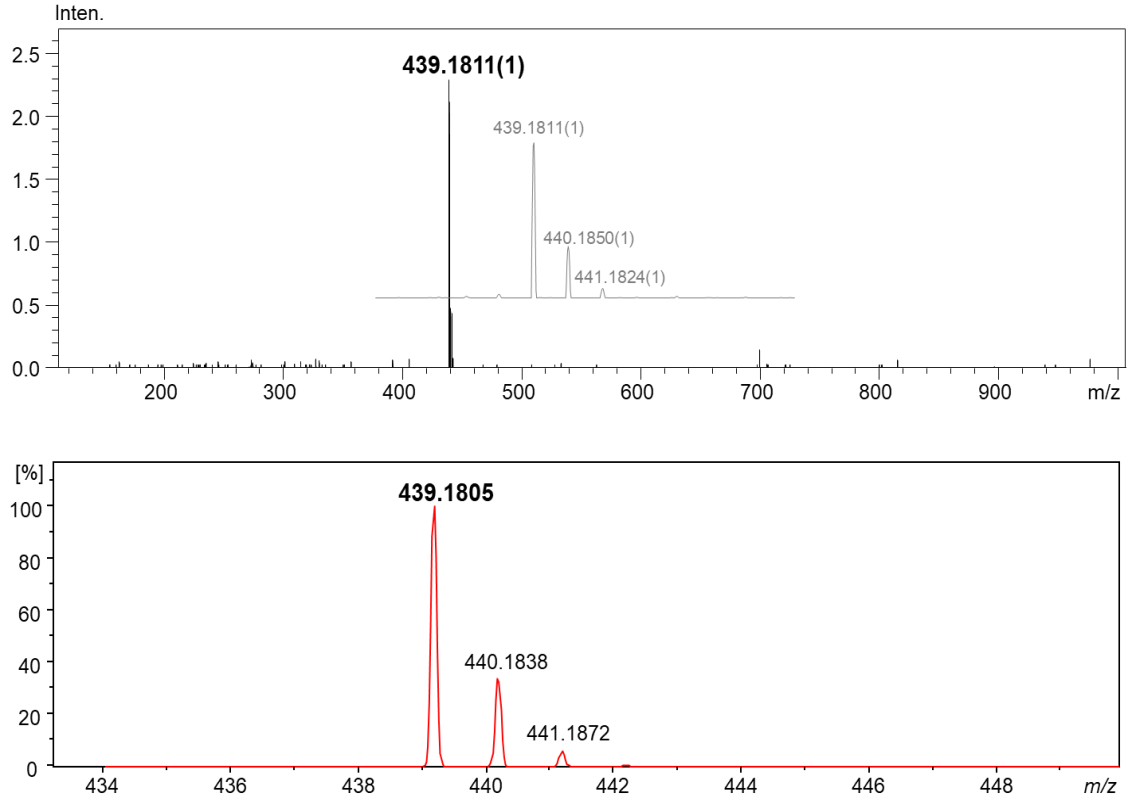

Figure S71. MS spectrum recorded for **1a** (above) compared with simulated pattern (below).

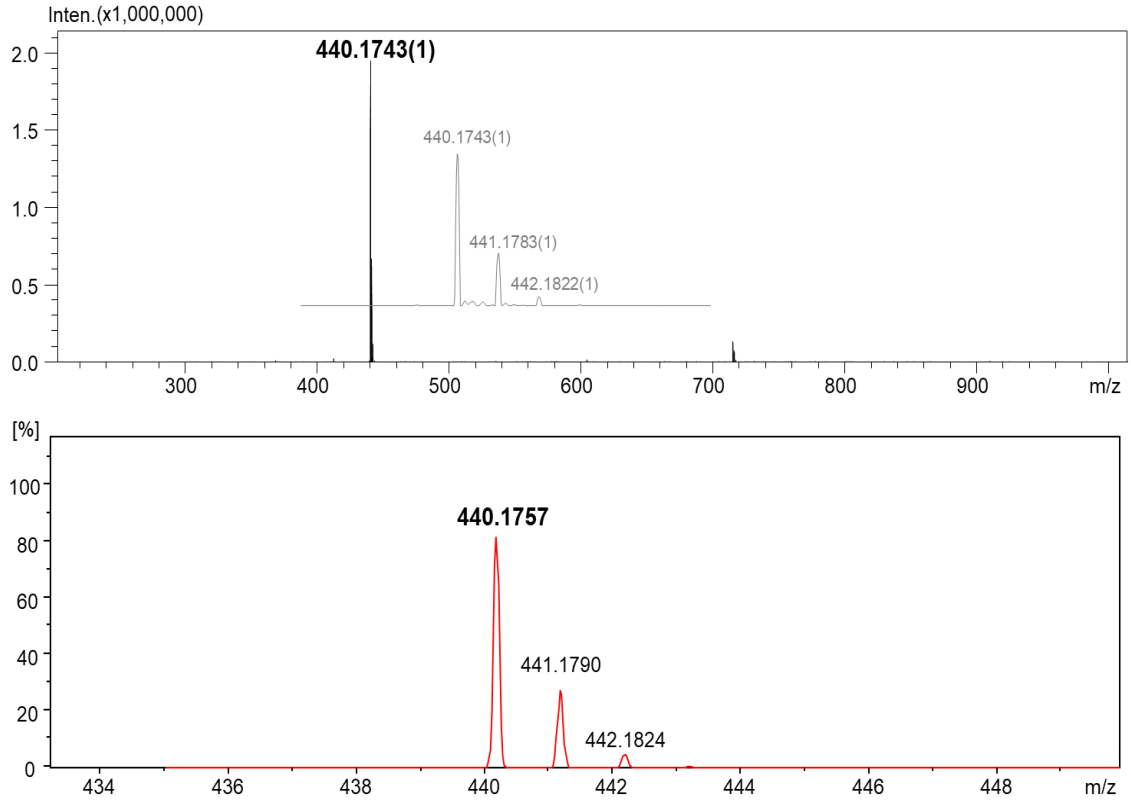

Figure S72. MS spectrum recorded for **1b** (above) compared with simulated pattern (below).

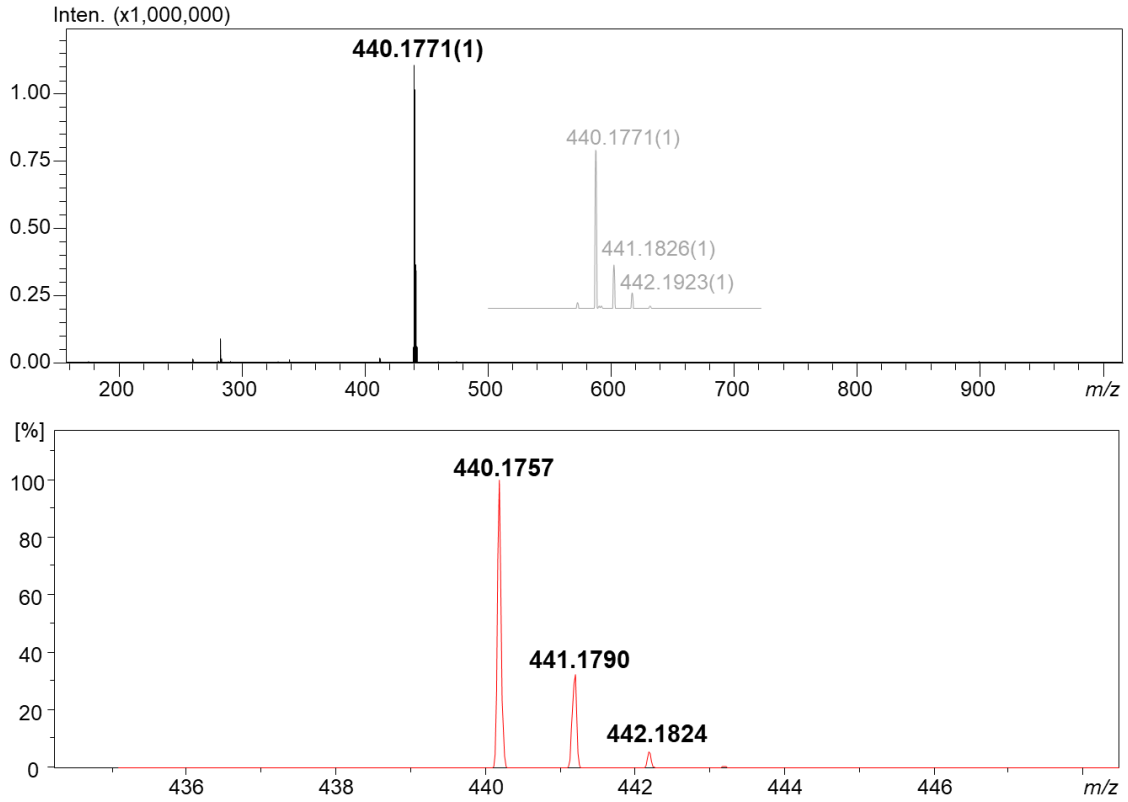

Figure S73. MS spectrum recorded for **1c** (above) compared with simulated pattern (below).

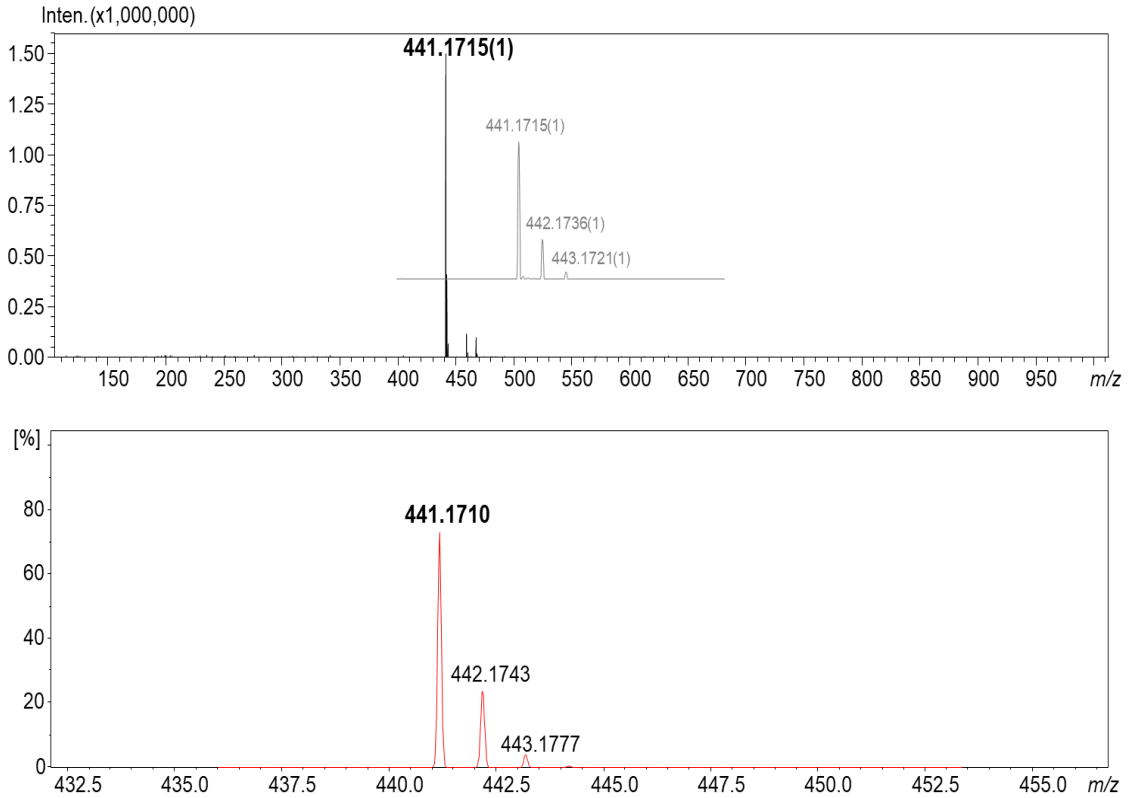

Figure S74. MS spectrum recorded for **1d** (above) compared with simulated pattern (below).

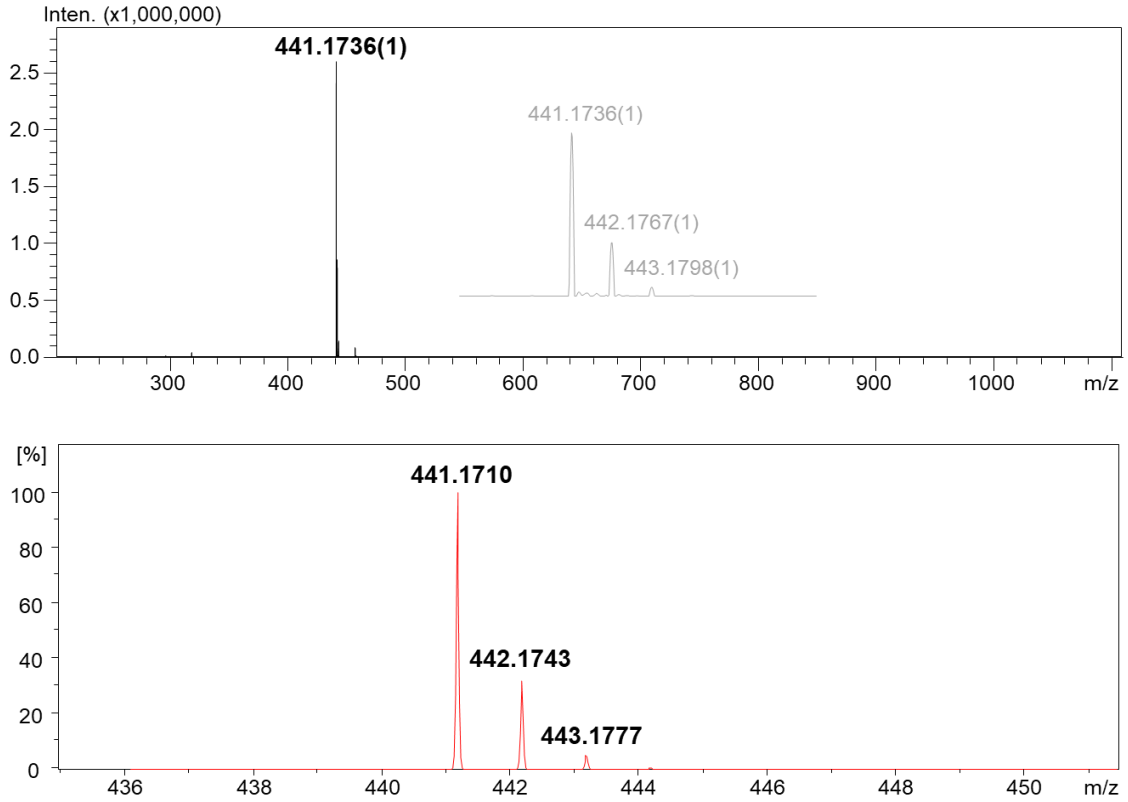

Figure S75. MS spectrum recorded for **1e** (above) compared with simulated pattern (below).

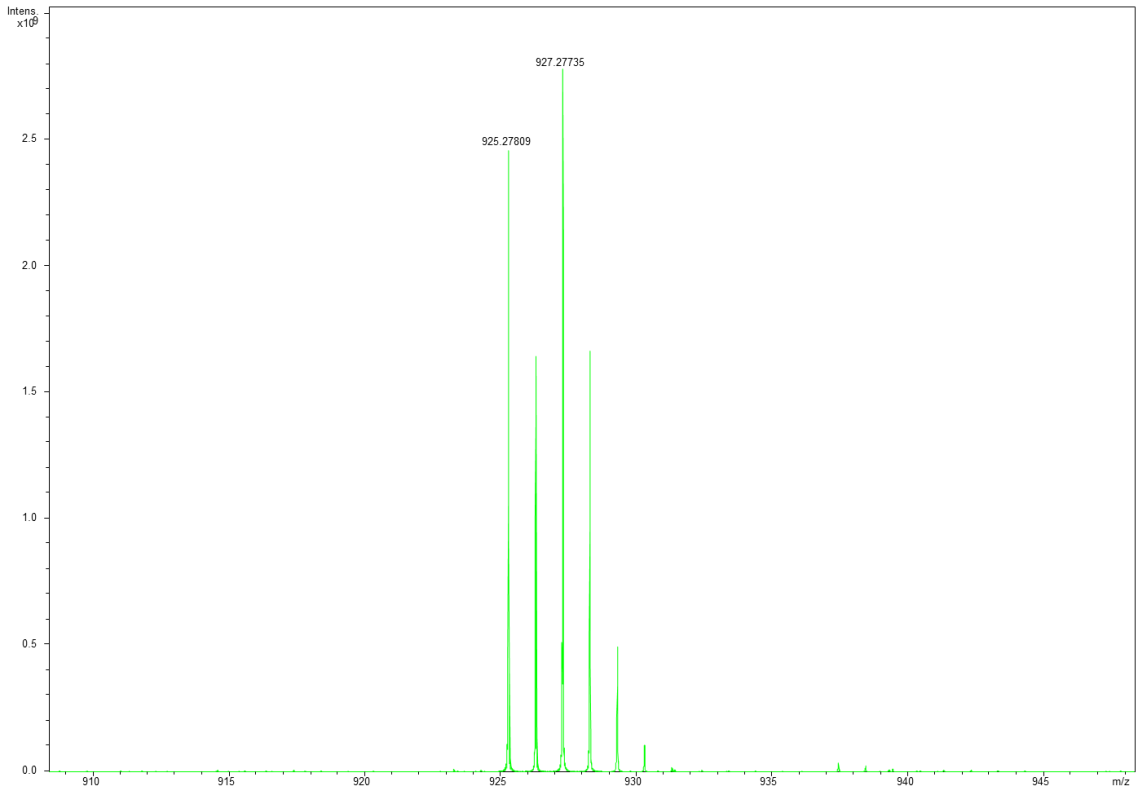

Figure S76. MS spectrum recorded for **2a**.

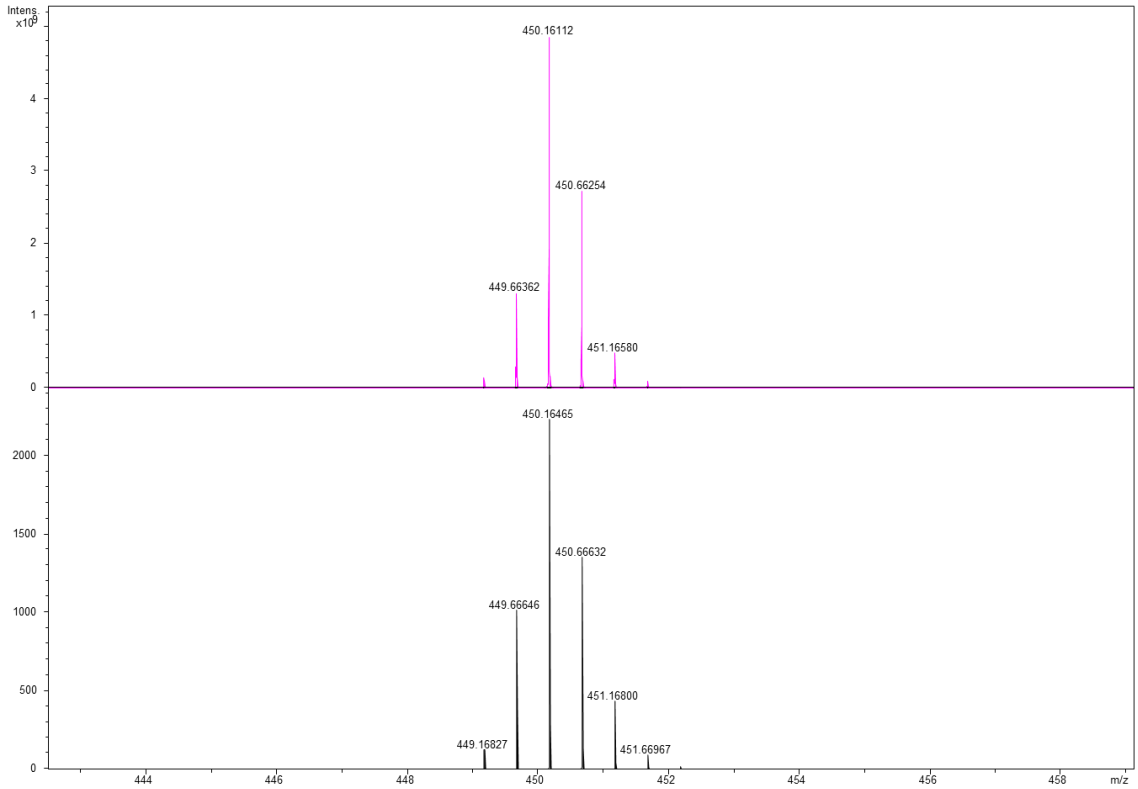

Figure S77. ESI-MS spectrum recorded for **3** (above) compared with simulated pattern (below).

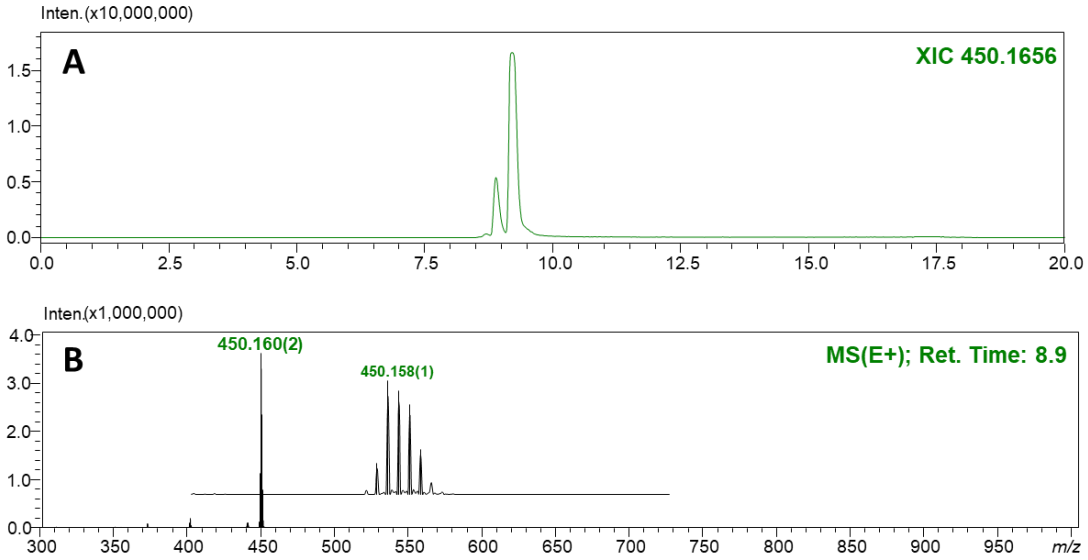

Figure S78. LC-MS analysis for compound **3** (A); ESI-MS spectra (B).

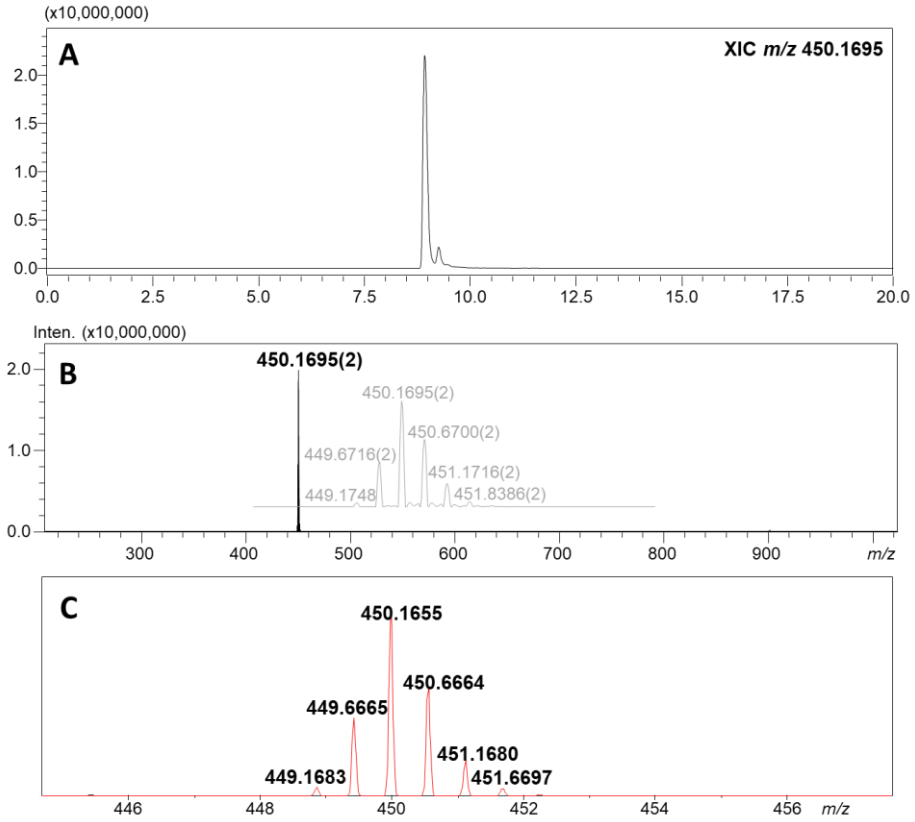

Figure S79. LC-MS analysis for compound **4** (A); ESI-MS spectra (B), simulated pattern (C).

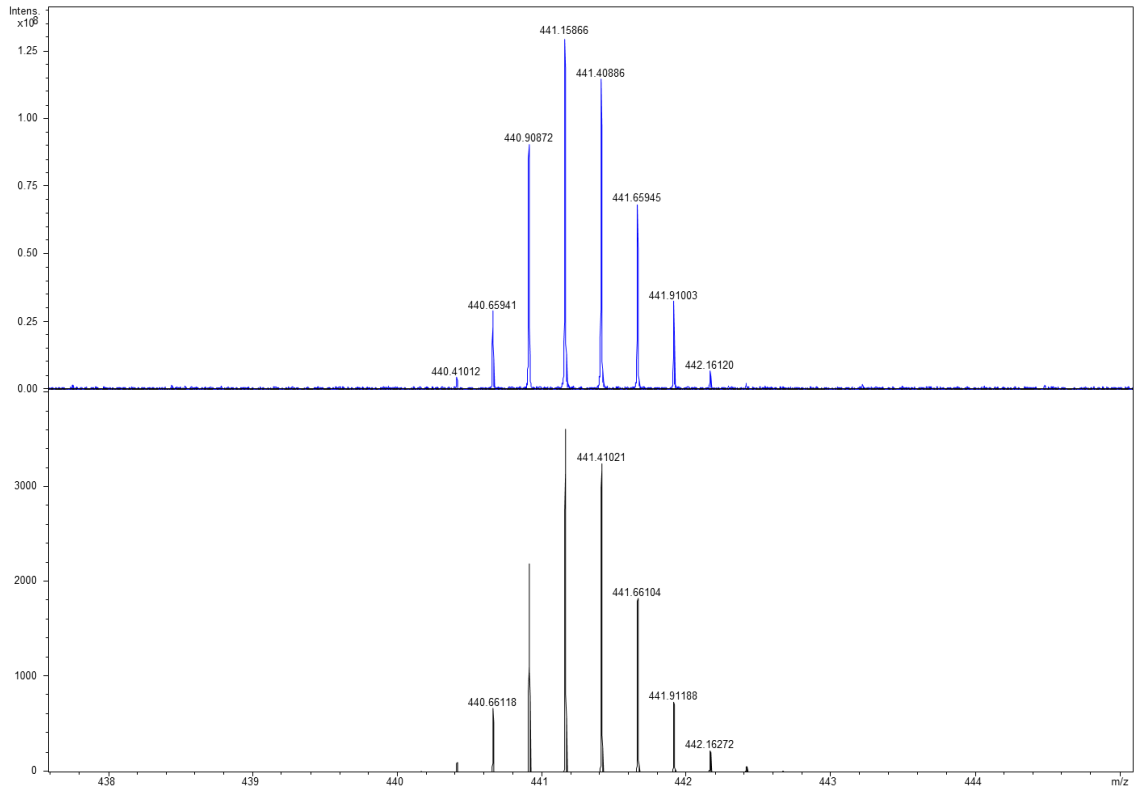

Figure S80. ESI-MS spectrum recorded for **3**-*O*-**3** (above) compared with simulated pattern (below).

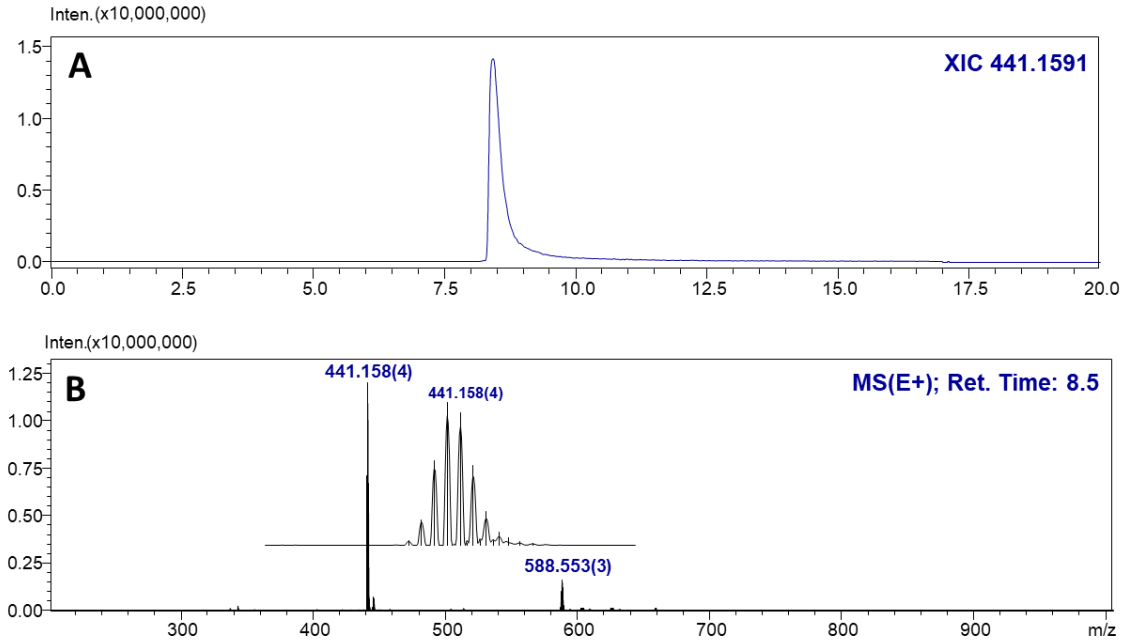

Figure S81. LC-MS analysis for compound **3**-*O*-**3** (A); ESI-MS spectra (B).

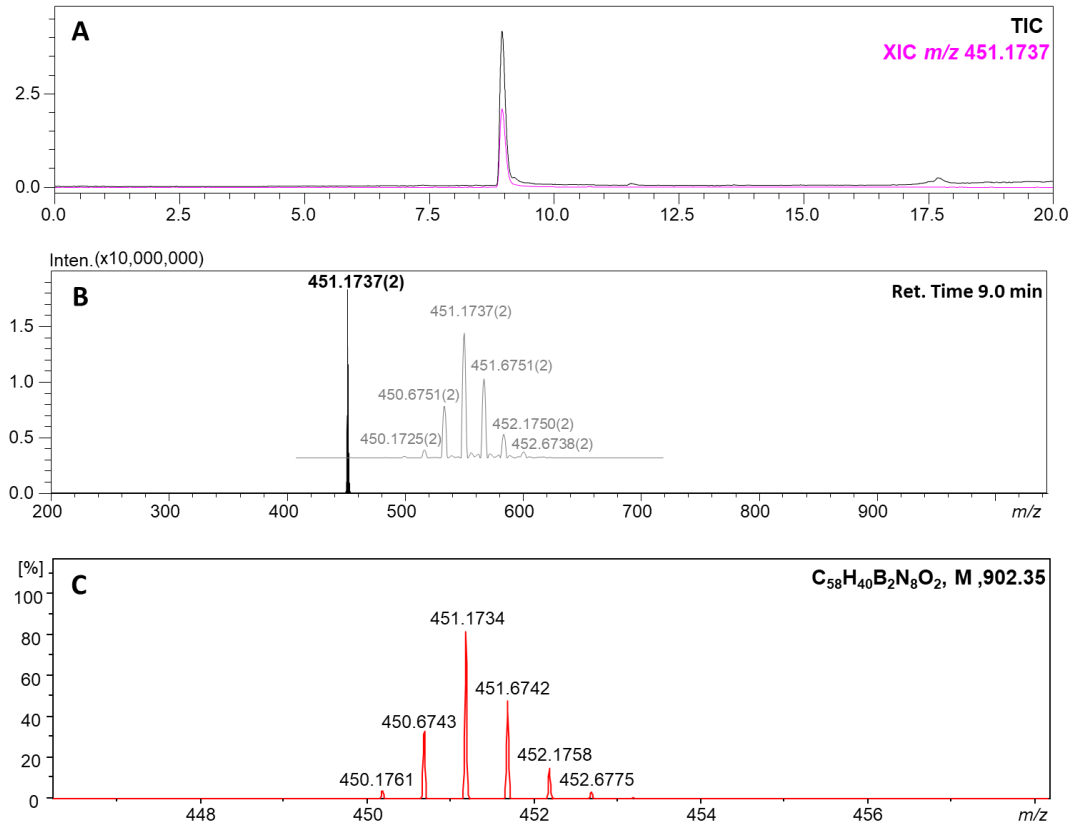

Figure S82. LC-MS analysis for compound **5** (A); ESI-MS spectra (B), simulated pattern (C).

5. UV-VIS spectra.

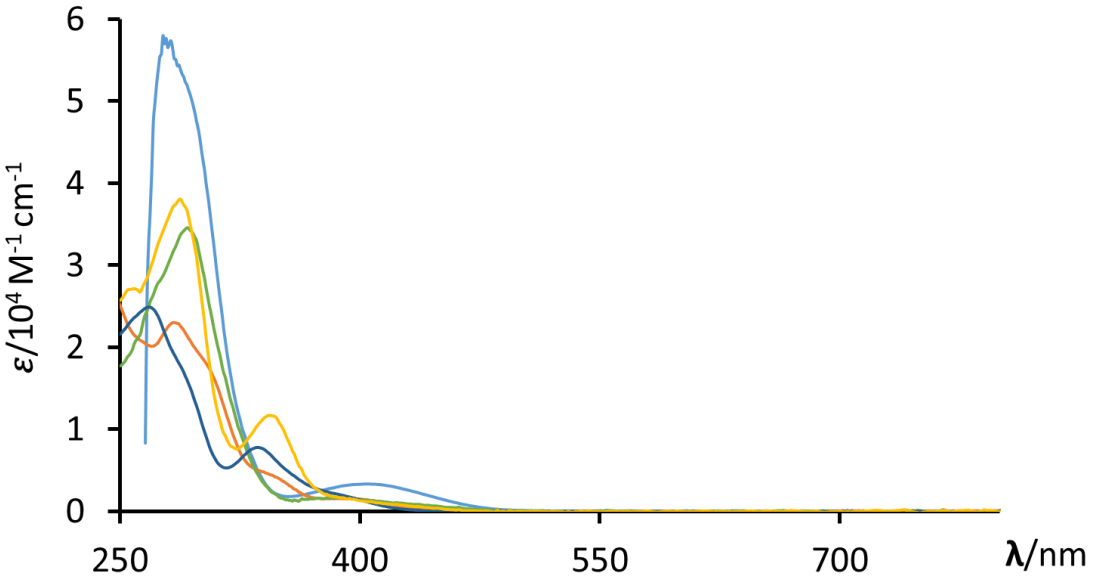

Figure S83. Extinction spectrum for macrocycles **1a-e**; **1a** (orange), **1b** (blue), **1c** (green), **1d** (cyan), **1e** (yellow) (CH_2Cl_2, 295 K).

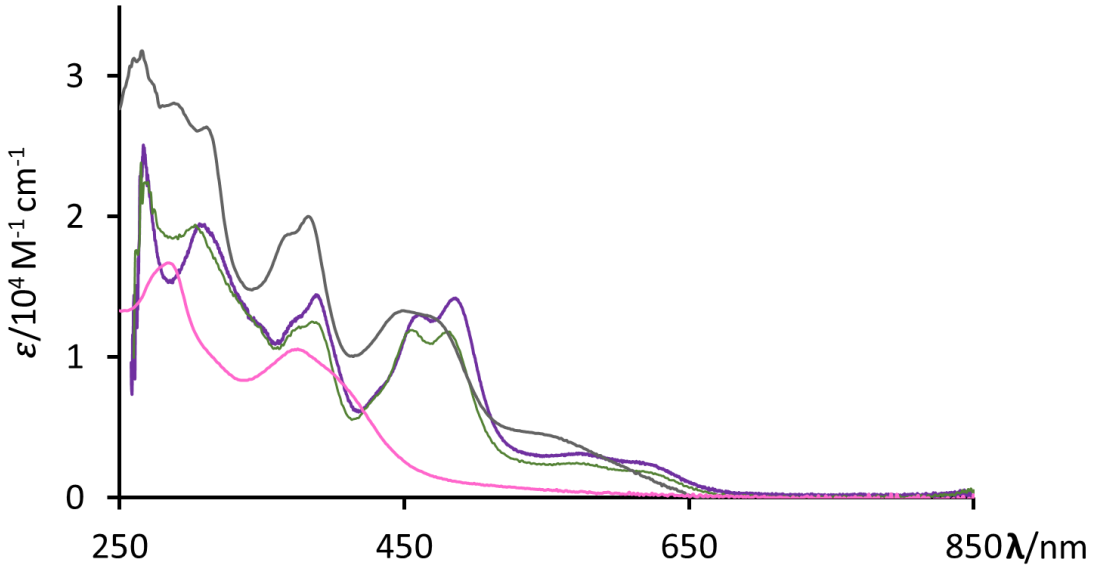

Figure S84. Extinction spectrum for boron(III) complexes, structures **3**, **4**, **3**-*O*-**3** and **5**; **3** (purple), **4** (grey), **3**-*O*-**3** (dark green), and **5** (pink), (CH_2Cl_2, 295 K).

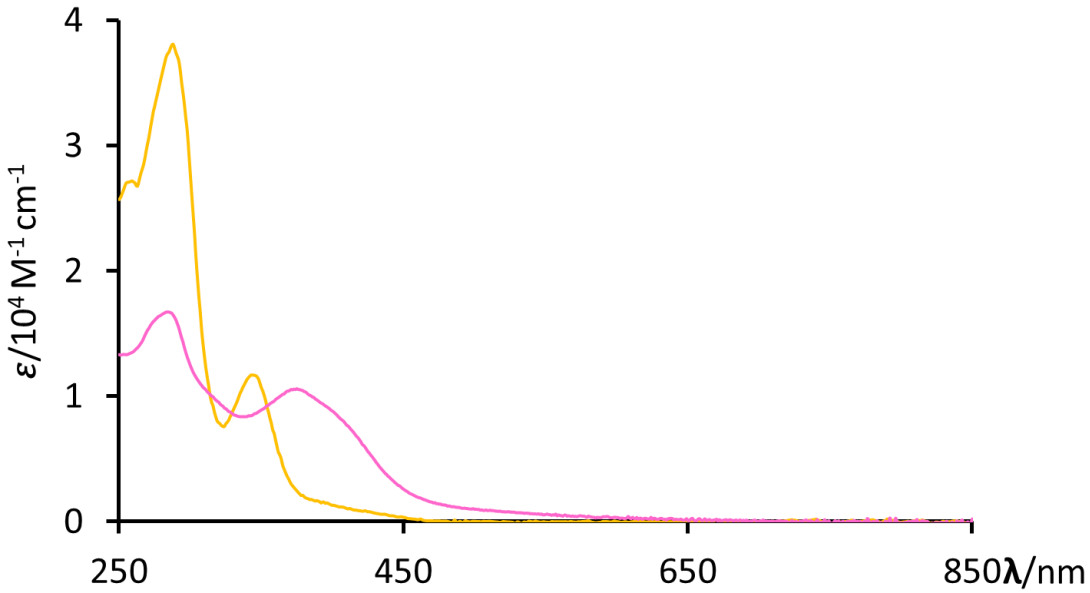

Figure S85. Extinction spectrum for structures **1e** and **5**; **1e** (yellow), **5** (pink) (CH_2Cl_2, 295 K).

6. Emission spectra.

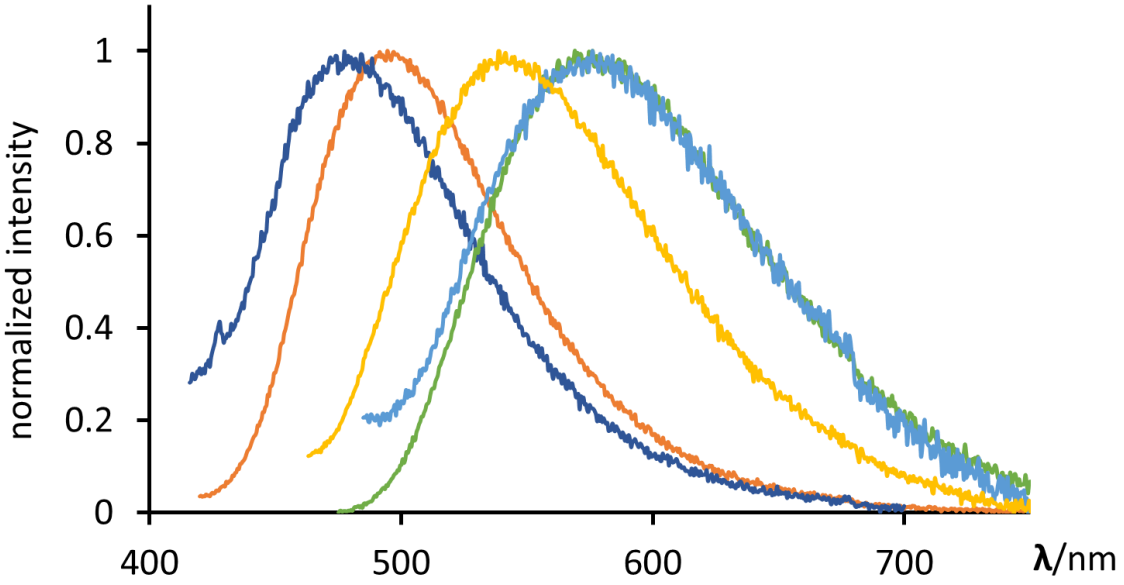

Figure S86. Normalized emission spectrum for the monomers **1a-1e**; **1a** (orange), **1b** (blue), **1c** (green), **1d** (cyan), **1e** (yellow) (CH_2Cl_2, 295 K).

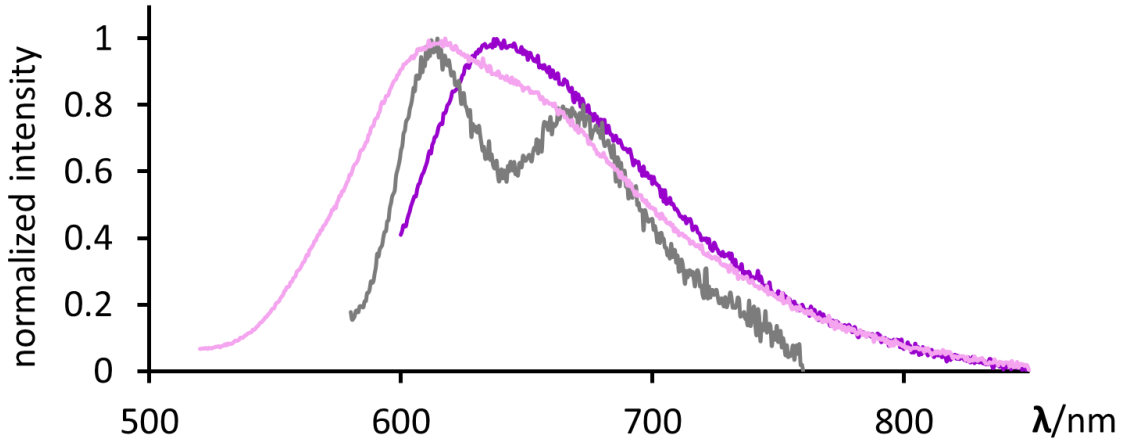

Figure S87. Normalized emission spectrum for the boron complexes **3**, **4** and **5**, **3** (purple), **4** (grey), **5** (pink).

Table S1. Emission properties for macrocycles **1a-e** and boron(III) complexes **3-5**.

Structure	$\lambda_{emission}$[a]	$\lambda_{exitation}$[b]	Φ[c]
-	nm	nm	%
1a	495	290	8.49
1b	478	270	5.45
1c	576	290	<1
1d	576	310	<1
1e	539	280	3.00
3	637	575	<1
4	615	425	<1
5	618	350	2.62

[a] Emission maxima. [b] Excitation wavelength. [c] Quantum yield.

7. Lifetime measurements.

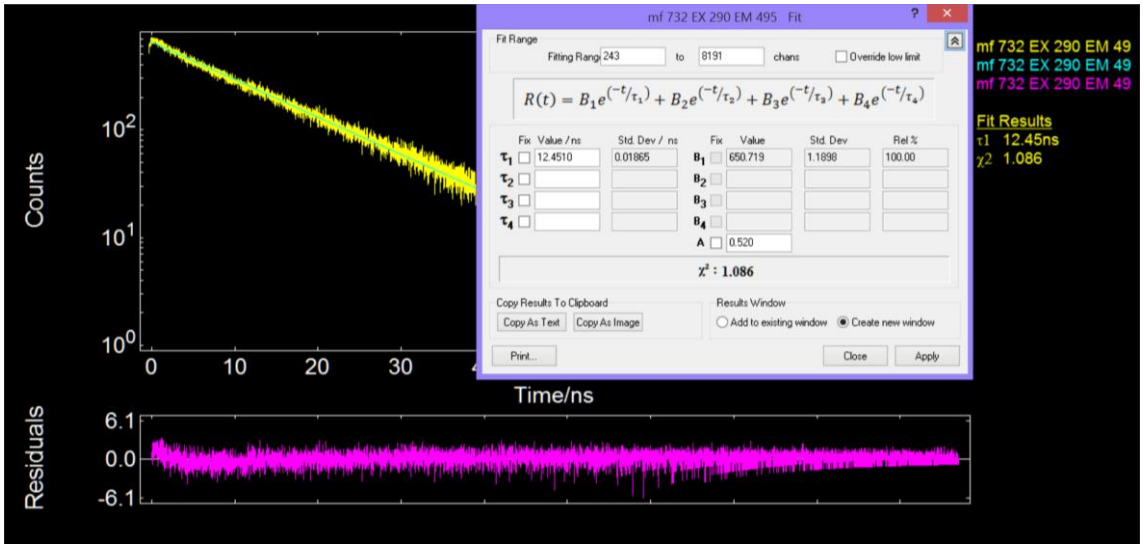

Figure S88. Linear fitting for **1a**.

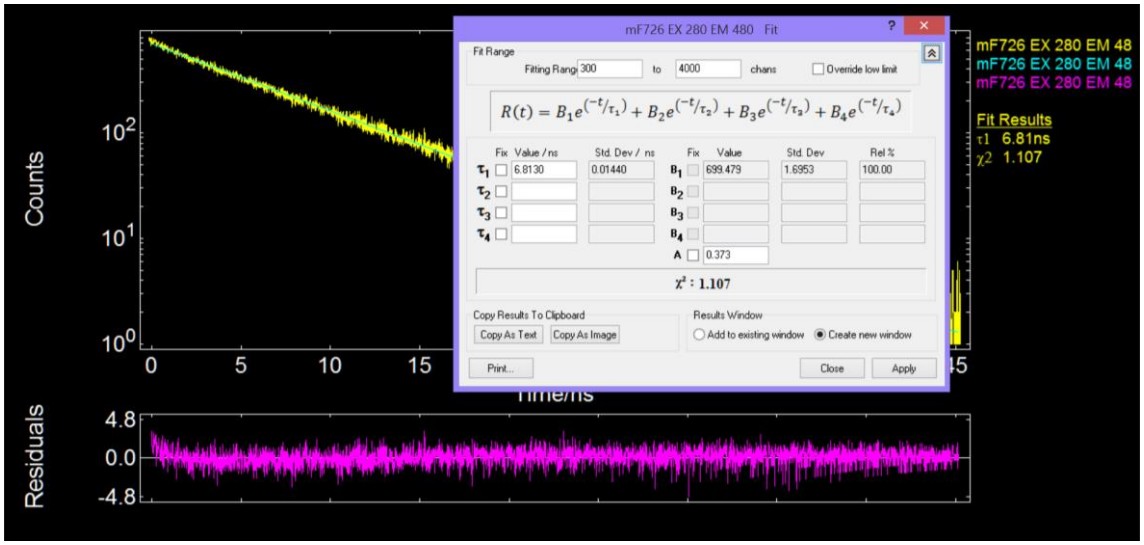

Figure S89. Linear fitting for **1b**.

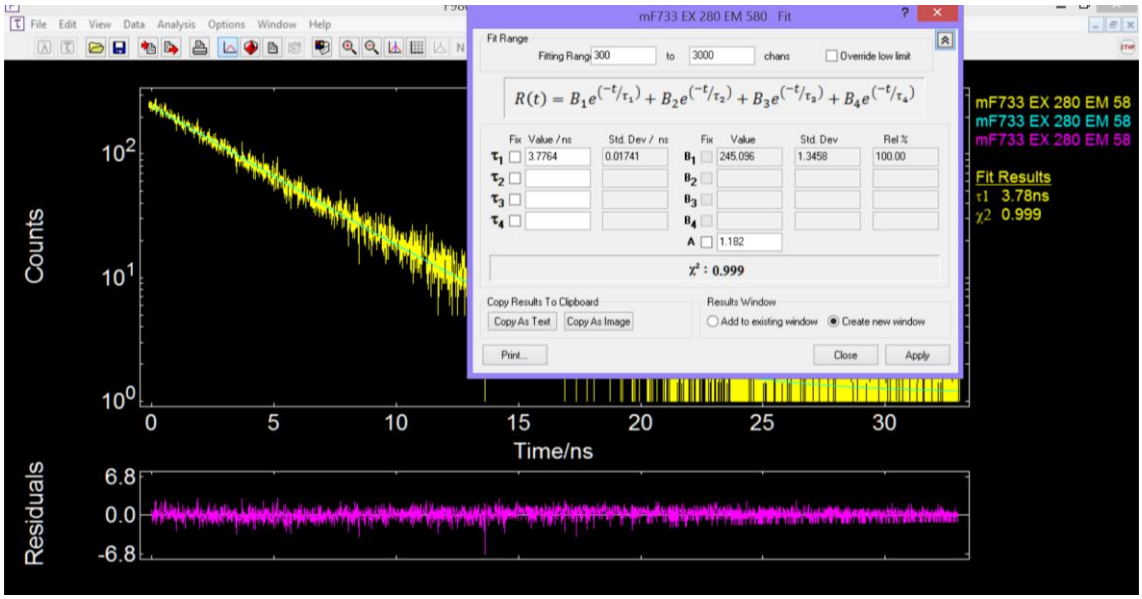

Figure S90. Linear fitting for **1c**.

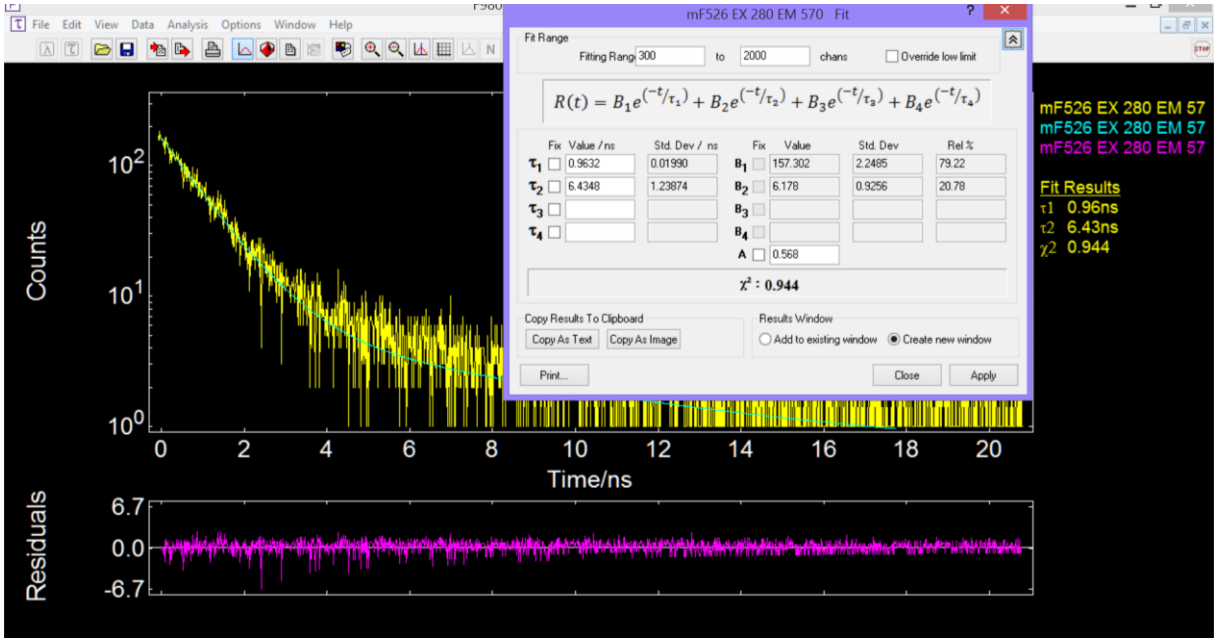

Figure S91. Linear fitting for **1d**.

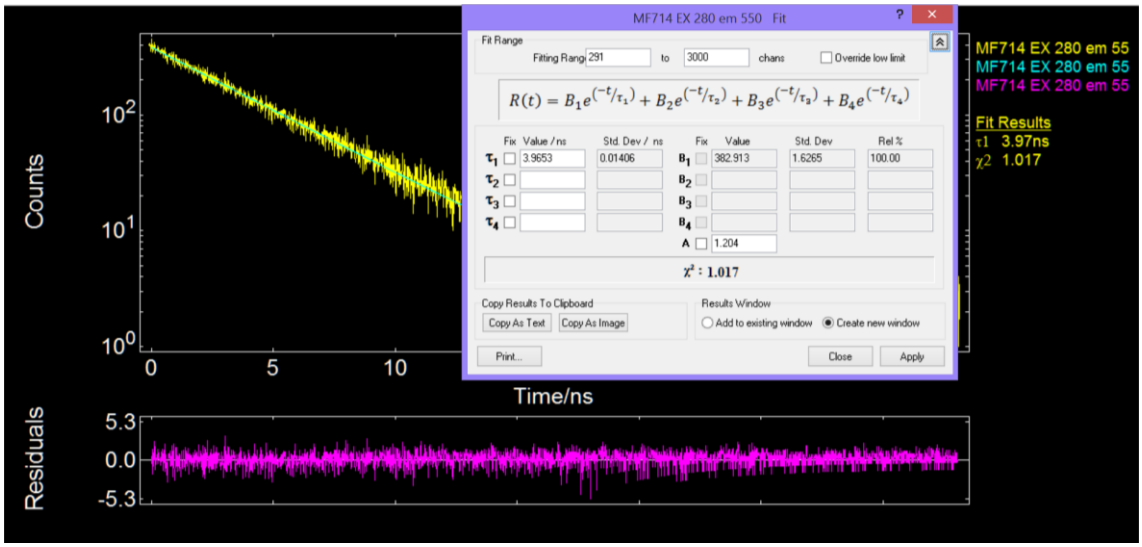

Figure S92. Linear fitting for **1e**.

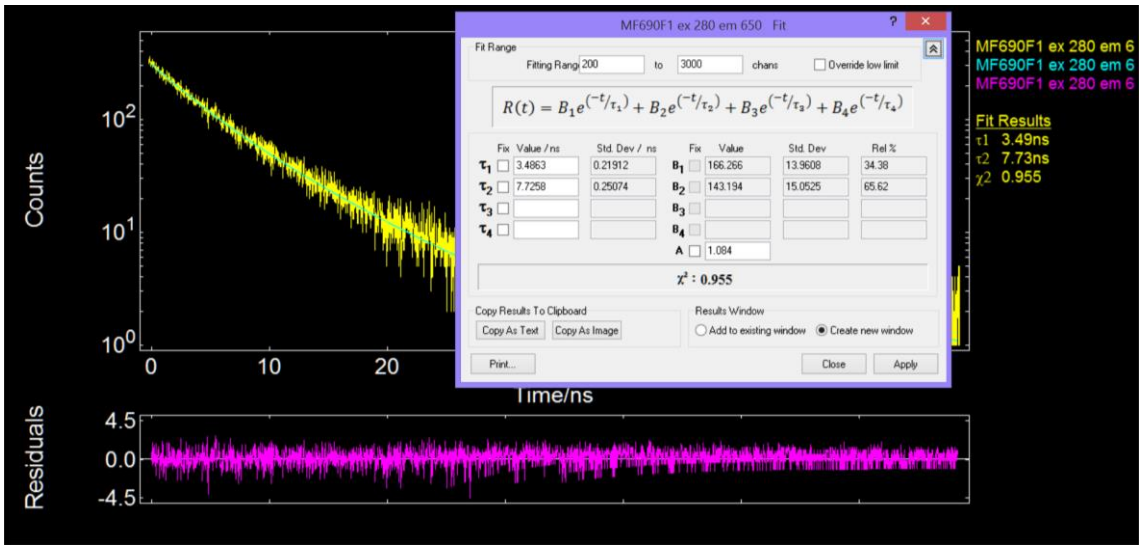

Figure S93. Linear fitting for **3**.

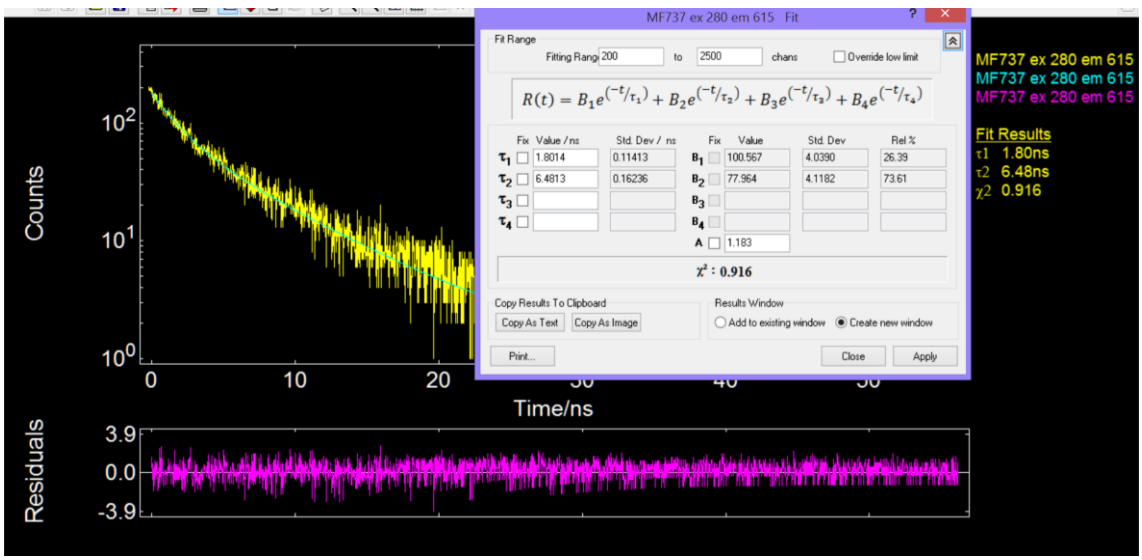

Figure S94. Linear fitting for **4**.

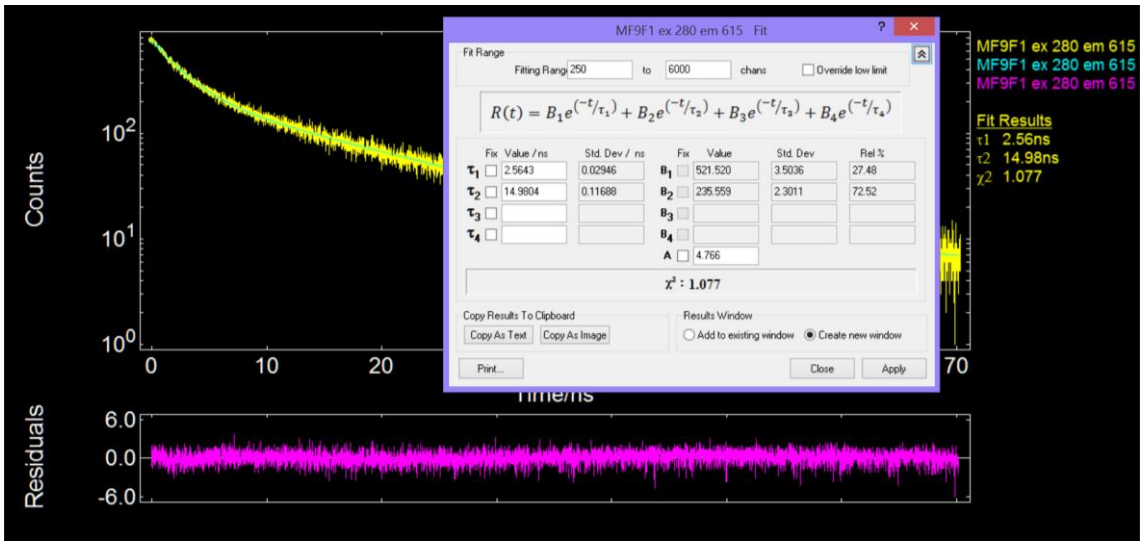

Figure S95. Linear fitting for **5**.

8. Theoretical calculations.

8.1. Optimization details.

Table S2. optimization details for macrocycles **1a-e** and boron(III) complexes **3-5**.

Structure	Code[a]	SCF *E*[b]	ZPV[c]	lowest freq. [d]	*G*[e]
		a.u.	a.u.	cm^{-1}	a.u.
1a	1a	-1379.290953	0.445233	21.63	-1378.845720
1b	1b	-1395.340741	0.433302	21.42	-1394.907439
1c	1c	-1395.346751	0.433585	21.85	-1394.913167
1d	1d	-1411.388286	0.421073	15.06	-1410.967213
1e	1e	-1411.393268	0.421353	19.58	-1410.971915
3	3	-2871.291011	0.842435	13.40	-2870.448575
4	4	-2871.293229	0.841793	12.68	-2870.451436
3-***O***-3	3-*O*-3	-5589.688333	1.634899	13.64	-5588.053434
5	5	-2872.462636	0.862617	10.17	-2871.600019

[a] Optimized geometry available as <code>.pdb file. [b] Electronic energy. [c] Zero-point vibrational energy. [d] Lowest vibrational frequency. [e] Gibbs free energy.

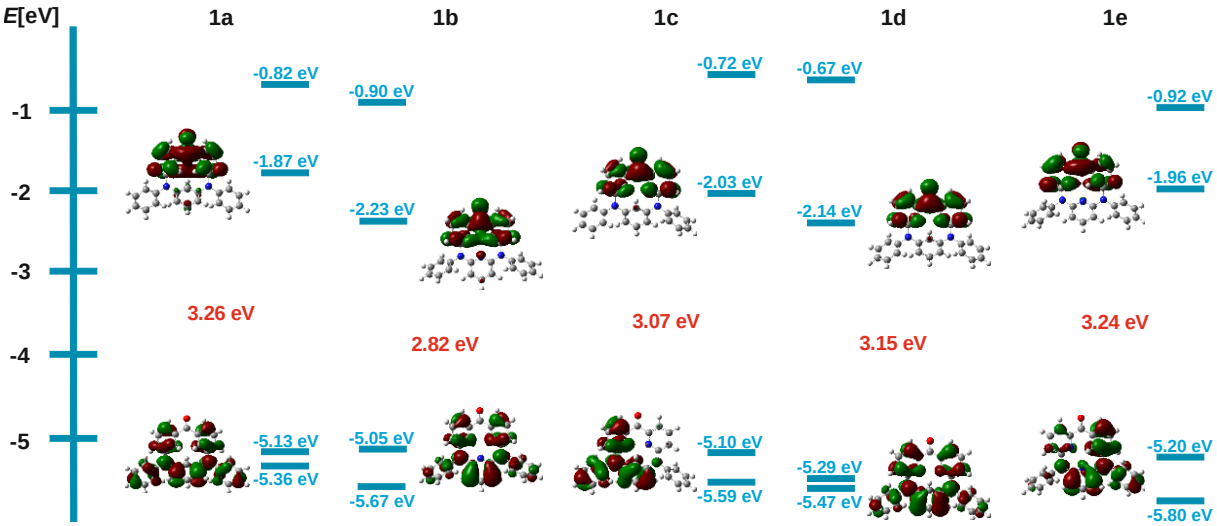

Figure S96. graphic representation of the frontier orbitals for **1a-e** with calculated energies (H+1, H, L, L-1).

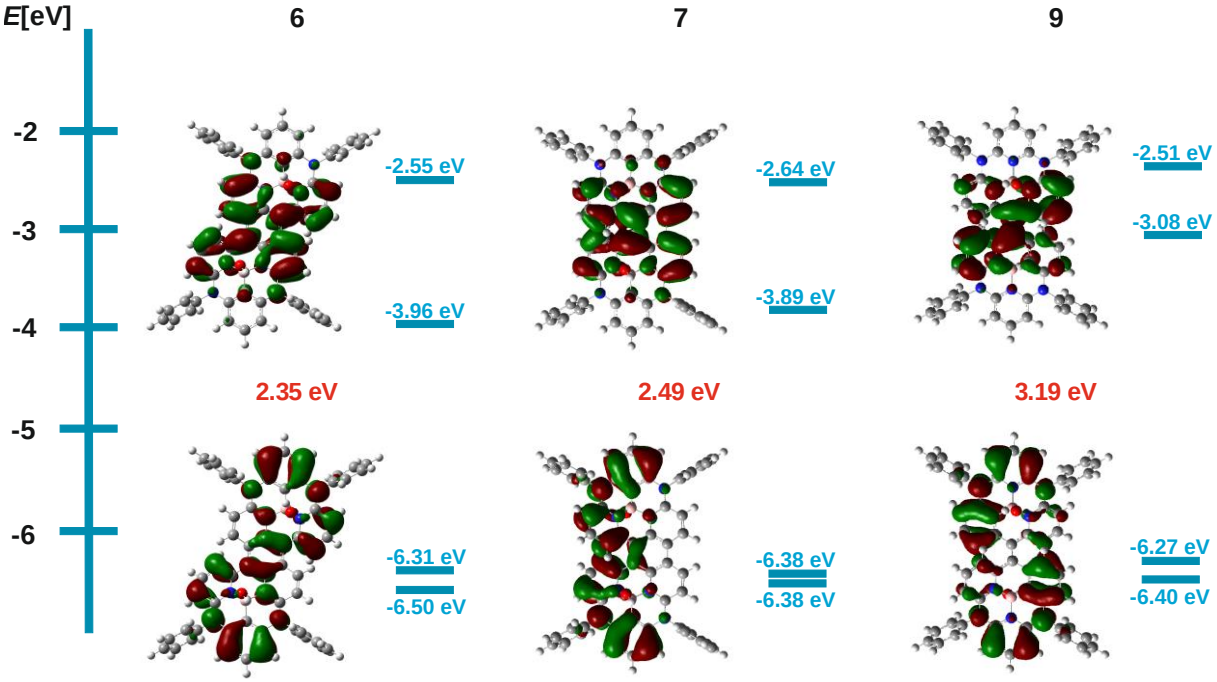

Figure S97. graphic representation of the frontier orbitals for **3**, **4** and **5** with calculated energies (H+1, H, L, L-1).

8.2. TD-DFT predicted UV Vis transitions.

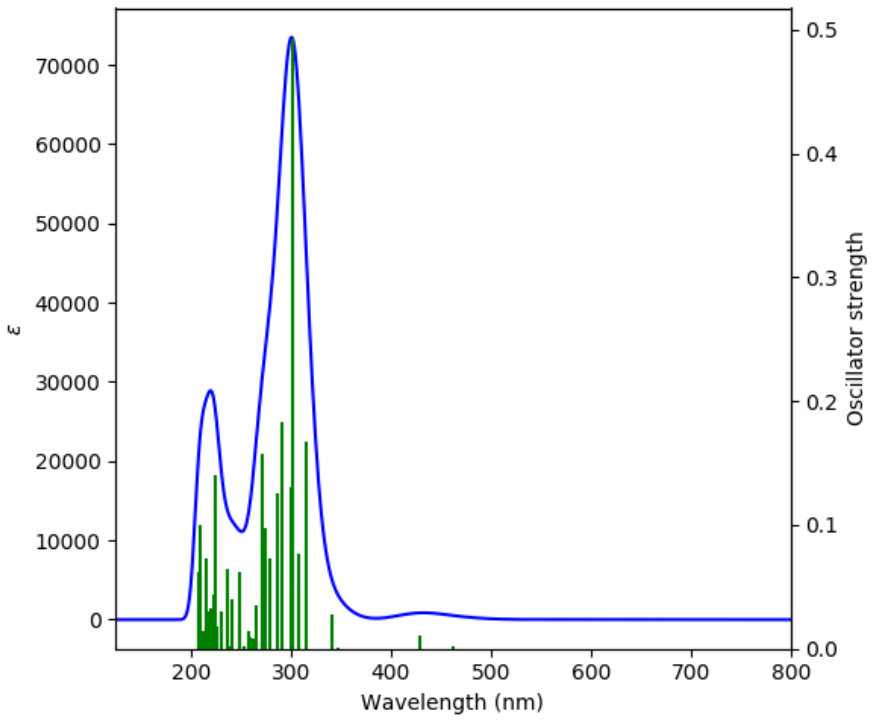

Figure S98. TD-DFT predicted absorption spectra for **1a** (solvent dichloromethane).

Table S3. UV-Vis transitions (oscillator strength > 0.01) calculated with TD-DFT for **1a**.

No.	Energy (cm-1)	Wavelength (nm)	Osc. Strength	Major contribs
1	21590.66	463.1633	0.0026	HOMO->LUMO (99%)
2	23282	429.5164	0.0108	H-1->LUMO (99%)
4	29255.34	341.8179	0.0278	H-2->LUMO (16%), HOMO->L+1 (66%)
5	31707.27	315.3851	0.1671	H-1->L+1 (97%)
6	32411.39	308.5335	0.0509	HOMO->L+2 (93%)
7	32495.27	307.7371	0.0772	H-1->L+2 (79%)
8	33079.22	302.3046	0.493	HOMO->L+3 (82%)
9	33234.88	300.8887	0.13	HOMO->L+4 (86%)
10	34259.21	291.8923	0.1834	H-6->LUMO (37%), H-2->LUMO (34%)
11	34853.64	286.9141	0.1259	HOMO->L+5 (78%)
14	35723.1	279.9309	0.0727	H-1->L+3 (77%)
15	36411.09	274.6416	0.097	H-9->LUMO (10%), H-3->LUMO (63%)
18	36857.92	271.3121	0.158	H-4->LUMO (90%)
19	37712.87	265.1615	0.0352	H-5->LUMO (97%)
23	38831.56	257.5225	0.0144	H-10->LUMO (18%), H-8->LUMO (70%)
25	40113.98	249.2896	0.0208	HOMO->L+8 (81%)
26	40259.16	248.3907	0.0624	H-10->LUMO (75%), H-8->LUMO (19%)
27	41547.23	240.6899	0.0406	H-2->L+1 (36%), HOMO->L+9 (45%)
29	42266.68	236.593	0.0649	H-2->L+1 (43%), HOMO->L+9 (43%)

30	43390.21	230.4667	0.0306	H-1->L+9 (83%)
31	44200.8	226.2403	0.0182	H-4->L+1 (14%), H-2->L+2 (14%), HOMO->L+10 (61%)
33	44593.59	224.2475	0.1403	H-3->L+1 (60%)
34	44683.12	223.7982	0.0435	H-4->L+1 (50%)
37	45383.2	220.3458	0.0325	H-5->L+1 (46%), H-4->L+1 (18%), H-2->L+4 (10%)
38	45603.39	219.2819	0.0251	H-5->L+1 (36%), H-2->L+4 (38%)
39	45752.61	218.5668	0.0299	H-4->L+2 (15%), H-2->L+3 (17%), H-1->L+10 (51%)
43	46254.28	216.1962	0.073	H-9->L+1 (32%), H-4->L+2 (32%), H-3->L+1 (18%)
45	47111.65	212.2617	0.0146	H-8->L+1 (26%), H-3->L+2 (39%), H-2->L+5 (21%)
47	47681.88	209.7233	0.0994	H-5->L+2 (60%), H-5->L+4 (13%)
48	47770.61	209.3337	0.0268	H-6->L+2 (41%), H-6->L+4 (14%)
49	47967.41	208.4749	0.0626	H-11->LUMO (46%), H-8->L+1 (19%), H-6->L+2 (11%)
50	48031.93	208.1948	0.0322	H-9->L+1 (13%), H-4->L+4 (49%)

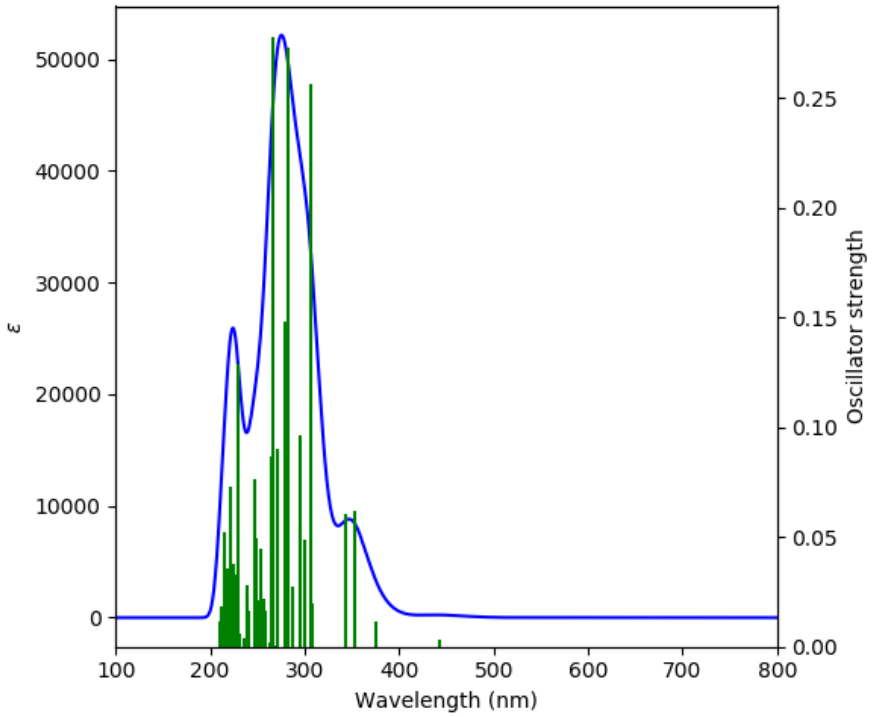

Figure S99. TD-DFT predicted absorption spectra for **1b** (solvent dichloromethane).

Table S4. UV-Vis transitions (oscillator strength > 0.01) calculated with TD-DFT for **1b**.

No.	Energy (cm-1)	Wavelength (nm)	Osc. Strength	Major contribs
1	22604.4944272	442.389898709	0.0033	HOMO->LUMO (99%)
2	26662.2697595	375.061841704	0.0114	H-1->LUMO (98%)
3	28314.8997845	353.170948021	0.0618	H-2->LUMO (10%), HOMO->L+1 (85%)
4	29159.3622716	342.943028275	0.0602	H-5->LUMO (22%), H-3->LUMO (10%), H-2->LUMO (46%), HOMO->L+1 (12%)
5	32423.4880458	308.418390578	0.0197	HOMO->L+2 (89%)
6	32573.5071696	306.997952291	0.2561	HOMO->L+3 (95%)
7	33320.3765708	300.116656207	0.0486	H-1->L+1 (86%)
8	33794.6305751	295.904995256	0.0962	HOMO->L+4 (88%)
9	33939.8103723	294.639241949	0.0554	H-5->LUMO (24%), H-3->LUMO (26%), H-2->LUMO (38%)
10	34828.6333531	287.120080154	0.0277	H-1->L+2 (14%), HOMO->L+6 (76%)
11	35383.5428002	282.617262394	0.2732	HOMO->L+5 (88%)
12	35855.3771412	278.898195956	0.1483	H-1->L+2 (64%), H-1->L+5 (11%), HOMO->L+6 (15%)
13	36911.1568888	270.920795849	0.0905	H-9->LUMO (16%), H-5->LUMO (18%), H-3->LUMO (46%)

15	37452.3549106	267.005907208	0.278	H-4->LUMO (75%), HOMO->L+7 (11%)
16	37658.8328444	265.541952437	0.0868	H-1->L+3 (91%)
18	38753.3272046	258.042359749	0.0164	H-1->L+5 (65%)
19	38974.3231181	256.57918342	0.022	H-6->LUMO (91%)
21	39459.06233	253.427208087	0.0445	H-1->L+4 (10%), HOMO->L+8 (67%)
22	39926.0573444	250.462997479	0.0212	H-8->LUMO (66%), H-1->L+6 (16%)
23	40080.9157947	249.495297244	0.0497	H-9->LUMO (20%), H-7->LUMO (41%), H-2->L+1 (17%)
25	40530.1666117	246.729802416	0.0761	H-9->LUMO (38%), H-2->L+1 (21%), H-1->L+7 (13%)
26	41452.058324	241.242543901	0.0164	H-10->LUMO (92%)
27	41748.0637995	239.532066637	0.0279	H-2->L+1 (28%), H-1->L+7 (50%)
28	41828.7192424	239.070193425	0.0241	H-4->L+1 (54%), H-1->L+8 (10%)
32	43579.7489077	229.464378539	0.1285	H-5->L+1 (12%), H-3->L+1 (66%), H-2->L+3 (12%)
33	43893.4985806	227.824172676	0.0103	H-2->L+2 (81%)
34	44241.9300939	226.029921813	0.0332	H-5->L+1 (18%), H-4->L+2 (10%), H-3->L+1 (16%), H-2->L+3 (40%)
35	44561.3256478	224.409840924	0.0375	H-5->L+1 (49%)
37	44902.4981713	222.704758249	0.0186	H-6->L+1 (11%), H-6->L+3 (13%), HOMO->L+10 (16%)
38	44918.6292599	222.62478096	0.0117	H-7->L+1 (18%), H-6->L+2 (12%), H-4->L+2 (25%), H-4->L+5 (11%)
39	45104.1367785	221.709153843	0.0726	H-5->L+1 (11%), H-4->L+2 (15%), H-2->L+3 (37%)
41	45342.8768895	220.541806916	0.0102	H-6->L+1 (23%), H-2->L+5 (16%), H-1->L+9 (27%)
42	45665.4986611	218.983703084	0.0359	H-2->L+4 (69%)
43	46317.1946398	215.902540682	0.0521	H-2->L+5 (32%), H-1->L+9 (16%)
47	47037.4477449	212.596568892	0.0145	H-4->L+3 (18%), H-3->L+4 (14%), H-1->L+9 (11%)
48	47272.1550837	211.541022031	0.0172	H-4->L+3 (16%), H-3->L+2 (44%)
49	47289.8992811	211.461647244	0.0182	H-3->L+3 (12%), H-2->L+6 (76%)
50	47674.6257438	209.755186202	0.0115	H-10->L+1 (24%), H-5->L+4 (13%), H-2->L+7 (20%)

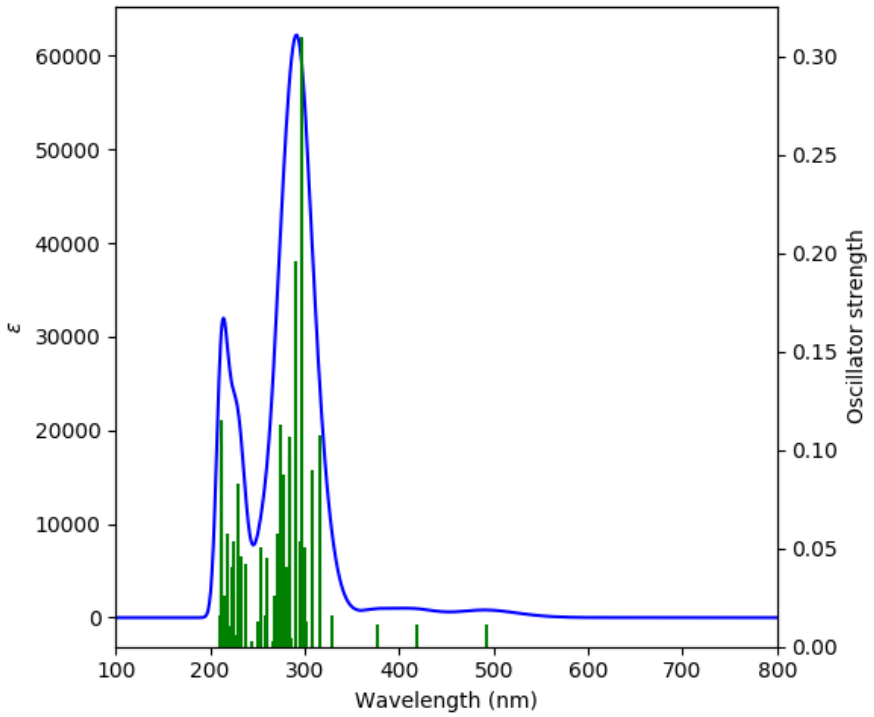

Figure S100. TD-DFT predicted absorption spectra for **1c** (solvent dichloromethane).

Table S5. UV-Vis transitions (oscillator strength > 0.01) calculated with TD-DFT for **1c**.

	Energy (cm-1)	Wavelength (nm)	Osc. Strength	Major contribs
1	20306.6208589	492.45022446	0.0111	HOMO->LUMO (99%)
2	23911.1126021	418.215587304	0.0117	H-1->LUMO (97%)
3	26521.9292888	377.04647694	0.0117	H-2->LUMO (83%)
4	30339.3514013	329.604936762	0.0162	HOMO->L+1 (85%)
5	31648.3892395	315.971846918	0.1073	HOMO->L+2 (80%)
6	32511.4024786	307.584393094	0.0896	HOMO->L+3 (16%), HOMO->L+4 (63%)
7	33055.0201637	302.525908333	0.0125	H-10->LUMO (20%), H-7->LUMO (16%), H-6->LUMO (38%)
8	33354.2518569	299.811851362	0.0504	HOMO->L+3 (66%), HOMO->L+4 (16%)
9	33600.2509577	297.616824725	0.31	HOMO->L+5 (80%)
10	33949.4890255	294.555243306	0.054	H-3->LUMO (55%), H-1->L+1 (25%)
11	34429.3889107	290.449535016	0.1956	H-3->LUMO (28%), H-1->L+1 (60%)
13	35185.1304107	284.210968761	0.0968	H-4->LUMO (13%), H-1->L+3 (15%), HOMO->L+7 (56%)
14	35268.2055169	283.54150299	0.1066	H-4->LUMO (20%), H-1->L+3 (31%), HOMO->L+7 (19%)

15	35570.6634278	281.130545128	0.0403	H-1->L+3 (14%), HOMO->L+6 (59%)
16	36090.08448	277.084416511	0.0877	H-1->L+2 (69%), HOMO->L+7 (10%)
17	36490.9420312	274.040609624	0.1126	H-5->LUMO (21%), H-4->LUMO (13%), H-1->L+4 (46%)
18	36824.8555649	271.55571547	0.0572	H-5->LUMO (53%), H-1->L+4 (27%)
19	37103.1168429	269.519136151	0.0126	H-8->LUMO (17%), H-7->LUMO (19%), H-6->LUMO (38%)
20	37226.5196705	268.625702551	0.0256	H-8->LUMO (48%), H-7->LUMO (26%)
23	38445.2234127	260.110336534	0.0451	H-10->LUMO (24%), H-9->LUMO (33%), H-8->LUMO (13%)
24	38721.0650274	258.257359216	0.0159	H-10->LUMO (10%), H-1->L+5 (27%), H-1->L+6 (40%), HOMO->L+8 (11%)
25	39525.1997931	253.003148683	0.0505	H-1->L+6 (11%), HOMO->L+8 (74%)
26	39855.887109	250.903962384	0.0128	H-2->L+1 (71%)
28	42193.2818443	237.004555296	0.0424	H-11->LUMO (31%), H-2->L+2 (35%)
29	43070.813063	232.175788866	0.0456	H-11->LUMO (23%), H-2->L+2 (10%), H-2->L+4 (23%), HOMO->L+9 (15%)
30	43242.6091564	231.253390928	0.0317	H-3->L+1 (11%), H-2->L+2 (18%), H-2->L+4 (20%), H-1->L+8 (23%)
31	43508.772118	229.838708683	0.0288	HOMO->L+9 (70%)
32	43595.0734419	229.383717253	0.083	H-11->LUMO (16%), H-2->L+4 (12%), H-1->L+8 (39%)
34	44598.4271516	224.223154014	0.0538	H-3->L+1 (41%)
36	44962.9897535	222.405139312	0.0407	H-4->L+1 (23%), H-3->L+4 (11%)
37	45128.3334114	221.59027919	0.0103	H-6->L+1 (10%), H-3->L+1 (10%), H-3->L+2 (12%), H-2->L+5 (17%)
39	45873.5897038	217.990352719	0.0575	H-4->L+1 (16%), H-3->L+2 (10%), H-1->L+9 (11%), HOMO->L+10 (17%)
41	46402.6894092	215.504750421	0.0263	H-2->L+6 (40%), HOMO->L+10 (14%)
45	47002.7659044	212.753437113	0.0537	H-12->LUMO (15%), H-6->L+1 (11%), H-3->L+2 (21%)
46	47114.0704156	212.250818318	0.027	H-12->LUMO (14%), H-3->L+2 (19%), H-1->L+9 (10%)
47	47148.7522561	212.094690135	0.1017	H-3->L+4 (25%)
48	47216.5028281	211.790357206	0.1151	H-3->L+3 (20%)
50	47581.06543	210.167635164	0.0159	H-8->L+1 (20%), H-7->L+1 (14%), H-6->L+1 (10%), H-3->L+5 (11%)

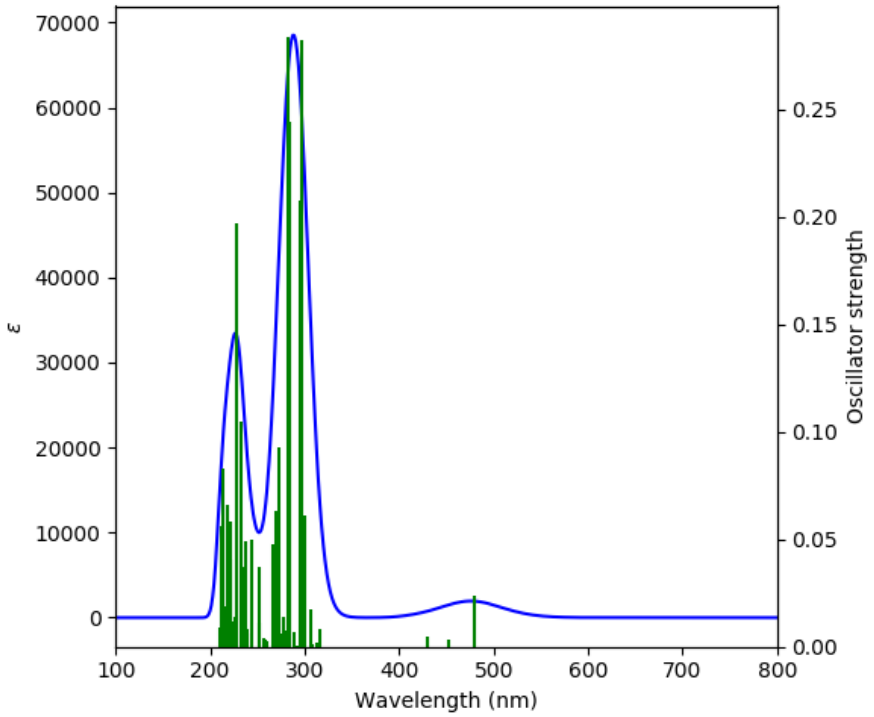

Figure S101. TD-DFT predicted absorption spectra for **1d** (solvent dichloromethane).

Table S6. UV-Vis transitions (oscillator strength > 0.01) calculated with TD-DFT for **1d**.

No.	Energy (cm-1)	Wavelength (nm)	Osc. Strength	Major contribs
1	20833.3009011	480.000747241	0.0241	HOMO->LUMO (97%)
7	32542.0515469	307.294700999	0.0177	HOMO->L+1 (79%)
8	33270.3701962	300.567740636	0.0614	H-1->L+1 (75%)
9	33694.6178259	296.78330384	0.2824	H-1->L+2 (58%), HOMO->L+3 (29%)
10	33793.0174662	295.919120274	0.2076	H-4->LUMO (11%), H-1->L+3 (13%), H-1->L+5 (11%), HOMO->L+4 (55%)
13	35207.7139347	284.028665381	0.2445	HOMO->L+5 (63%)
14	35409.352542	282.411263752	0.284	H-4->LUMO (12%), H-1->L+5 (51%), HOMO->L+5 (10%)
17	36074.7599459	277.202121788	0.0142	H-5->LUMO (96%)
19	36463.5191807	274.246705329	0.0061	H-6->LUMO (10%), H-2->L+2 (10%), H-1->L+3 (24%), H-1->L+6 (10%), HOMO->L+7 (30%)
20	36629.669393	273.002737008	0.0929	H-6->LUMO (62%), HOMO->L+7 (10%)
22	37166.8346427	269.057079951	0.0634	H-1->L+4 (28%), HOMO->L+6 (34%)
23	37264.4277287	268.35243715	0.0167	H-8->LUMO (29%), H-6->LUMO (11%), H-2->L+2 (32%)
24	37573.338075	266.146169394	0.0477	H-8->LUMO (47%), H-2->L+2 (33%)
28	39618.7601069	252.405677841	0.0373	H-10->LUMO (76%)

29	39801.8479623	251.244615815	0.0111	H-11->LUMO (43%), H-2->L+3 (16%), H-2->L+5 (17%)
30	40854.4014921	244.77166804	0.0498	HOMO->L+8 (74%)
33	42140.8558064	237.299404785	0.0493	H-12->LUMO (38%), H-2->L+3 (10%), H-2->L+5 (11%), H-1->L+8 (30%)
34	42461.0579147	235.509911696	0.0371	H-12->LUMO (15%), H-3->L+2 (17%), H-1->L+8 (50%)
35	43099.042468	232.023716244	0.1045	H-3->L+1 (79%)
36	43936.2459653	227.602513148	0.1971	H-3->L+2 (60%), H-1->L+8 (12%)
37	44171.7598586	226.388987715	0.0139	H-2->L+6 (17%), H-2->L+7 (65%)
39	44533.0962428	224.552093694	0.0119	HOMO->L+9 (63%)
41	45023.4813356	222.106325485	0.0409	H-3->L+3 (12%), H-3->L+5 (16%), H-1->L+9 (27%)
42	45050.9041862	221.971127564	0.0583	H-4->L+3 (10%), H-3->L+5 (12%), H-1->L+9 (10%), HOMO->L+9 (14%)
44	45810.6784583	218.289716209	0.0143	H-3->L+3 (55%), H-3->L+5 (13%)
45	45942.9533847	217.661235582	0.0659	H-4->L+1 (38%), H-3->L+4 (37%)
46	46389.7845384	215.564700279	0.0191	H-13->LUMO (30%), H-4->L+1 (14%), H-3->L+4 (37%)
48	46901.1400464	213.214433383	0.0832	H-5->L+1 (14%), H-4->L+2 (23%), H-3->L+5 (12%), H-2->L+8 (14%), HOMO->L+10 (10%)
49	47133.4277219	212.163648674	0.0559	H-2->L+8 (68%)

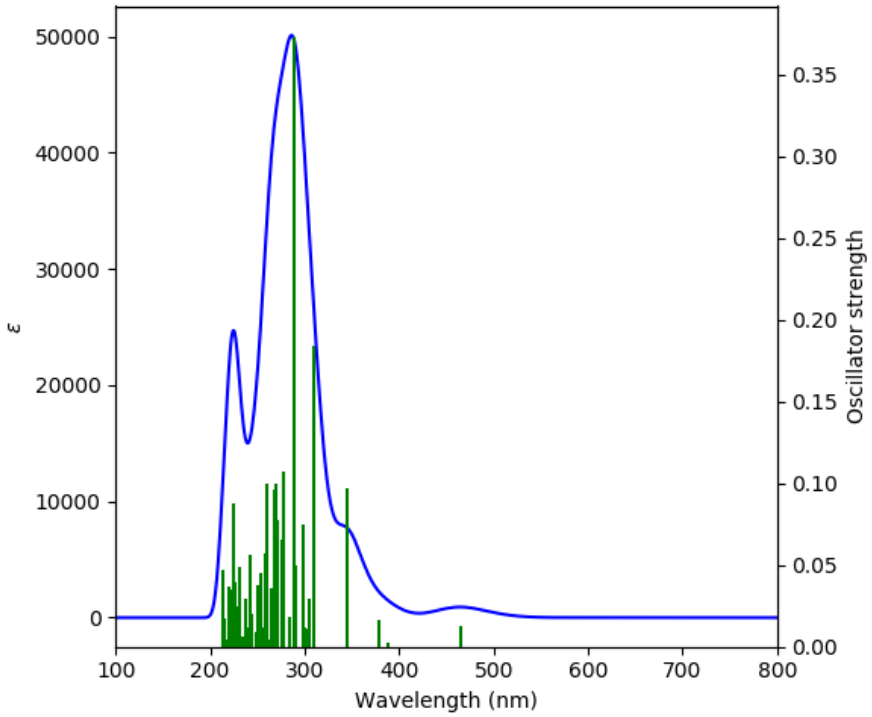

Figure S102. TD-DFT predicted absorption spectra for **1e** (solvent dichloromethane).

Table S7. UV-Vis transitions (oscillator strength > 0.01) calculated with TD-DFT for **1e**.

No.	Energy (cm-1)	Wavelength (nm)	Osc. Strength	Major contribs
1	21518.0656113	464.725788119	0.0126	HOMO->LUMO (99%)
3	26446.1131725	378.12739947	0.0164	H-2->LUMO (49%), H-1->LUMO (42%)
4	29001.2776036	344.812395395	0.0973	HOMO->L+1 (94%)
5	32287.1803473	309.720449182	0.1843	HOMO->L+2 (80%)
6	32714.6541947	305.673412914	0.0298	H-6->LUMO (39%)
7	33039.6956296	302.666226473	0.0108	HOMO->L+3 (74%)
8	33397.805796	299.420867978	0.0115	H-3->LUMO (18%), H-1->L+1 (18%), HOMO->L+3 (14%), HOMO->L+4 (34%)
9	33575.2477704	297.838457318	0.0744	H-3->LUMO (36%), HOMO->L+4 (45%)
10	34331.7958248	291.27517975	0.0493	H-3->LUMO (27%), H-1->L+1 (46%), HOMO->L+5 (16%)
11	34575.3752624	289.223180489	0.3731	H-1->L+1 (12%), HOMO->L+5 (61%)
12	35298.0480308	283.3017846	0.0179	HOMO->L+6 (70%)
13	35982.0061865	277.916688362	0.107	H-4->LUMO (61%)
14	36118.313885	276.867852465	0.0658	H-1->L+2 (11%), H-1->L+3 (13%), HOMO->L+7 (53%)

15	36778.075408	271.901122858	0.0778	H-1->L+2 (32%), H-1->L+3 (12%), HOMO->L+7 (25%)
16	37104.7299517	269.507418947	0.0993	H-1->L+2 (25%), H-1->L+3 (55%)
17	37351.535607	267.72660983	0.0958	H-2->L+1 (53%), H-1->L+2 (12%)
18	37750.7800493	264.895188574	0.0355	H-5->LUMO (83%)
20	38336.3385648	260.84911534	0.0993	H-8->LUMO (13%), H-7->LUMO (14%), H-1->L+4 (42%)
21	38587.9835466	259.148032131	0.0572	H-8->LUMO (54%), H-7->LUMO (10%), H-6->LUMO (13%), H-1->L+4 (11%)
22	39138.0536672	255.505807341	0.0115	H-9->LUMO (60%)
23	39472.7737553	253.339176568	0.0451	H-1->L+5 (24%), HOMO->L+8 (39%)
24	39506.6490413	253.121948904	0.0196	H-9->LUMO (15%), H-1->L+5 (36%), HOMO->L+8 (26%)
25	39881.6968508	250.741587988	0.0373	H-11->LUMO (22%), H-1->L+6 (23%), HOMO->L+8 (10%)
27	40847.1425023	244.815166678	0.0203	H-3->L+1 (16%), H-2->L+2 (41%)
28	41118.9513448	243.196863561	0.056	H-3->L+1 (33%), H-2->L+1 (10%), H-2->L+2 (17%)
30	41885.9846068	238.743343242	0.012	H-1->L+7 (68%)
31	42169.8917658	237.136012953	0.0298	H-12->LUMO (22%), H-10->LUMO (21%), H-2->L+3 (23%)
33	43253.094364	231.197331591	0.0491	H-12->LUMO (26%), H-11->LUMO (19%), H-1->L+8 (11%)
34	43649.1125886	229.09973209	0.0247	H-3->L+2 (43%), H-3->L+3 (10%), H-2->L+2 (12%)
35	43908.0165603	227.748843682	0.0134	H-4->L+1 (23%), H-2->L+5 (40%)
36	44199.9892636	226.244398847	0.0397	H-4->L+1 (20%), H-2->L+5 (21%), H-1->L+8 (17%)
37	44270.159499	225.885791088	0.0158	H-6->L+1 (31%)
38	44533.0962428	224.552093694	0.0875	H-4->L+1 (21%), H-1->L+8 (28%), HOMO->L+9 (22%)
40	44708.1185539	223.673022338	0.032	H-7->L+1 (11%), H-4->L+2 (14%)
41	44810.5509664	223.161728306	0.0348	H-8->L+1 (10%), H-6->L+1 (19%), HOMO->L+9 (17%)
44	45578.3907828	219.402217328	0.0368	H-3->L+2 (16%), H-3->L+3 (31%), H-2->L+6 (10%)
47	46513.9939204	214.989063659	0.0174	H-8->L+1 (22%), H-2->L+7 (11%)
48	46590.6165912	214.635493832	0.0102	H-3->L+3 (12%), H-3->L+4 (19%), HOMO->L+10 (30%)
49	46671.2720341	214.264569277	0.0471	H-2->L+7 (33%)

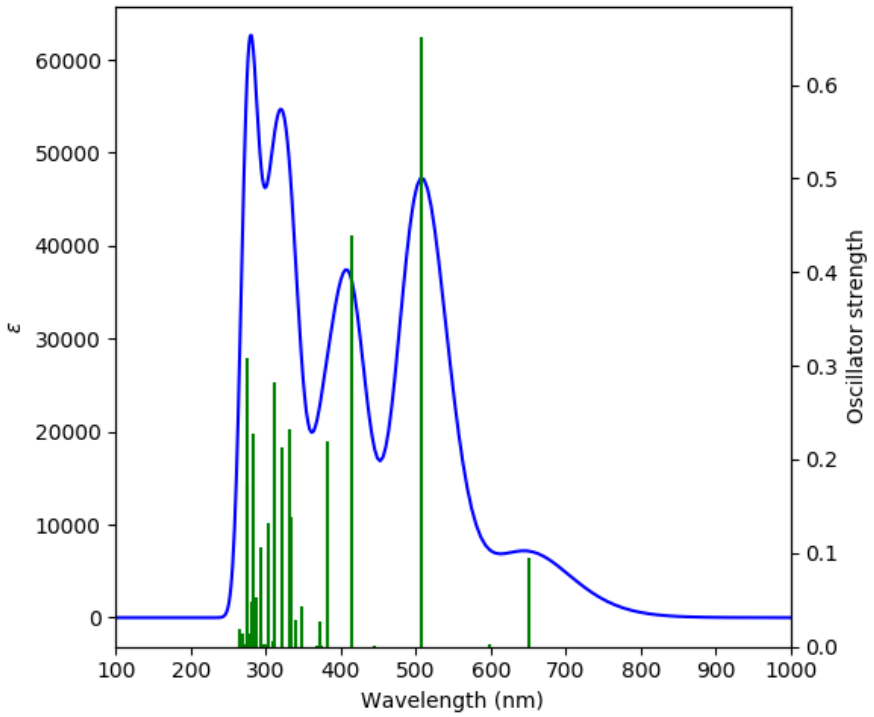

Figure S103. TD-DFT predicted absorption spectra for **3** (solvent dichloromethane).

Table S8. UV-Vis transitions (oscillator strength > 0.01) calculated with TD-DFT for **3**.

No.	Energy (cm-1)	Wavelength (nm)	Osc. Strength	Major contribs
1	15347.117675	651.588149108	0.0946	HOMO->LUMO (99%)
3	19668.6363056	508.423657066	0.6515	H-2->LUMO (98%)
5	24115.9774271	414.662852884	0.4385	H-4->LUMO (96%)
6	26206.5665071	381.583752961	0.219	HOMO->L+1 (90%)
8	26826.0003085	372.77267893	0.0104	H-11->LUMO (11%), H-9->LUMO (12%), H-6->LUMO (68%)
10	26849.390387	372.44793479	0.0273	H-9->LUMO (66%), H-8->LUMO (27%)
17	28686.7213762	348.593339366	0.0429	H-13->LUMO (92%)
19	29324.7059296	341.009387239	0.0288	H-15->LUMO (12%), H-2->L+1 (60%), H-1->L+2 (13%)
22	29892.5202476	334.531846668	0.1385	H-1->L+2 (79%)
23	30106.2571713	332.156865037	0.2328	H-1->L+3 (31%), HOMO->L+4 (56%)
25	31131.3878505	321.219216053	0.2136	H-1->L+3 (54%), HOMO->L+4 (32%)
26	31144.2927214	321.086116466	0.0016	H-16->LUMO (66%), H-2->L+2 (20%)
27	32168.6168462	310.861982279	0.2827	HOMO->L+5 (76%)

29	32949.3615335	303.496017361	0.1317	H-17->LUMO (73%), H-4->L+1 (10%)
32	33947.8759166	294.569239753	0.0117	H-2->L+3 (21%), H-1->L+5 (54%)
33	34172.9046023	292.629500371	0.1059	H-4->L+1 (58%)
35	34782.6597506	287.499577999	0.0533	H-4->L+1 (14%), H-3->L+2 (42%), H-2->L+4 (32%)
36	35079.4717805	285.067006213	0.0234	H-18->LUMO (60%), HOMO->L+6 (25%)
37	35194.8090638	284.132810093	0.2282	H-3->L+2 (13%), H-2->L+4 (44%), H-2->L+5 (26%)
38	35548.8864582	281.302763499	0.0474	H-3->L+2 (19%), H-2->L+4 (11%), H-2->L+5 (57%)
39	35932.8063664	278.2972167	0.0133	H-4->L+2 (74%)
40	36240.1036038	275.937400989	0.3082	H-3->L+3 (10%), H-1->L+6 (70%)
41	36394.1554998	274.769392576	0.1734	H-3->L+3 (73%), H-1->L+6 (11%)
45	37262.8146198	268.364054139	0.0134	H-1->L+8 (19%), HOMO->L+7 (50%), HOMO->L+11 (11%)
46	37432.1910499	267.149737152	0.0117	H-4->L+3 (10%), H-3->L+5 (17%), H-2->L+6 (26%), HOMO->L+12 (12%)
50	37641.088647	265.667130241	0.0194	H-20->LUMO (19%), H-8->L+1 (24%), H-6->L+1 (32%), H-5->L+2 (19%)

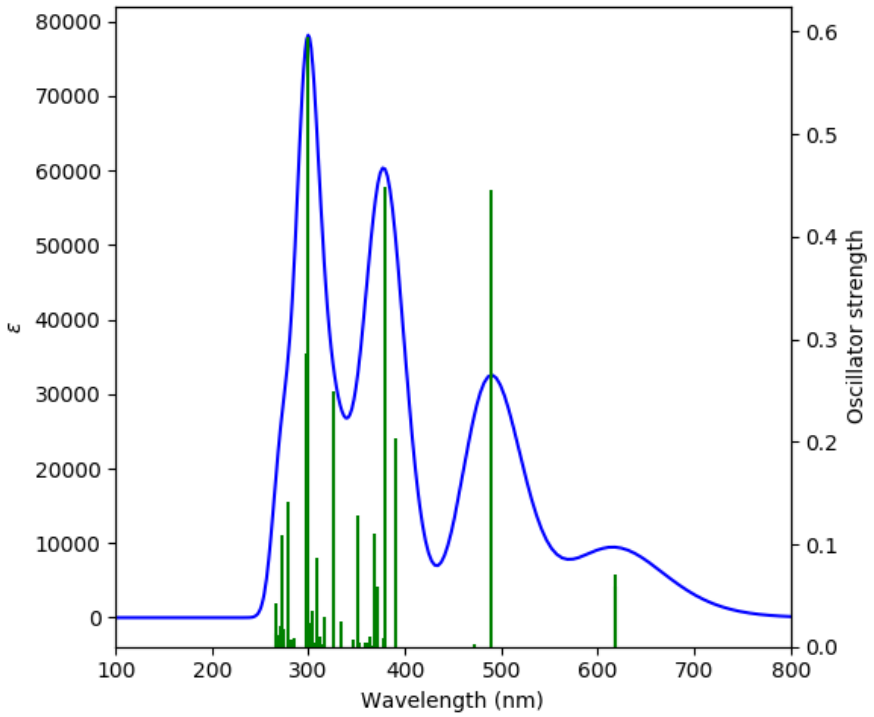

Figure S104. TD-DFT predicted absorption spectra for **4** (solvent dichloromethane).

Table S9. UV-Vis transitions (oscillator strength > 0.01) calculated with TD-DFT for **4**.

No.	Energy (cm-1)	Wavelength (nm)	Osc. Strength	Major contribs
1	16164.1573116	618.652726971	0.0584	H-1->LUMO (99%)
2	16187.54739	617.758809229	0.0703	HOMO->LUMO (99%)
3	20412.2794891	489.901189396	0.4461	H-2->LUMO (99%)
5	25658.1094953	389.740327588	0.2029	H-4->LUMO (90%)
6	26336.4217701	379.702303042	0.4492	H-1->L+1 (96%)
8	26867.1345844	372.201954346	0.0593	H-5->LUMO (84%)
9	27143.7827536	368.408489369	0.1107	H-8->LUMO (28%), H-1->L+3 (15%), HOMO->L+2 (45%)
19	28418.1387514	351.887929308	0.1282	H-1->L+3 (77%), HOMO->L+2 (14%)
21	29944.9462855	333.946165896	0.0245	H-2->L+1 (70%)
24	30645.8420843	326.308540405	0.2491	H-3->L+1 (62%), H-2->L+2 (24%)
25	31637.904032	316.076564045	0.0288	H-3->L+1 (27%), H-2->L+2 (62%)
27	32075.8630869	311.760901738	0.01	H-16->LUMO (32%), H-3->L+2 (48%)
28	32373.4816712	308.894795486	0.086	H-17->LUMO (13%), HOMO->L+4 (66%)
30	32917.9059108	303.786031442	0.0344	H-17->LUMO (61%), H-3->L+3 (28%)

31	33151.0001408	301.650024359	0.0228	H-3->L+3 (10%), H-1->L+5 (72%), HOMO->L+4 (11%)
33	33394.5795783	299.449794735	0.5953	H-17->LUMO (15%), H-3->L+3 (48%), H-1->L+5 (20%), HOMO->L+4 (10%)
34	33617.1886007	297.46687383	0.2856	H-16->LUMO (17%), H-3->L+2 (29%), H-2->L+3 (30%), H-1->L+4 (10%)
38	35781.9806882	279.470275476	0.1421	H-4->L+1 (22%), HOMO->L+6 (60%)
39	36429.6438946	274.501722524	0.0172	H-2->L+4 (60%), H-1->L+6 (21%)
41	36655.4791348	272.810511172	0.1091	H-11->L+1 (10%), H-9->L+1 (36%), H-5->L+1 (25%)
45	36896.638909	271.027396958	0.0196	H-4->L+2 (67%)
47	37303.1423413	268.073930837	0.0119	H-1->L+8 (26%), H-1->L+11 (16%), HOMO->L+7 (24%), HOMO->L+10 (23%)
49	37445.0959208	267.057668143	0.0421	H-19->LUMO (13%), H-6->L+1 (10%), H-4->L+3 (15%), H-3->L+4 (29%) H-10->L+1 (9%), H-8->L+1 (3%), H-5->L+2 (8%), H-4->L+1 (5%)
50	37528.9775814	266.460762975	0.0132	H-9->L+1 (14%), H-7->L+1 (22%), H-6->L+2 (15%), H-5->L+1 (36%) H-11->L+1 (3%), H-7->L+3 (2%), H-5->L+3 (2%)

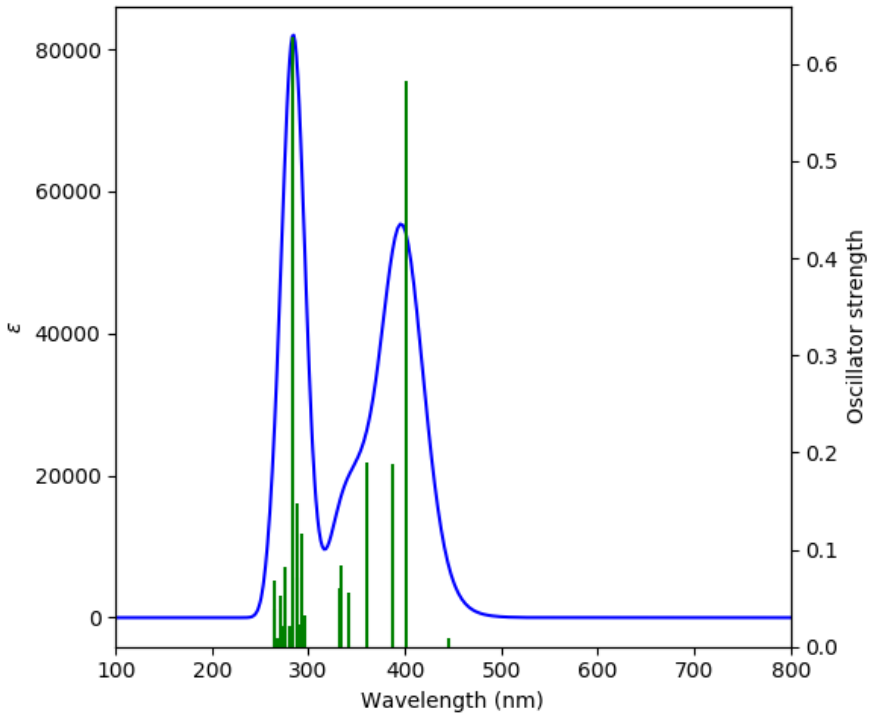

Figure S105. TD-DFT predicted absorption spectra for **5** (solvent dichloromethane).

Table S10. UV-Vis transitions (oscillator strength > 0.01) calculated with TD-DFT for **5**.

No.	Energy (cm-1)	Wavelength (nm)	Osc. Strength	Major contribs
1	21412.4069811	467.01895816	0.0	HOMO->LUMO (98%)
3	24941.8891624	400.931939633	0.583	H-2->LUMO (81%), HOMO->L+2 (12%)
5	25862.9743203	386.65313108	0.1889	H-2->LUMO (18%), H-1->L+1 (19%), HOMO->L+2 (59%)
6	27716.4363982	360.796743721	0.1902	H-1->L+1 (63%), HOMO->L+2 (24%), HOMO->L+3 (12%)
8	29248.0832588	341.902746635	0.0557	H-2->L+1 (18%), H-1->L+1 (11%), HOMO->L+3 (63%)
10	29928.0086425	334.135161462	0.0844	H-3->LUMO (68%), H-2->L+1 (12%), HOMO->L+3 (15%)
12	30140.9390117	331.774666878	0.0606	H-3->LUMO (24%), H-2->L+1 (66%)
17	33686.5522816	296.854362429	0.033	H-6->LUMO (79%)
20	34055.1476557	293.641363741	0.1164	H-6->LUMO (10%), H-4->L+2 (20%), H-3->L+1 (24%), H-1->L+4 (23%), HOMO->L+5 (16%)
22	34320.5040628	291.371011967	0.0232	H-10->LUMO (91%)
25	34686.6797736	288.295105363	0.0718	H-12->LUMO (64%), H-1->L+4 (18%)

26	34752.0106823	287.753134384	0.1469	H-12->LUMO (30%), H-4->L+2 (10%), H-1->L+4 (45%)
28	35170.612431	284.32828742	0.6283	HOMO->L+5 (75%)
29	35673.9023947	280.316963627	0.0208	H-4->L+2 (41%), H-3->L+1 (38%)
32	36262.6871278	275.765553853	0.0827	H-15->LUMO (65%), H-2->L+4 (13%)
34	36356.2474416	275.055890079	0.0827	H-15->LUMO (20%), H-2->L+4 (11%), H-1->L+8 (10%), HOMO->L+7 (28%), HOMO->L+10 (12%)
37	36604.6662057	273.189214287	0.0213	H-5->L+2 (41%), H-1->L+6 (10%), HOMO->L+10 (16%)
41	36995.0385494	270.306516552	0.0527	H-5->L+2 (13%), H-2->L+4 (26%), HOMO->L+7 (24%)
47	37684.6425862	265.360086065	0.0681	H-11->L+2 (15%), H-10->L+1 (14%), H-9->L+2 (24%), H-6->L+1 (18%)
48	37793.5274341	264.595571753	0.0383	H-10->L+1 (15%), H-9->L+2 (11%), H-6->L+1 (15%), H-1->L+6 (13%)

8.3. GIAO-DFT predicted NMR values.

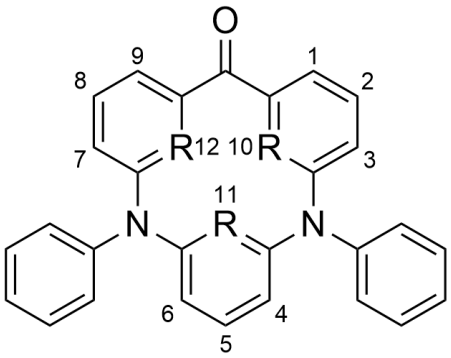

Figure S106. general macrocyclic structure with numbering for GIAO analysis, phenyl substituents decorating the cavity are omitted for clarity, R = CH, if not specified.

Table S11. summary of NMR spectra (SCF GIAO method) calculated at b3lyp/6-31g(d,p) degree of theory for **1a** and compared with experimental values using $CDCl_3$ as solvent.

	1/9	**2/8**	**3/7**	**4/6**	**5**	**10/12**	**11**
theoretical	6.98	7.20	7.04	6.54	7.15	7.97	7.49
experimental	7.47	7.37	7.58	6.98	7.16	7.01	7.58

Table S12. summary of NMR spectra (SCF GIAO method) calculated at b3lyp/6-31g(d,p) degree of theory for **1b** (R(11) = N) and compared with experimental values using $CDCl_3$ as solvent.

	1/9	**2/8**	**3/7**	**4/6**	**5**	**10/12**
theoretical	7.08	7.17	6.57	5.93	7.17	8.48
experimental	7.68	7.34	7.00	6.23	7.24	8.66

Table S13. summary of NMR spectra (SCF GIAO method) calculated at b3lyp/6-31g(d,p) degree of theory for **1c** (R(12) = N) and compared with experimental values using $CDCl_3$ as solvent.

	1	**2**	**3**	**4**	**5**	**6**	**7**	**8**	**9**	**10**	**11**
theoretical	7.28	7.28	7.28	6.70	7.12	6.27	6.59	7.56	7.73	9.02	8.02
experimental	7.50	7.16	7.18	6.33	7.01	6.72	7.16	7.41	7.16	8.77	8.00

Table S14. summary of NMR spectra (SCF GIAO method) calculated at b3lyp/6-31g(d,p) degree of theory for **1d** (R(10/12) = N) and compared with experimental values using $CDCl_3$ as solvent.

	1	**2/8**	**3**	**4/6**	**5**	**7**	**9**	**11**
theoretical	7.53	7.53	6.82	6.34	7.07	6.76	7.68	8.36
experimental	7.50	7.50	6.77	6.42	6.98	6.77	7.50	8.51

Table S15. summary of NMR spectra (SCF GIAO method) calculated at b3lyp/6-31g(d,p) degree of theory for **1e** (R(11/12) = N) and compared with experimental values using $CDCl_3$ as solvent.

	1	**2**	**3**	**4**	**5**	**6**	**7**	**8**	**9**	**10**
theoretical	7.30	7.23	6.80	6.17	7.23	5.79	6.25	7.59	7.59	9.88
experimental	7.30	7.15	6.88	6.28	7.26	5.94	6.44	7.50	7.60	9.67

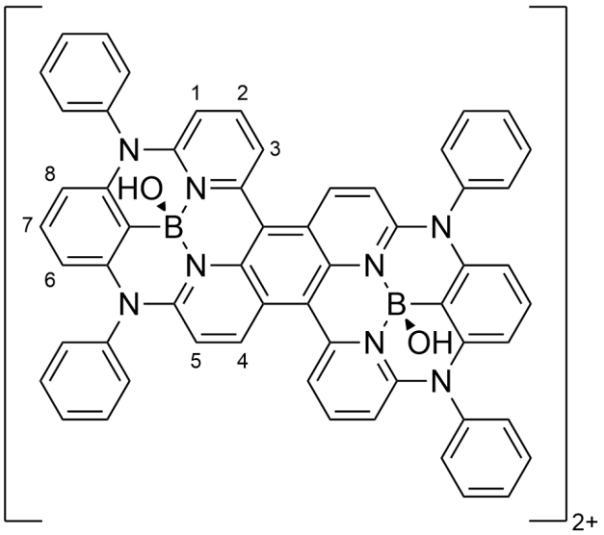

Figure S107. boron(III) complex structure **3** with numbering for GIAO analysis, phenyl substituents decorating the cavity are omitted for clarity (two-fold symmetry present).

Table S16. summary of NMR spectra (SCF GIAO method) calculated at b3lyp/6-31g(d,p) degree of theory for **3** and compared with experimental values using $MeOD_4$ as solvent.

	1	**2**	**3**	**4**	**5**	**6**	**7**	**8**
theoretical	6.91	7.94	7.41	8.69	7.03	6.41	7.41	6.56
experimental	7.03	8.14	7.81	9.01	7.24	6.45	7.34	6.52

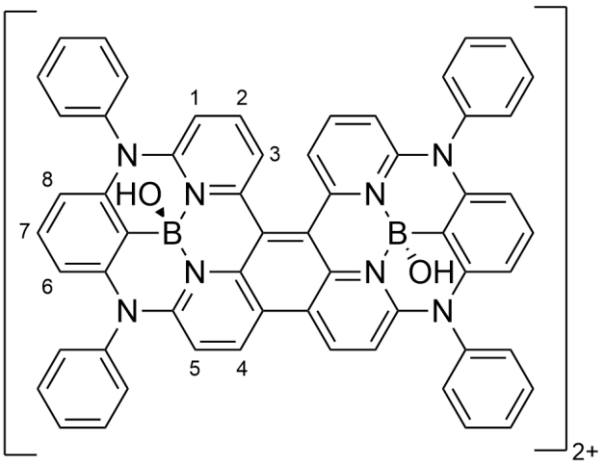

Figure S108. boron(III) complex structure **4** with numbering for GIAO analysis (two-fold symmetry present).

Table S17. summary of NMR spectra (SCF GIAO method) calculated at b3lyp/6-31g(d,p) degree of theory for **4** and compared with experimental values using $MeOD_4$ as solvent.

	1	**2**	**3**	**4**	**5**	**6**	**7**	**8**
theoretical	6.83	7.74	7.74	8.69	7.12	6.47	7.41	6.52
experimental	6.95	7.65	7.68	9.13	7.30	6.52	7.29	6.46

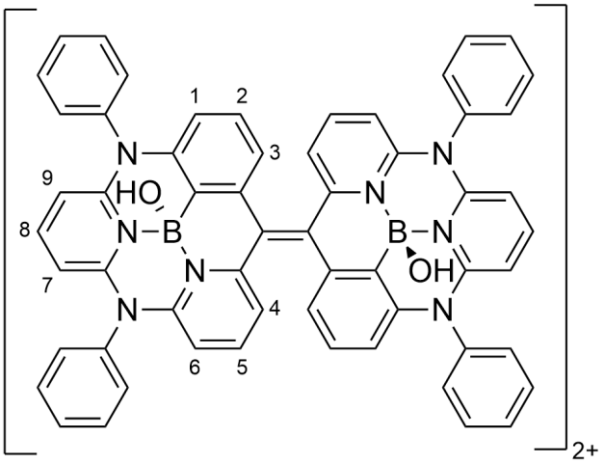

Figure S109. boron(III) complex structure **5** with numbering for GIAO analysis (two-fold symmetry present).

Table S18. summary of NMR spectra (SCF GIAO method) calculated at b3lyp/6-31g(d,p) degree of theory for **5** and compared with experimental values using $MeOD_4$ as solvent.

	1	**2**	**3**	**4**	**5**	**6**	**7**	**8**	**9**
theoretical	6.41	7.19	7.02	7.26	7.71	6.75	6.07	7.53	6.17
experimental	6.44	7.09	6.93	7.41	7.82	6.79	6.14	7.71	6.35

9. Crystallographic data.

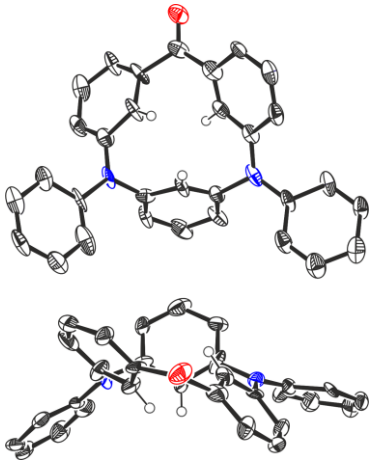

Figure S110. X-ray crystal structures of **1a**, thermal ellipsoids present 50% probability. External protons (outside the cavity) have been removed for clarity.

Table S19. Crystal data and structure refinement for **1a**.

Identification code	**1a**
Depisition number	2153360
Empirical formula	$C_{31}H_{22}N_2O$
Formula weight	438.50
Temperature/K	100(2)
Crystal system	orthorhombic
Space group	$Pna2_1$
a/Å	14.420(5)
b/Å	37.960(9)
c/Å	8.121(3)
Volume/Å^3	4445(2)
Z	8
ρ_{calc}g/cm^3	1.310
μ/mm^{-1}	0.621
F(000)	1840.0
Crystal size/mm^3	0.04 × 0.03 × 0.01
Radiation	CuK_α (λ = 1.54184)
2Θ range for data collection/°	9.298 to 136.326
Index ranges	-13 ≤ h ≤ 17, -44 ≤ k ≤ 37, -9 ≤ l ≤ 9
Reflections collected	14528
Independent reflections	6598 [R_{int} = 0.1911, R_{sigma} = 0.2776]
Data/restraints/parameters	6598/19/613
Goodness-of-fit on F^2	0.982
Final R indexes [I>=2σ (I)]	R_1 = 0.1329, wR_2 = 0.2932
Final R indexes [all data]	R_1 = 0.2719, wR_2 = 0.3942
Largest diff. peak/hole / e Å^{-3}	0.51/-0.37
Flack parameter	-2.1(10)

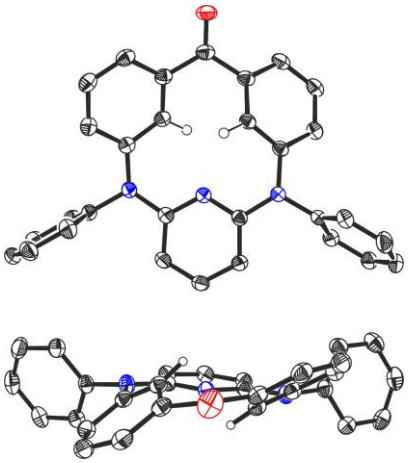

Figure S111. X-Ray crystal structures of **1b**, thermal ellipsoids present 50% probability. External protons (outside the cavity) have been removed for clarity.

Table S20. Crystal data and structure refinement for **1b**.

Identification code	**1b**
Deposition number	2153365
Empirical formula	$C_{30}H_{21}N_3O$
Formula weight	439.50
Temperature/K	151(2)
Crystal system	monoclinic
Space group	$P2_1/c$
a/Å	14.826(4)
b/Å	5.850(3)
c/Å	25.150(7)
β/°	94.3900(9)
Volume/Å^3	2174.9(14)
Z	4
ρ_{calc}g/cm^3	1.342
μ/mm^{-1}	0.650
F(000)	920.0
Crystal size/mm^3	0.40 × 0.10 × 0.04
Radiation	CuK_α (λ = 1.54184)
2Θ range for data collection/°	5.978 to 147.836
Index ranges	-18 ≤ h ≤ 18, -7 ≤ k ≤ 7, -31 ≤ l ≤ 31
Reflections collected	37790
Independent reflections	4384 [R_{int} = 0.0186, R_{sigma} = 0.0089]
Data/restraints/parameters	4384/0/308
Goodness-of-fit on F^2	1.027
Final R indexes [I>=2σ (I)]	R1 = 0.0324, wR2 = 0.0818
Final R indexes [all data]	R1 = 0.0337, wR2 = 0.0828
Largest diff. peak/hole / e Å^{-3}	0.20/-0.17

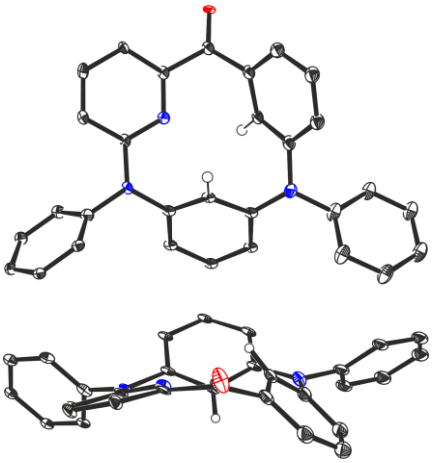

Figure S112. X-Ray crystal structures of **1c**, thermal ellipsoids present 50% probability. External protons (outside the cavity) and solvent atoms have been removed for clarity.

Table S21. Crystal data and structure refinement for **1c**.

Identification code	**1c**
Deposition number	2153363
Empirical formula	$C_{30.9}H_{22.8}Cl_{1.8}N_3O$
Exact composition	$C_{30}H_{21}N_3O{\cdot}0.9(CH_2Cl_2)$
Formula weight	515.93
Temperature/K	100(2)
Crystal system	monoclinic
Space group	$P2_1/n$
a/Å	8.416(6)
b/Å	31.033(9)
c/Å	9.694(6)
β/°	98.93(3)
Volume/Å^3	2501(2)
Z	4
ρ_{calc}g/cm^3	1.370
μ/mm^{-1}	0.269
F(000)	1071.0
Crystal size/mm^3	0.200 × 0.150 × 0.090
Radiation	MoK_α (λ = 0.71073)
2Θ range for data collection/°	4.998 to 50.078
Index ranges	-9 ≤ h ≤ 10, -36 ≤ k ≤ 34, -10 ≤ l ≤ 11
Reflections collected	10562
Independent reflections	4382 [R_{int} = 0.0747, R_{sigma} = 0.1202]
Data/restraints/parameters	4382/0/328
Goodness-of-fit on F^2	1.190
Final R indexes [I>=2σ (I)]	R1 = 0.1160, wR2 = 0.1931
Final R indexes [all data]	R1 = 0.1647, wR2 = 0.2102
Largest diff. peak/hole / e Å^{-3}	0.62/-0.37

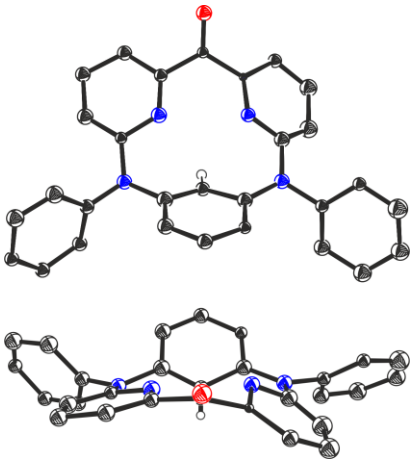

Figure S113. X-Ray crystal structures of **1d**, thermal ellipsoids present 50% probability. External protons (outside the cavity) and solvent atoms have been removed for clarity.

Table S22. Crystal data and structure refinement for **1d**.

Identification code	**1d**
Deposition number	2153361
Empirical formula	$C_{30}H_{22}Cl_2N_4O$
Exact composition	$C_{29}H_{20}N_4O{\cdot}CH_2Cl_2$
Formula weight	525.41
Temperature/K	100(2)
Crystal system	monoclinic
Space group	$P2_1/n$
a/Å	8.438(5)
b/Å	29.605(3)
c/Å	9.885(7)
β/°	96.74(5)
Volume/Å^3	2452(2)
Z	4
ρ_{calc}g/cm^3	1.423
μ/mm^{-1}	2.640
F(000)	1088.0
Crystal size/mm^3	0.52 × 0.30 × 0.13
Radiation	Cu K_α (λ = 1.54184)
2Θ range for data collection/°	5.97 to 134.994
Index ranges	-7 ≤ h ≤ 10, -35 ≤ k ≤ 32, -11 ≤ l ≤ 11
Reflections collected	8913
Independent reflections	4372 [R_{int} = 0.0804, R_{sigma} = 0.0944]
Data/restraints/parameters	4372/4/358
Goodness-of-fit on F^2	1.077
Final R indexes [I>=2σ (I)]	R1 = 0.1087, wR2 = 0.2766
Final R indexes [all data]	R1 = 0.1346, wR2 = 0.2956
Largest diff. peak/hole / e Å^{-3}	0.73/-0.52

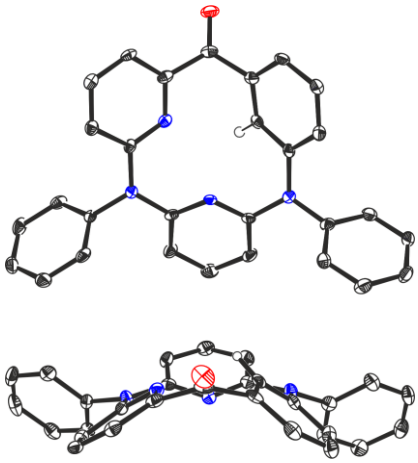

Figure S114. X-Ray crystal structures of **1e**, thermal ellipsoids present 50% probability. External protons (outside the cavity) have been removed for clarity.

Table S23. Crystal data and structure refinement for **1e**.

Identification code	**1e**
Deposition number	2153364
Empirical formula	$C_{29}H_{20}N_4O$
Formula weight	440.49
Temperature/K	100(2)
Crystal system	triclinic
Space group	P-1
a/Å	8.829(4)
b/Å	9.614(4)
c/Å	25.805(9)
α/°	91.74(2)
β/°	94.62(3)
γ/°	92.97(3)
Volume/Å^3	2179.0(15)
Z	4
ρ_{calc}g/cm^3	1.343
μ/mm^{-1}	0.084
F(000)	920.0
Crystal size/mm^3	0.350 × 0.220 × 0.100
Radiation	MoK$_\alpha$ (λ = 0.71073)
2Θ range for data collection/°	4.48 to 50.122
Index ranges	-10 ≤ h ≤ 10, -11 ≤ k ≤ 11, 0 ≤ l ≤ 30
Reflections collected	7657
Independent reflections	7657 [R_{int} = ?, R_{sigma} = 0.0298]
Data/restraints/parameters	7657/0/614
Goodness-of-fit on F^2	1.248
Final R indexes [I>=2σ (I)]	R1 = 0.0767, wR2 = 0.1373
Final R indexes [all data]	R1 = 0.0824, wR2 = 0.1397
Largest diff. peak/hole / e Å^{-3}	0.29/-0.33

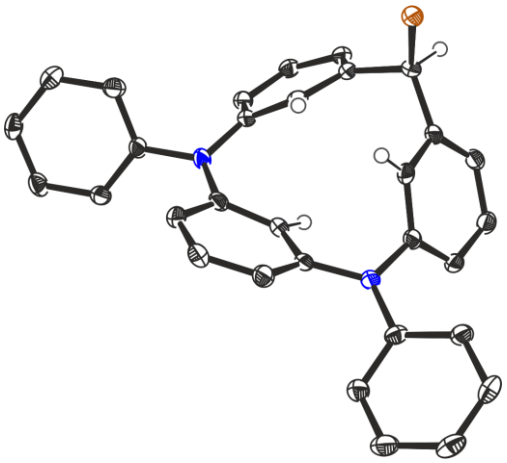

Figure S115. X-Ray crystal structures of **2a**, thermal ellipsoids present 50% probability. External protons (outside the cavity) and solvent atoms have been removed for clarity.

Table S24. Crystal data and structure refinement for **2a**.

Identification code	**2a**
Deposition number	2153366
Empirical formula	$C_{31}H_{23}BrN_2$
Formula weight	503.42
Temperature/K	100(2)
Crystal system	orthorhombic
Space group	Pccn
a/Å	33.181(7)
b/Å	22.852(5)
c/Å	5.966(3)
Volume/Å^3	4524(3)
Z	8
ρ_{calc}g/cm^3	1.478
μ/mm^{-1}	2.643
F(000)	2064.0
Crystal size/mm3	0.490 × 0.020 × 0.020
Radiation	CuK$_\alpha$ (λ = 1.54184)
2Θ range for data collection/°	4.696 to 150.882
Index ranges	-38 ≤ h ≤ 41, -28 ≤ k ≤ 27, -7 ≤ l ≤ 5
Reflections collected	22372
Independent reflections	4486 [R_{int} = 0.0470, R_{sigma} = 0.0359]
Data/restraints/parameters	4486/0/307
Goodness-of-fit on F^2	1.074
Final R indexes [I>=2σ (I)]	R1 = 0.0466, wR2 = 0.1168
Final R indexes [all data]	R1 = 0.0577, wR2 = 0.1232
Largest diff. peak/hole / e Å-3	1.18/-0.60

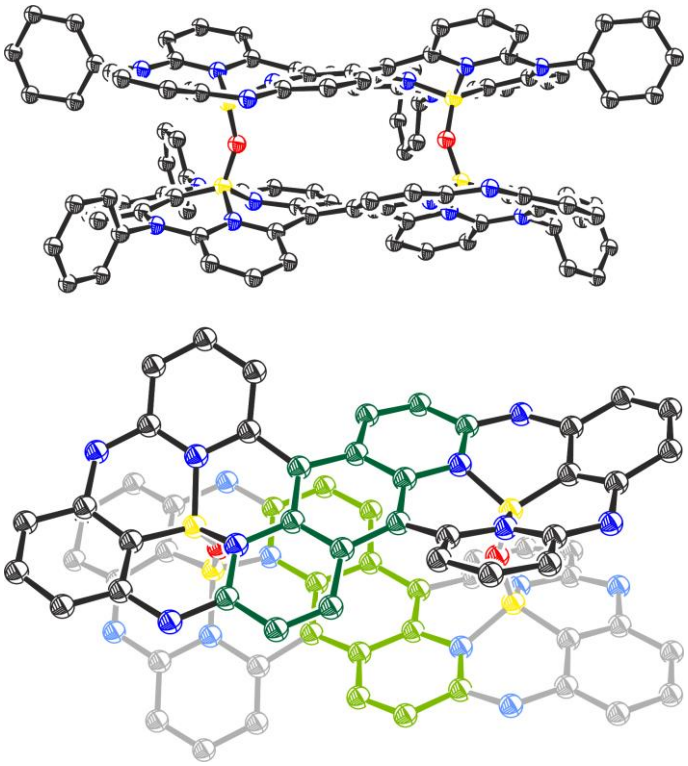

Figure S116. X-Ray crystal structures of **3**-*O*-**3**, thermal ellipsoids present 50% probability. External phenyl substituents, protons, solvent and counter anion atoms have been removed for clarity. Color scheme applied in the bottom part is intended to highlight the pyrido[2,3-g]quinoline frames.

Table S25. Crystal data and structure refinement for **3**-*O*-**3**.

Identification code	**3**-*O*-**3**
Deposition number	2153367
Empirical formula	$C_{141.09}H_{103.24}B_4Br_4Cl_2N_{16}O_{11.03}Zn'$
Exact composition	$[C_{116}H_{72}B_4N_{16}O_2]ZnBr_4[ClO_4]_2 \cdot 0.45H_2O \cdot 0.583CH_3OH \cdot 3.5C_7H_8$
Formula weight	2693.59
Temperature/K	100(2)
Crystal system	triclinic
Space group	P-1
a/Å	16.853(4)
b/Å	17.842(3)
c/Å	22.270(5)
α/°	73.04(2)
β/°	79.04(2)
γ/°	82.640(10)
Volume/Å^3	6269(2)
Z	2
ρ_{calc}g/cm^3	1.429
μ/mm^{-1}	2.712
F(000)	2748.0
Crystal size/mm^3	0.232 × 0.066 × 0.011

Radiation	CuK_α (λ = 1.54184)
2Θ range for data collection/°	7.058 to 148.054
Index ranges	-20 ≤ h ≤ 20, -21 ≤ k ≤ 12, -27 ≤ l ≤ 27
Reflections collected	84401
Independent reflections	24149 [R_{int} = 0.0766, R_{sigma} = 0.0861]
Data/restraints/parameters	24149/194/1649
Goodness-of-fit on F^2	1.336
Final R indexes [I>=2σ (I)]	R1 = 0.1345, wR2 = 0.3566
Final R indexes [all data]	R1 = 0.1788, wR2 = 0.3852
Largest diff. peak/hole / e $Å^{-3}$	1.27/-2.11

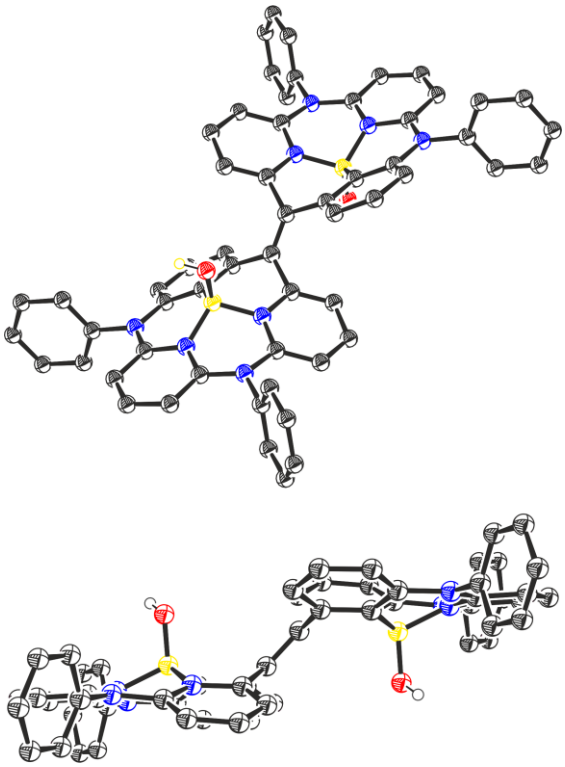

Figure S117. X-Ray crystal structures of **5**, thermal ellipsoids present 50% probability. External protons (outside the cavity) and solvent atoms have been removed for clarity.

Table S26. Crystal data and structure refinement for **5**.

Identification code	**5**
Deposition number	2153362
Empirical formula	$C_{72.1}H_{76.8}B_2Br_2N_8O_{8.6}$
Exact composition	$[C_{58}H_{40}B_2N_8O_2]Br_2 \cdot 2.3(C_4H_8O) \cdot 4.1(CH_4O) \cdot 0.2(C_4H_{10}O)$
Formula weight	1374.45
Temperature/K	100(2)
Crystal system	monoclinic
Space group	C2/c
a/Å	27.431(8)
b/Å	12.568(3)

c/Å	19.588(5)
β/°	90.23(3)
Volume/Å^3	6753(3)
Z	4
ρ_{calc}g/cm^3	1.352
μ/mm^{-1}	1.265
F(000)	2857.0
Crystal size/mm^3	0.490 × 0.220 × 0.100
Radiation	Mo K_α (λ = 0.71073)
2Θ range for data collection/°	5.102 to 51.11
Index ranges	-33 ≤ h ≤ 33, -15 ≤ k ≤ 15, -23 ≤ l ≤ 23
Reflections collected	50611
Independent reflections	6317 [R_{int} = 0.0299, R_{sigma} = 0.0194]
Data/restraints/parameters	6317/3/490
Goodness-of-fit on F^2	1.042
Final R indexes [I>=2σ (I)]	R_1 = 0.0747, wR_2 = 0.2060
Final R indexes [all data]	R_1 = 0.0870, wR_2 = 0.2168
Largest diff. peak/hole / e Å^{-3}	1.54/-1.56